

Turbulence Investigation and Reproduction for Assisting Downstream Migrating Juvenile Salmonids, Part I of II

**Final Report
2001 - 2002**



This Document should be cited as follows:

Hotchkiss, Rollin, "Turbulence Investigation and Reproduction for Assisting Downstream Migrating Juvenile Salmonids, Part I of II", Project No. 2001-01000, 138 electronic pages, (BPA Report DOE/BP-00004633-1)

Bonneville Power Administration
P.O. Box 3621
Portland, Oregon 97208

This report was funded by the Bonneville Power Administration (BPA), U.S. Department of Energy, as part of BPA's program to protect, mitigate, and enhance fish and wildlife affected by the development and operation of hydroelectric facilities on the Columbia River and its tributaries. The views in this report are the author's and do not necessarily represent the views of BPA.

Turbulence Investigation and Reproduction for Assisting Downstream
Migrating Juvenile Salmonids

WASHINGTON STATE UNIVERSITY

DEPARTMENT OF CIVIL AND ENVIRONMENTAL ENGINEERING
ALBROOK HYDRAULICS LABORATORY

Prepared for: Bonneville Power Administration

Principal Investigator: Dr. Rollin H. Hotchkiss

Date Work Performed: May 2001 through December 2002

DECEMBER 2002

ACKNOWLEDGEMENT

Data from the Bonneville Prototype Surface Collector was provided by Blaine Ebberts with the USACE, Portland District and Derrek Faber of Battelle Labs.

EXECUTIVE SUMMARY

This report is in partial fulfillment of the Innovative Project Proposals Grant Number 22022. The primary goal of this work has been to investigate the applicability of using appropriately scaled induced turbulence to assist downstream migrating juvenile salmonids.

Water in rivers and streams moves downstream with an average, or bulk velocity, but the velocity is by no means uniform from the streambed to the water surface or from one streambank to the other. Water velocities are in a continuous state of change, exhibiting circular motions and changes from the bulk velocity in all directions at all locations. The difference between the velocity at a point at any instant compared with the average velocity at the same point is called turbulence. Turbulence in rivers depends upon the depth of flow, the discharge, the size and shape of the stream channel, and the nature of the streambed and banks. Words associated with turbulence include eddies, vortices, secondary currents, and bursts.

Juvenile salmonids commonly migrate at night using their lateral line organ as the primary guidance sensor for movement. Understanding the turbulent flow experienced by the juveniles during their outmigration is therefore necessary if active guidance of juveniles is to be achieved. It has been the goal of this study to determine turbulence characteristics in the natural migration corridors and reproduce those characteristics in the laboratory for guidance of migrating juvenile salmonids.

Turbulence data were collected in unobstructed and obstructed flow in rivers of the Clearwater River Basin in Idaho to determine the range and character of turbulence that juveniles experience during outmigration. Mean flow velocity, turbulent kinetic energy (TKE), strain,

Reynolds shear stress tensors, and eddy length scales were investigated. This suite of parameters captures all the relevant information fish are thought to access through their lateral lines.

The turbulence characteristics recorded in the Clearwater River Basin were compared to those we measured in a large laboratory tank that was operated like a reservoir - very slow flow-through velocity. Since the reservoir-like turbulence levels were very low, various jets and mixers were installed and tested in the tank to attempt to reproduce the TKE, strain, and eddy length scales found in the Clearwater River Basin. If successful, we would be able to reproduce "natural" turbulence in large open water bodies, such as reservoir forebays, that would be similar to that experienced by juvenile salmonids during their riverine outmigration. Most turbulence parameters in natural migration corridors as measured in the gravel bed rivers of the Clearwater Basin were easily reproducible with turbulent jets. However, large mixers (>15cm in diameter) are required to reproduce natural eddy length scales, making proper reproduction of all parameters more difficult in the laboratory environment - but not inhibiting their use in larger water bodies. TKE, strain, and eddy length scales were reproduced using a single 1.4 cm diameter oscillating jet while TKE and strain were reproduced using a single 15 cm mixer. The ability to successfully reproduce most turbulent parameters with a single source demonstrates that complex arrays of jets and mixers may not be necessary for juvenile attraction. The one jet and one mixer that best reproduced the natural turbulence parameters were selected for testing with actively migrating juvenile salmonids. Results from those tests are still pending and are under the direction of Mr. Dennis Rondorf of the U.S. Geological Survey Cook Lab. Without final data on fish collection efficiencies, substantial conclusions cannot be made; however, preliminary data suggests that if TKE, strain, and eddy length scales are properly reproduced, fish collection efficiencies may be increased and delays may be decreased.

In an effort to look ahead to future applications, we compared the turbulence characteristics from the natural river, jet, and mixer to those upstream from the Bonneville Prototype Surface Collector (PSC). The Bonneville PSC was selected as a typical manmade fishway to demonstrate the applicability of this research to fish passage technologies. Results show that the turbulent fluctuations upstream of the Bonneville PSC are similar to the turbulent fluctuations found in the natural migration corridor of the Clearwater River Basin with the exception that turbulent length scales. The length scale, or "size" of the eddies in the Bonneville Reservoir are one to two orders of magnitude larger than turbulent structures in the Clearwater River Basin. The Bonneville PSC has generally had positive results collecting juvenile salmonids, but according to our preliminary results using an oscillating jet, fish passage efficiencies might further be increased and fish delays decreased at this and other attractors if eddy length scales more closely match those found in natural migration corridors.

TABLE OF CONTENTS

INTRODUCTION	1
BACKGROUND	2
Turbulence in Gravel Bed Rivers	3
Turbulent Flow behind Geometric Objects.....	5
Turbulent Plumes	6
METHODS	8
Site Selection	8
Experimental Setup.....	11
<i>Field Data Collection</i>	11
<i>Laboratory Data Collection</i>	12
Sampling Protocol.....	13
<i>Field Data Collection</i>	13
<i>Laboratory Data Collection</i>	15
Data Manipulation	15
RESULTS	17
Unobstructed Turbulent Flow in Gravel Bed Rivers	17
Turbulent Flow Downstream from a Boulder.....	20
Turbulence in Natural and Manmade Fishways	28
DISCUSSION.....	30
Unobstructed Turbulent Flow in Gravel Bed Rivers	30
Obstructed Turbulent Flow in Gravel Bed Rivers	30

Turbulence in Natural and Manmade Fishways	34
<i>Natural Fish Corridors</i>	35
<i>Bonneville Prototype Surface Collector</i>	35
<i>Turbulent Mixer</i>	36
<i>Turbulent Jet</i>	37
CONCLUSIONS.....	38
REFERENCES	41
APPENDIX A – LITERATURE REVIEW	45
Introduction.....	46
Measurement Techniques	49
<i>Flow Visualization</i>	49
<i>Hot Wire Anemometers</i>	49
<i>Doppler Technology</i>	50
<i>Numerical Modeling</i>	52
Flow Measurements Behind Bluff Geometric Objects	52
<i>Object Shape</i>	52
Studies on the Turbulent Flow behind Circular Cylinders	56
Studies on the Turbulent Flow behind Square Cylinders	58
Flow Measurements behind Nongeometric Objects	59
References.....	60
APPENDIX B – GRAVEL BED RIVER RESULTS.....	65
Reach Figures.....	66
Sampling Platform Pictures and Specifications.....	68

Survey Results	70
USGS Gauging Station Results	77
Wolman Method Results.....	78
Shear Velocity Calculations.....	80
Relative Roughness and Coles’ Parameter Calculations	82
Incipient Motion Calculations.....	86
Turbulence Data Manipulation Process for Point 8-16-8-14.....	88
Vertical Profile Figures.....	99
Obstructed Flow Figures.....	103
References.....	106
 APPENDIX C – JET, MIXER, AND BONNEVILLE	
PROTOTYPE SURFACE COLLECTOR RESULTS.....	107
Flume Configuration.....	108
Summary of Jets and Mixers Tested.....	109
Results from Selected Jet.....	110
Results from Selected Mixer.....	114
Results from Bonneville Prototype Surface Collector.....	118
References.....	122
 APPENDIX D – CONTACT INFORMATION FOR	
ALBROOK HYDRAULIC LABORATORY	123
Contact Information for Albroom Hydraulic Laboratory	124

LIST OF FIGURES

1. General Trends Observed in the Wake of a Natural Boulder (Literature Review)	6
2. Plan View of a Directed Jet Issuing into Ambient Flow	7
3. Clearwater River Sampling Sites	9
4. Typical Sample Setup for Data Collection in Gravel Bed Rivers	12
5. Reservoir Style Flume.....	13
6. Dimensionless Velocity Profiles for Unobstructed Flow	18
7. Dimensionless Turbulent Kinetic Energy Profiles for Unobstructed Flow	19
8. Mean Streamwise Velocity Directly Downstream from the Boulders	21
9. Turbulent Kinetic Energy Directly Downstream from the Boulders.....	22
10. Absolute Value of Strain Directly Downstream from the Boulders	23
11. Reynolds Shear Stress Tensor $\overline{u'v'}$ Directly Downstream from the Boulders	24
12. Reynolds Shear Stress Tensor $\overline{u'w'}$ Directly Downstream from the Boulders	25
13. Eddy Length Scale Directly Downstream from the Boulders	26
14. Relevant Flow Parameters at 3 Meters Downstream from Boulder A on 8/7/01	27
15. Streamwise Decay of Turbulent Kinetic Energy Along the Wake Centerline Downstream from Boulders B and C.....	28
16. Summary of Gravel Bed River Findings	34
A1. A Self Portrait by Leonardo da Vinci Along with a Qualitative Discussion of Flow Behind an Object.....	47
A2. Quantitative Measurement of Turbulent Flow Behind a Boulder Using an ADV. .	51
A3. Vortex Shedding Modes for Circular and Rectangular Cylinders	56

B1. Selected Reach on the South Fork of the Clearwater (Boulder A)	66
B2. Selected Reach on the South Fork of the Clearwater (Boulder B)	66
B3. Selected Reach on the Lochsa River (Boulder C)	67
B4. Sampling Platform	68
B5. Grain Size Distribution for Site 1 on the S.F. of the Clearwater River	78
B6. Grain Size Distribution for Site 2 on the S.F. of the Clearwater River	78
B7. Grain Size Distribution on the Lochsa River	79
B8. Determination of Local U^*	81
B9. Streamwise Velocity Distribution, Relative Roughness, and Coles' Parameter on 7/27/01	83
B10. Streamwise Velocity Distribution, Relative Roughness, and Coles' Parameter on 8/1/01	83
B11. Streamwise Velocity Distribution, Relative Roughness, and Coles' Parameter on 8/7/01	84
B12. Streamwise Velocity Distribution, Relative Roughness, and Coles' Parameter on 8/16/01	84
B13. Streamwise Velocity Distribution, Relative Roughness, and Coles' Parameter on 8/22/01	85
B14. Data Rotation Angles for Orientation to Mean Streamwise Direction	90
B15. Autocorrelation Calculation Diagram	97
B16. Length Scale Diagram for Point 8-16-8-14	98
B17. Strain Profiles for Unobstructed Flow	99

B18. Dimensionless Streamwise Turbulence Intensity Profiles for Unobstructed Flow	99
B19. Dimensionless Transverse Turbulence Intensity Profiles for Unobstructed Flow	100
B20. Dimensionless Vertical Turbulence Intensity Profiles for Unobstructed Flow	100
B21. Dimensionless Reynolds Shear Stress Tensor $-\overline{u'w'}/U_*^2$ Profiles For Unobstructed Flow	101
B22. Dimensionless Reynolds Shear Stress Tensor $-\overline{u'v'}/U_*^2$ Profiles For Unobstructed Flow	101
B23. Dimensionless Reynolds Shear Stress Tensor $-\overline{v'w'}/U_*^2$ Profiles For Unobstructed Flow	102
B24. Transverse Velocity Directly Downstream from the Boulders.....	103
B25. Vertical Velocity Directly Downstream from the Boulders	103
B26. Streamwise Turbulent Intensity Downstream from the Boulders.....	104
B27. Transverse Turbulent Intensity Downstream from the Boulders.....	104
B28. Vertical Turbulent Intensity Downstream from the Boulders	105
C1. Flume Configuration.....	108
C2. Streamwise Velocity from Selected Jet	110
C3. Turbulent Kinetic Energy from Selected Jet.....	111
C4. Strain from Selected Jet	112

C5. Eddy Length Scales from Selected Jet.....	113
C6. Streamwise Velocity from Selected Mixer	114
C7. Turbulent Kinetic Energy from Selected Mixer	115
C8. Strain from Selected Mixer	116
C9. Eddy Length Scales from Selected Mixer	117

LIST OF TABLES

1. Site and Boulder Parameters for Each Sample Date.....	10
2. Location of Windows and Cross Sections with Respect to Apparent Vortex Shedding Location	14
3. Summary Table of Selected Turbulence Parameters in Natural and Manmade Fishways.....	29
B1. USGS Gauging Station Results for Each Sampling Event	77
B2. Global and Local Shear Stress Values for Each Sample Date	80
B3. Incipient Motion Calculations.....	87
B4. Raw ADV Data for Point 8-16-8-14	88
B5. Filtered ADV Data for Point 8-16-8-14	89
B6. Rotated Data for Point 8-16-8-14.....	91
B7. Example Batch Input File for FORTRAN-90 Program	93
B8. Example Output File for FORTRAN-90 Program.....	94
C1. Summary Table of Jets and Mixers Tested	109
C2. Eddy Length Scales Upstream from the Bonneville Prototype Surface Collector ...	118

NOTATION

ADV = acoustic doppler velocimeter;

D = boulder diameter;

d_{50} = mean particle diameter;

Fr = stream Froude Number;

f = shedding frequency;

g = gravitational constant;

Hz = Hertz;

h = water depth;

κ = Von Karman's Constant (taken as 0.41);

k_s = apparent roughness height;

L = eddy length scale;

PSC = prototype surface collector;

Q = volumetric discharge;

R = hydraulic radius;

Re = stream Reynolds Number;

RPM = rotations per minute;

R(t) = autocorrelation function;

S = bed slope;

St = Strouhal Number;

s'_i = instantaneous fluctuation component of the velocity magnitude;

t = time;

TI_i = turbulent intensity, where i = x, y, and z directions;

TKE = turbulent kinetic energy;

U_{avg} = depth averaged streamwise velocity;

U_{mag} = time averaged magnitude of the velocity vector;

U_* = shear velocity;

u = time averaged streamwise velocity;

u' = fluctuation component of the instantaneous streamwise velocity;

v' = fluctuation component of the instantaneous transverse velocity;

WSS = water surface slope;

w' = fluctuation component of the instantaneous vertical velocity;

X_w = total wake length;

x = streamwise direction;

y = transverse direction;

z = vertical direction and distance above streambed;

β = pressure-gradient parameter;

Δt = time lag;

Π = Coles' Parameter; and

σ = particle diameter geometric standard deviation.

INTRODUCTION

Turbulence in gravel bed rivers plays a critical role in most stream processes including contaminant and nutrient transport, aquatic habitat selection, and natural channel design. While most hydraulic designs and fluid models are based on bulk velocity, migrating juvenile salmon experience and react to the temporally varied turbulent fluctuations. Without properly understanding and accounting for the continuous turbulent motions proper fishway design and guidance are impossible. Matching temporally varied flow to fish reactions is the key to guiding juvenile salmonids to safe passageways. While the ideal solution to fish guidance design would be to use specific fluid action-fish reaction mechanisms, such concrete cause and effect relations have not been established. One way to approach the problem of guidance is to hypothesize that in an environment lacking obvious bulk flow cues (like the reservoir environment), turbulent flow conditions similar to those experienced by juvenile salmonids in natural migration corridors will be attractive to juvenile salmonids. Proof of this hypothesis requires three steps: (1) gathering data on turbulence characteristics in natural migration corridors, (2) reproduction of the turbulence parameters in a controlled environment, and (3) testing the reproduced turbulence on actively migrating juvenile salmonids for increased passage efficiencies. The results from the third step have not been finalized, therefore this report will focus on understanding turbulent processes in gravel bed rivers and reproduction of turbulence in controlled environments for use in fish passage technologies. The purposes of this report are to (1) present data collected in natural gravel bed rivers, (2) present a simple method for reproduction of appropriate turbulence levels in a controlled environment, (3) compare these results to those from one prototype surface collector (PSC), and (4) discuss the implications on fish passage design.

BACKGROUND

Most investigations of turbulent flow over gravel beds have occurred in the laboratory (Papanicolaou *et al.*, 2001) or in controlled environments such as irrigation channels (Nikora and Goring, 1998). This report attempts to relate such studies to two natural gravel bed rivers with gradually varied flow (temporal and spatial) while also considering the effect of natural boulders on turbulent flow patterns with the overall goal of identifying and reproducing typical migration corridor habitat. The field investigation was designed to test turbulence relationships proposed by previous studies as well as the effects of spatial diversity in gravel bed rivers. Most studies have avoided regions of spatial diversity and have focused on uniform channels while treating the flow as steady. This methodology, while useful in establishing fundamental trends, should necessarily be expanded to match the spatial variability of turbulence in natural migration corridors. The most prevalent cause of spatial variability in gravel bed rivers is the ubiquitous occurrence of natural obstructions such as boulders, woody debris, and clusters (Papanicolaou *et al.* 2003). These natural obstructions often shape turbulence and bulk flow characteristics more than the gravel bed itself and provide important aquatic habitat (Nowell and Jumars, 1984).

Turbulence data collected in unobstructed gravel bed flow will be compared to studies of gravel bed turbulence in uniform and gradually varied flow. Very little published research has been conducted to quantitatively described turbulence patterns behind natural river objects in gravel bed rivers. In order to understand the processes that create the turbulence patterns behind boulders a brief review of the literature on turbulence behind geometric objects and velocity patterns behind natural obstructions has been included in the body of the text while a more complete investigation of flow around bluff objects and sampling techniques is included as Appendix A. Additionally, a summary of literature on induced turbulence is presented.

Turbulence in Gravel Bed Rivers

The mean streamwise velocity distribution in an unobstructed gravel bed channel is expected to follow the log-wake law for hydraulically rough gradually varied flows (Nezu and Nakagawa, 1993):

$$\frac{u}{U_*} = \frac{1}{\kappa} \ln\left(\frac{z}{k_s}\right) + 8.5 + \frac{2\Pi}{\kappa} \sin^2\left(\frac{\pi z}{2h}\right) \dots\dots\dots (1)$$

where u is the time averaged streamwise velocity at distance z from the bed, U_* is the shear velocity, κ is Von Karman's Constant (taken as 0.41 in this report), k_s is the apparent roughness height, Π is Coles' parameter, and h is the depth of the water column. Song and Chiew (2001) investigated turbulence in nonuniform open channel flow and showed that Π is a function of the pressure-gradient parameter β , the aspect ratio, and bed roughness. The relationship between Π and β indicates that negative values of Π are attributable to accelerating flow and positive values of Π are attributable to decelerating flow (Song and Chiew, 2001).

The intensity of turbulent fluctuations are often quantified using turbulent intensities ($TI_x = (\overline{u'^2})^{1/2}$, $TI_y = (\overline{v'^2})^{1/2}$, and $TI_z = (\overline{w'^2})^{1/2}$) and the turbulent kinetic energy ($TKE = 0.5 \left[(\overline{u'^2})^{1/2} + (\overline{v'^2})^{1/2} + (\overline{w'^2})^{1/2} \right]$), where u' , v' , and w' are the velocity fluctuation components in the streamwise (x), transverse (y), and vertical (z) directions, respectively and an overbar denotes the temporal mean. Turbulent intensities and TKE decay exponentially from the bed (Nezu and Nakagawa, 1993). Nezu and Nakagawa (1993) and Nikora and Goring (1998, 2000) derived separate but similar expressions for the vertical TKE distribution:

$$\frac{TKE}{U_*^2} = 4.78 * \exp\left(-2 \frac{z}{h}\right) \text{ (Nezu and Nakagawa, 1993)} \dots\dots\dots(2)$$

$$\frac{TKE}{U_*^2} = 1.84 - 1.02 \ln\left(-\frac{z}{h}\right) \text{ (Nikora and Goring, 1998, 2000)} \dots\dots\dots(3)$$

These relationships were developed from the k-ε turbulence model assuming that turbulent generation is balanced by turbulent dissipation. Additionally, it is shown that $TI_x > TI_y > TI_z$ should hold for the entire profile and that the following ratios should remain constant throughout the vertical profile in uniform flow:

$$\frac{TI_y}{TI_x} = 0.71 \text{ (Nezu and Nakagawa, 1993) to } 0.75 \text{ (Song and Chiew, 2001)} \dots\dots\dots(4)$$

$$\frac{TI_z}{TI_x} = 0.5 \text{ (Song and Chiew, 2001) to } 0.55 \text{ (Nezu and Nakagawa, 1993)} \dots\dots\dots(5)$$

Rennie *et al.* (1999) indicate that TKE for different stream morphologies was largest in ripple areas ($500\text{cm}^2/\text{s}^2$) and smallest in areas designated as pools ($<100\text{cm}^2/\text{s}^2$) which is supported by the large hydraulic roughness in ripples and less hydraulic roughness in pools.

Eddy length scales can be calculated by integrating the autocorrelation function (Schlichting, 1979):

$$L = U_{\text{mag}} \int_0^t R(t) dt \dots\dots\dots(6)$$

where $R(t)$ is the autocorrelation function, L is the eddy length scale, U_{mag} is the velocity vector magnitude, and t is time. The autocorrelation function is defined as:

$$R(t) = \frac{\overline{s'_t s'_{t+\Delta t}}}{(\overline{s'_t})^2} \dots\dots\dots(7)$$

where s'_t is the instantaneous fluctuation component of the velocity magnitude and $s'_{t+\Delta t}$ is the instantaneous fluctuation component of the velocity magnitude for the time lag Δt . The eddy length scale is a measure of the amount of mass that moves as a unit thus giving an idea of the average size of the macroscale eddies (Schlichting, 1979). Rennie *et al.* (1999) found that eddy length scales were smallest in ripples (14cm) and largest in pools (30cm). The length scales in the ripple regions scaled well with depth as proposed by Nezu and Nakagawa (1993) while the length scales in the pool were larger but did not encompass the entire pool depth.

Turbulent Flow behind Geometric Objects

The mechanisms that drive fluid movement in the wake region of a circular cylinder are a function of the Reynolds Number and the Strouhal Number (Schlichting, 1979). The Strouhal Number describes the vortex shedding frequency for a given velocity and particle diameter and is defined by:

$$St = \frac{fD}{U} \dots\dots\dots(8)$$

where D is the cylinder diameter, f is the shedding frequency, and U is the approach velocity.

For the Reynolds Numbers occurring in most gravel bed rivers, the Strouhal Number remains relatively constant at a value of 0.21. The turbulent flow behind a square cylinder is more complex due to the four corners of the object. At most Reynolds numbers there may be as many as four vortices being shed at one time (Nakamura, 1993). Turbulent kinetic energies are shown to be maximum at the zone of separation, which is coincidental with the mean eddy path (Djilali and Gartshore, 1991). General observations of velocity and turbulence parameters

around natural boulders by various researchers are summarized in Figure 1. For this report the wake edge is defined as the center of the two vortex streets trailing from a boulder.

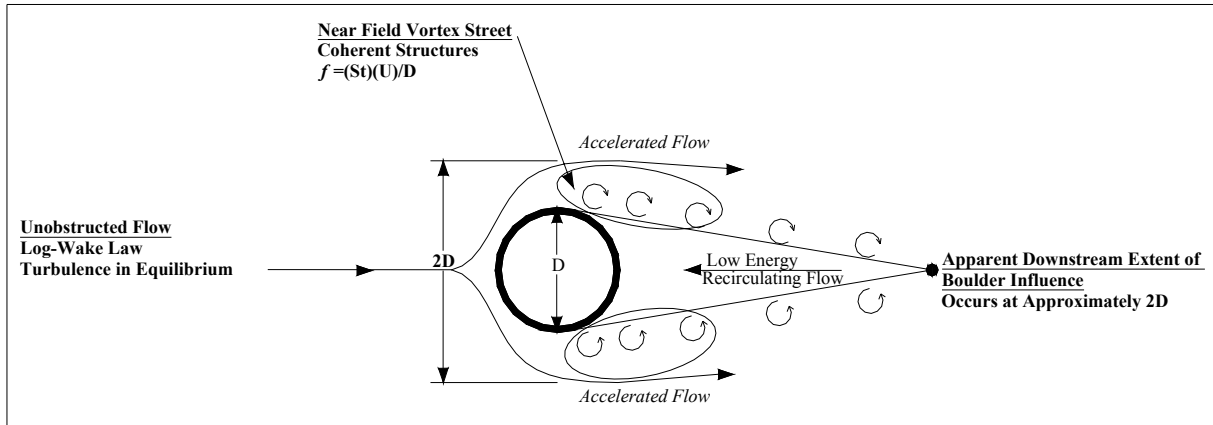


Figure 1. Plan View Schematic of General Trends Observed in the Wake of a Natural Boulder (Shamloo, 2001; Cullen, 1989; Okamoto and Sunabashiri, 1992; Nowell and Jumars, 1984)

Appendix A contains a more complete discussion of turbulence behind bluff objects and measurement techniques.

Turbulent Plumes

Turbulent plumes issuing from jets and mixers are well understood and have been summarized in many books (Schlichting, 1979 and White, 1991). Turbulent plumes scale with the source diameter and become fully developed as they issue downstream. A plan view schematic of typical jet parameters as described by White (1991) and sample locations are presented in Figure 2. As fluid issues from a jet it is uniform across the diameter of the jet and a potential uniform flow core exists for a length ten times the diameter of the jet. At twenty times

the diameter of the jet self-similar velocities form and then at fifty times the diameter of the jet self similar streamwise fluctuation components (u') form. At seventy times the jet diameter the fluctuation components in all directions are self similar. At one-hundred fifty jet diameters the flow becomes isotropic.

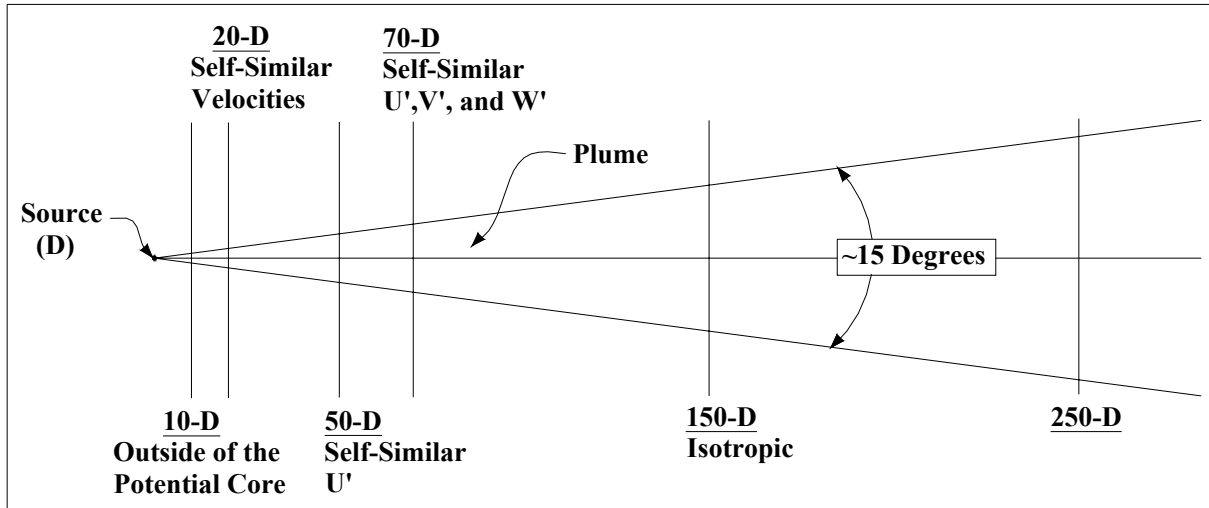


Figure 2. Plan View of a Directed Jet Issuing Into Ambient Flow (White, 1991). The cross sections represent the streamwise station where important turbulence quantities are attained based upon the jet diameter (D). The cross sections also represent the six transverse cross sections where data were collected.

METHODS

Site Selection

Turbulence was characterized at two reaches on the South Fork of the Clearwater River and one reach on the Lochsa River within the Clearwater River Basin of Idaho (Figure 3). Relatively straight reaches were selected to reduce the potential for secondary currents. Acoustic Doppler Velocimeter (ADV) measurements on the South Fork of the Clearwater River were taken in (1) an unobstructed reach and (2) behind two protruding boulders, designated Boulders A and B. Measurements near Boulder A were collected on three different occasions in 2001 (7/27, 8/1, and 8/7). Measurements near Boulder B were collected on 8/16/01. Stream discharge varied less than three percent during each sampling event (Table 1 and Appendix B) but decreased from approximately 12.7 m³/s in late July to 5.4 m³/s in mid August (USGS, 2002). The median grain size of the channel bed was 50 mm as determined by the Wolman method (Wolman, 1954). Grain size distributions based on the Wolman Method are presented in Appendix B. Boulder A was “stingray” shaped while Boulder B was approximately cylindrical in shape (Figure 3). One reach was investigated on 8/22/01 in the Lochsa River near a protruding boulder designated Boulder C that was cubical in shape (Table 1). Stream discharge varied less than one percent with a mean discharge of 11.3 m³/s (Appendix B). The median grain size of the channel bed was 62 mm (Appendix B). Reach and boulder data for each of the five days sampled are presented in Table 1 and Appendix B.

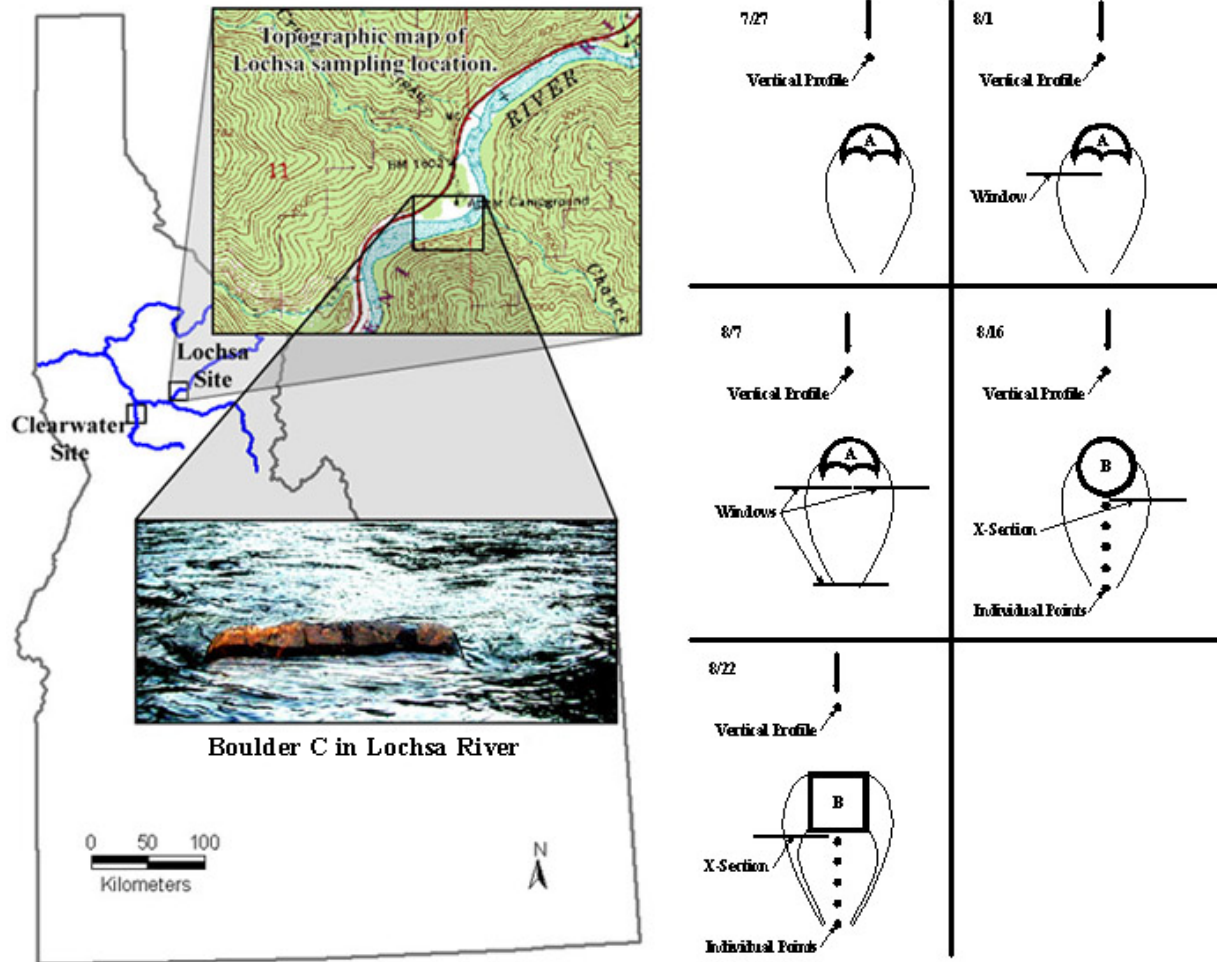


Figure 3. Clearwater River Sampling Sites. Detailed topographic map, and photograph of Boulder C in the Lochsa River along with elevation views of ADV sample locations showing approximate paths followed by shed vortices.

Parameter	Unit	Sample Date				
		7/27	8/1	8/7	8/16	8/22
River	1	S.F. Clearwater	S.F. Clearwater	S.F. Clearwater	S.F. Clearwater	Lochsa
Boulder	1	A	A	A	B	C
Obstr. Shape	1	Sting Ray	Sting Ray	Sting Ray	Cylindrical	Cubical
Q	m ³ /s	9.2	12.7	7.5	5.4	11.3
ΔQ	m ³ /s	-0.09	0.35	-0.24	-0.06	-0.04
U_{avg}	cm/s	42.8	55.6	42.7	72.3	59.0
h	cm	26	32	24	42	44
Width	m	46.7	46.7	46.7	32.4	50.8
WSS	%	0.28	0.34	0.28	0.44	0.37
D	cm	97.6	97.6	97.6	96.5	101.8
d_{50}	mm	48	48	48	55	62
σ	1	2.2	2.2	2.2	2.2	3.1
Re	1	1.1E+05	1.8E+05	1.0E+05	3.0E+05	2.6E+05
Fr	1	0.27	0.31	0.28	0.36	0.28
U^*	cm/s	3.29	5.04	4.65	5.99	5.24
Π	1	0.25	0.17	0.41	-0.32	0.13
k_s	cm	1.9	5.8	10.4	3.0	0.5
Observed f	Hz	2	2	2	2.2	2

Table 1. Site and Boulder Parameters for Each Sample Date. Q is the volumetric discharge, ΔQ is the change in volumetric discharge that occurred during the daily sampling period, U_{avg} is the depth averaged streamwise velocity, h is the flow depth, Width is the average stream width, WSS is the water surface slope, D is the boulder diameter transverse to mean flow direction, d_{50} is the median bed particle diameter, σ is the particle diameter geometric standard deviation, Re is the stream Reynolds Number, Fr is the stream Froude Number, U^* is the shear velocity, Π is Coles' Parameter, k_s is the apparent roughness height, and Observed f is the observed frequency of vortex shedding from the boulder. Determination of the d_{50} , U^* , Π , and k_s is presented in Appendix B.

Experimental Setup

Field Data Collection

Information on the ADV sampling platform and pictures of each reach are presented in Appendix B. Figure 4 presents a typical sample setup for data collection in gravel bed rivers. A detailed survey of each stream reach was conducted using a Leica total station. Each stand leg, the top of the ADV probe, and major reference points including the Boulder, channel bottom, and water surface elevations were located, results are presented in Appendix B.



Figure 4. Typical Sample Setup for Data Collection in Gravel Bed Rivers.

Quantitative measurement of turbulent flow behind Obstruction A on the South Fork of the Clearwater River using an ADV and stand.

Laboratory Data Collection

A reservoir style flow through flume (8.8m x 5.2m x 1.4m) was constructed to mimic bulk flow properties in a typical reservoir (Appendix B). Because we were interested in flow conditions in the upper ten feet of reservoirs (typically upper 90% of the water column) bed roughness was not important therefore to reduce wall effects painted steel walls and beds were

used. Flow was pumped into the flume at $0.13 \text{ m}^3/\text{s}$ to produce a mean streamwise velocity of 2 cm/s . A moveable sampling platform over the flume was used to position the ADV for data collection. Jets were mounted to a slender rod one meter downstream from the honeycomb inlet of the head tank in the center of the planview area and piped such that the plumes were horizontal and oriented downstream. The mixers were tested with the same location and orientation and driven by a variable speed electric motor. Figure 5 presents a picture of the flume and experimental setup.

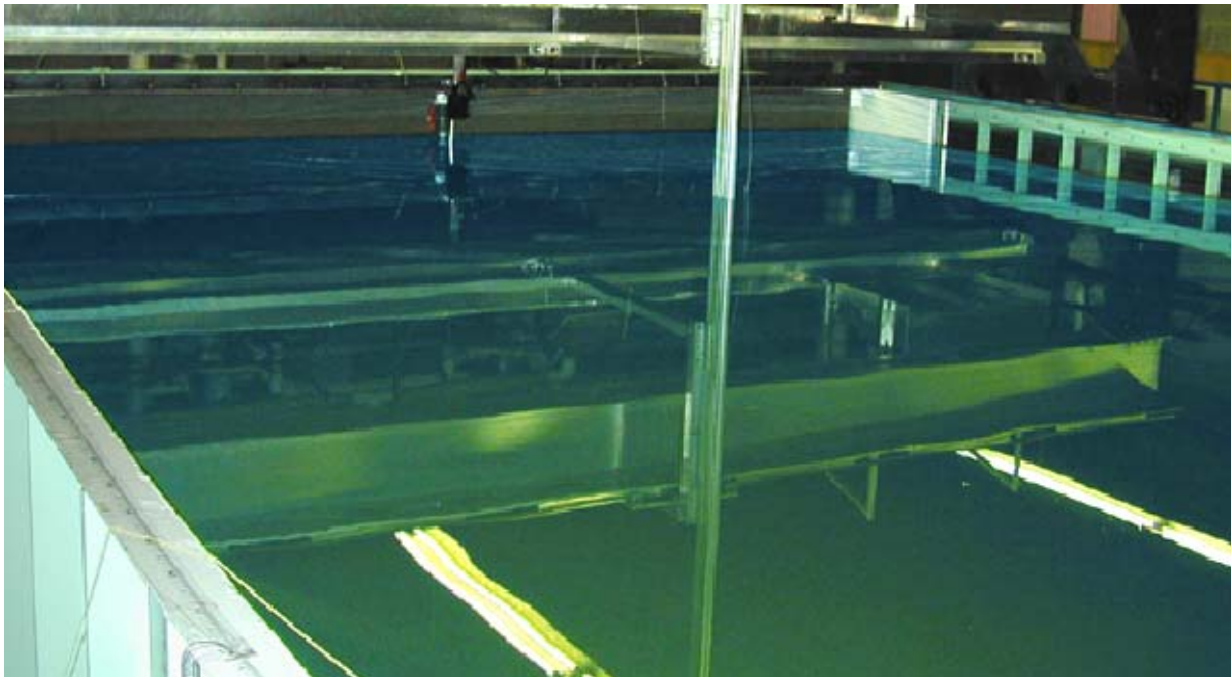


Figure 5. Reservoir Style Flume. ADV Sampling of Turbulent Jet.

Sampling Protocol

Field Data Collection

Velocity measurements were collected with a SonTek Field ADV fitted with a waterproof canister and cables to make it suitable for field applications. Measurements were collected for 2

minutes at a 25 Hz frequency for each sample location. Statistical parameters such as TKE and Reynolds shear stress tensors did not change significantly beyond a one minute sampling period, therefore the 2 minute sample periods were deemed acceptable. The orientation of the mean stream velocity at each unobstructed profile location was used for downstream orientation of data collected behind the boulder sampled that day. Five vertical velocity profiles were collected to characterize turbulence in unobstructed flow reaches.

Transverse profiles were collected downstream from Boulder A perpendicular to the obstructed flow direction. Four vertical windows of between two and four transverse cross sections of data were created with a 10cm grid spacing in both the transverse and vertical directions. Each window was centered over the mean eddy path. See Figure 3 for event sample locations and Table 2 for window and cross section locations with respect to vortex shedding paths.

Boulder		A	A	A	A	B	C
Date		8/1	8/7	8/7	8/7	8/16	8/22
Setup	Unit	Right	Right	Left	Downstream	Left	Right
Streamwise	cm	83	106	87	311	23	83
Transverse	cm	11-89	58-42	76-24	-125-85*	35-65	37-63
Vertical	cm	10, 20, 30, 33	4, 14, 21	10, 20	6, 16	33	28

Table 2. Location of Windows and Cross Sections with Respect to Apparent

Vortex Shedding Location. Streamwise – Streamwise distance downstream from apparent vortex shedding location; Transverse – Transverse distance inside of the wake edge to distance outside of the wake edge e.g. 11cm inside of the wake edge to 89cm outside of the wake edge; * – Transverse distances for the downstream window represent distance from wake center line where negative numbers are

oriented toward the left bank; Vertical – Vertical distance from the bed for each cross section.

A series of fine scaled cross sections perpendicular to the flow were collected behind Boulder B and Boulder C to increase data resolution in important flow areas (Figure 3 and Table 2). Samples were collected in a single plane at sixty percent of the total water depth from the bed due to its relevance as the location at which mean velocities are expected. Sixty percent of the water depth is within the buffer region of each vertical profile. Sample volumes were spaced such that the distance between samples was smallest near the mean eddy path (1cm) and largest away from the mean eddy path (10cm). Samples were also collected at sixty percent of the flow depth downstream from the boulder along the wake centerlines of Boulders B and C to the apparent downstream extent of the Boulder influence.

Laboratory Data Collection

Turbulence data downstream from four jets and four mixers were recorded. Laboratory data from turbulent jets and mixers were collected with the same Field ADV used in the gravel bed river investigations. Cross sections transverse to the jet or mixer orientations were collected at six streamwise stations along the plume centerline at the cross sections shown in Figure 2. Eleven data points were collected in each transverse cross section such that the entire plume width was captured. One vertical cross section was collected on each plume to ensure that radial symmetry existed.

Data Manipulation

ADV data were processed and filtered using standard techniques to create an initial data set that was then rotated and manipulated to calculate point and grouped turbulence

characteristics (Wahl, 2000). The very clear water of the Lochsa River yielded a SNR of 12.85 (standard deviation 2.25). Even though the SNR for the Lochsa was relatively low, the measurements appeared to be consistent, showed high correlation, and were judged to be acceptable (SonTek personal communication, 2002) based on a filtering scheme of $SNR > 10$ and $correlation > 70$ (Appendix B). Data for autocorrelation calculations were not filtered due to the nature of the calculations (Appendix B). TKE, Reynolds shear stress tensors, and eddy length scales were calculated at each point. Strain was calculated using a centered difference method and is defined as the change in streamwise velocity over relevant distance (dU/dz for unobstructed flow and dU/dy for obstructed flow). Eddy lengths were calculated by multiplying the integration of the autocorrelation function by the approach velocity magnitude. The data manipulation process is demonstrated on point 8-16-8-14 in Appendix B. The raw data can be obtained from Dr. Rollin Hotchkiss at Albrook Hydraulic Laboratory in CD format upon request; contact information for Dr. Hotchkiss and Albrook Hydraulic Laboratory are provided in Appendix D.

RESULTS

Unobstructed Turbulent Flow in Gravel Bed Rivers

Velocity profiles for unobstructed flow in gravel bed rivers are presented in Figure 6. Data were made dimensionless with the shear velocity, U_* . Due to the complex geometry and spatial variability within each reach global shear velocity calculations did not properly predict the shear velocity at each vertical profile. The local shear velocity was calculated using (Nezu and Nakagawa, 1993) (Appendix B):

$$U_* = \frac{\sqrt{-\overline{u'w'}}}{\sqrt{1 - \left(\frac{z}{h}\right)}} \dots\dots\dots (9)$$

This method requires curve fitting the $\overline{u'w'}$ vertical profile and extrapolating to the bed. Each Reynolds Shear Stress tensor profile followed a linear trend and the $\overline{u'w'}$ component at the bed was determined using linear extrapolation to the bed. Use of the standard U_* equation ($U_* = \sqrt{gRS}$) resulted in improperly high values of U_* due to the nonuniform nature of the flow. Using the calculated values of U_* and a Von Karman constant of 0.41, Π and k_s were calculated based on curve fitting techniques (Appendix B). Shear velocities, Coles' parameters, and apparent roughness heights for each profile are presented in Table 1. Streamwise velocity profiles collapse reasonably well (Figure 6). Variations between individual U/U_* profiles in Figure 6 are due to the fact that the plots have been made dimensionless by the total distance from the bed when the log-wake law is a function of both the distance from the bed and the relative roughness of the bed. Dimensionless transverse and vertical velocity profiles show no appreciable secondary currents. The absolute value of strain ($|dU/dz|$) for these profiles varied from a maximum of 4.3 s^{-1} near the bed on August 1st to zero near the surface (Appendix B).

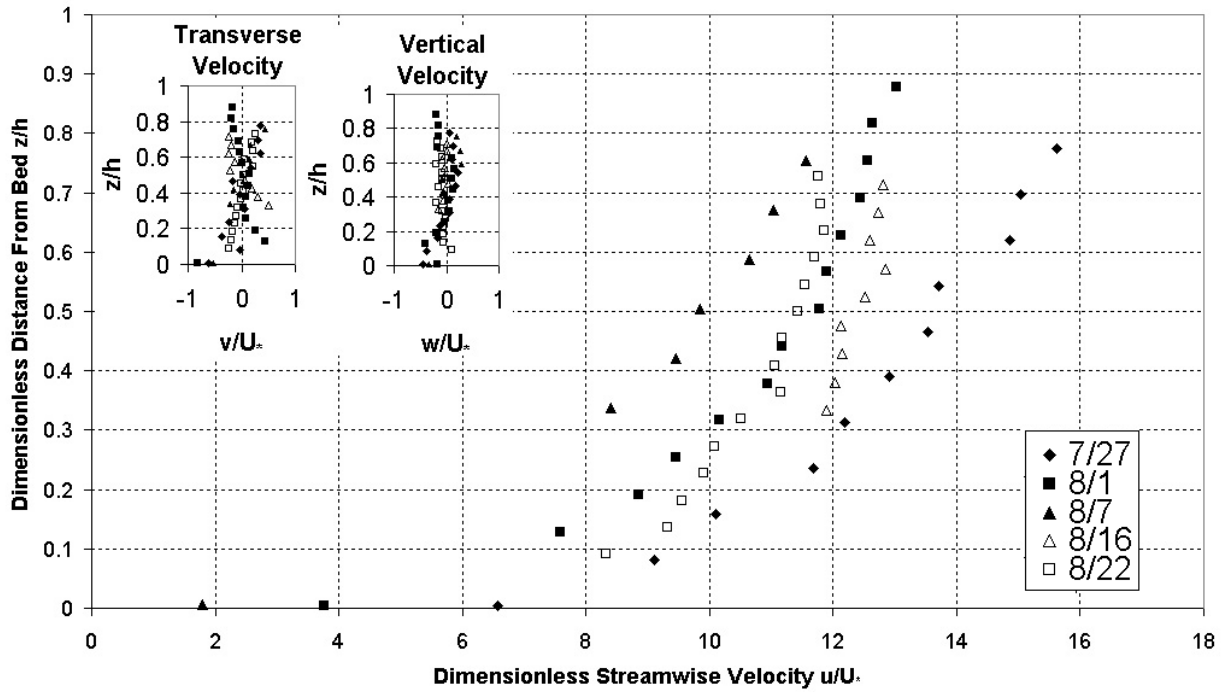


Figure 6. Dimensionless Velocity Profiles for Unobstructed Flow

The dimensionless turbulent kinetic energy profiles ($TKE^{1/2}/U_*$) are presented as Figure 7 along with semi-empirical Equations 2 and 3 (Nezu and Nakagawa, 1993 and Nikora and Goring, 1998). The turbulent intensity ratios were found to be: $TI_y/TI_x=0.77$ and $TI_z/TI_x=0.51$ which are similar to Equations 4 and 5 (Nezu and Nakagawa, 1993, and Song and Chiew, 2001).

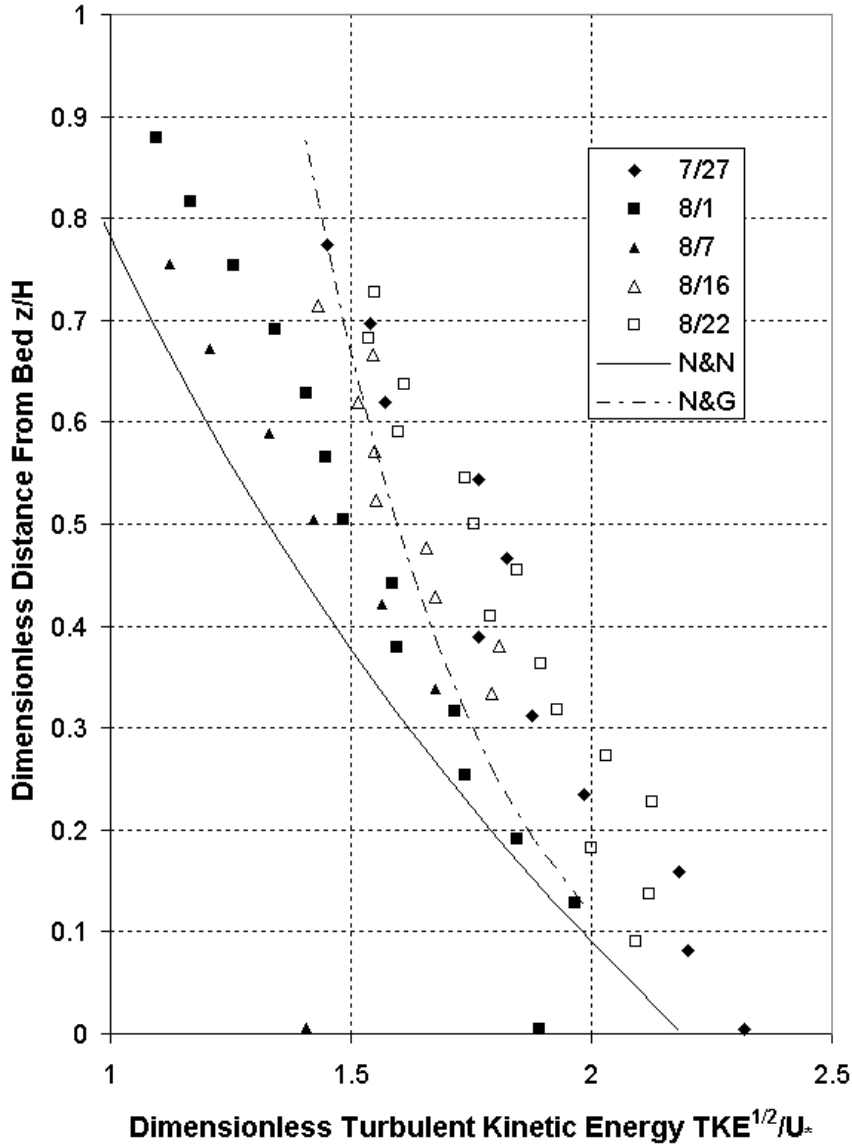


Figure 7. Dimensionless Turbulent Kinetic Energy Profiles for Unobstructed Flow ($TKE^{1/2}/U_*$). N&N = Nezu and Nakagawa (1993); N&G = Nikora and Goring (1998).

The Reynolds shear stress tensor $\overline{u'w'}$ reached a maximum negative value near the bed of $-27.5\text{cm}^2/\text{s}^2$ upstream of Boulder C and decreased toward zero at the surface (Appendix B). The bed shear stresses are significantly less than the required bed shear stress for incipient motion of

the mean particle size based on the Shield's Diagram (Chang, 1992). Incipient motion calculations are shown in Appendix B. No distinguishable trends were present in the other off diagonal Reynolds shear stress tensor components (Appendix B).

Turbulent Flow Downstream from a Boulder

Turbulent flow downstream from Boulders A through C was investigated using both visual and Doppler shifting techniques. All boulders blocked the entire flow profile preventing overtopping and produced coherent structures with vertical axes of rotation. The vortices were observed to be approximately 10cm in diameter and were shed from each side of the boulder at approximately 1Hz (shedding frequency, f , of 2Hz). The structures traveled downstream following narrow bands of motion consistent with vortex streets.

One window of data directly downstream from Boulder A and one cross section from Boulders B and C are presented in Figures 8-13. The Figures present data centered on the wake edge of each boulder such that negative values are within the wake and positive values are outside of the wake. Figure 8 depicts the mean streamwise velocity. For reference, streamwise velocities are a maximum just outside of the wakes while secondary currents are apparent within the wakes (negative transverse distance values). Figure 9 presents the TKE, and Figures 11 and 12 present two of the off-diagonal Reynolds shear stress tensors $\overline{u'v'}$ and $\overline{u'w'}$, respectively. The difference in sign for the $\overline{u'v'}$ values presented in the Figure 11 cross sections are related to opposite circulation associated with shedding from opposite boulder edges (left edge of Boulder B and right edge of Boulder C). Figure 10 depicts the absolute value of strain as $|dU/dy|$ since velocity change is primarily in the transverse direction. Figure 13 presents the eddy lengths scaled by the approach velocity magnitude. Contours in Figure 13 have been made sparse due to

the large variability in data outside the vortex street. Transverse and vertical velocity windows and turbulent intensities in each direction are presented in Appendix C.

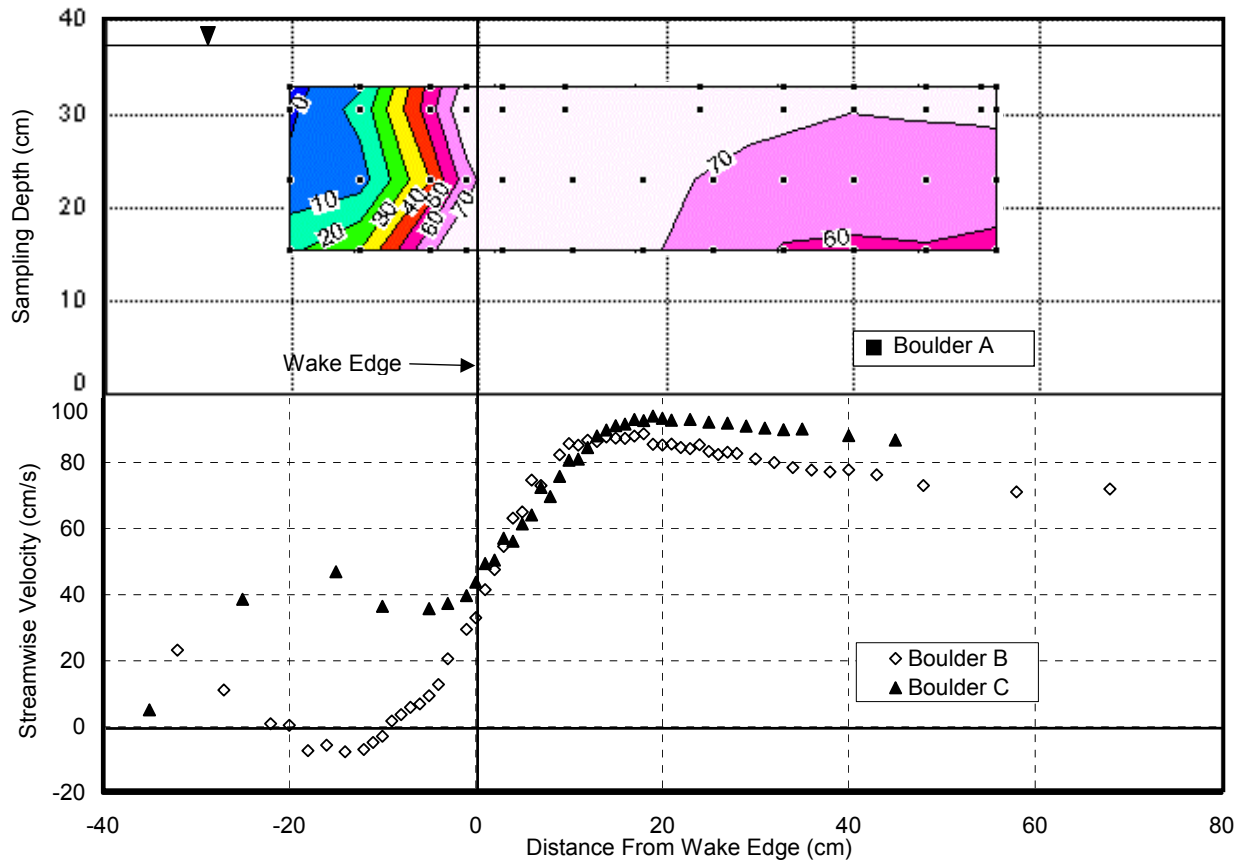


Figure 8. Mean Streamwise Velocity Directly Downstream From the Boulders: window (Boulder A) and cross sections (Boulders B and C). Mean streamwise velocity values are in cm/s. Negative distance values on the x-axis indicate locations within the wake.

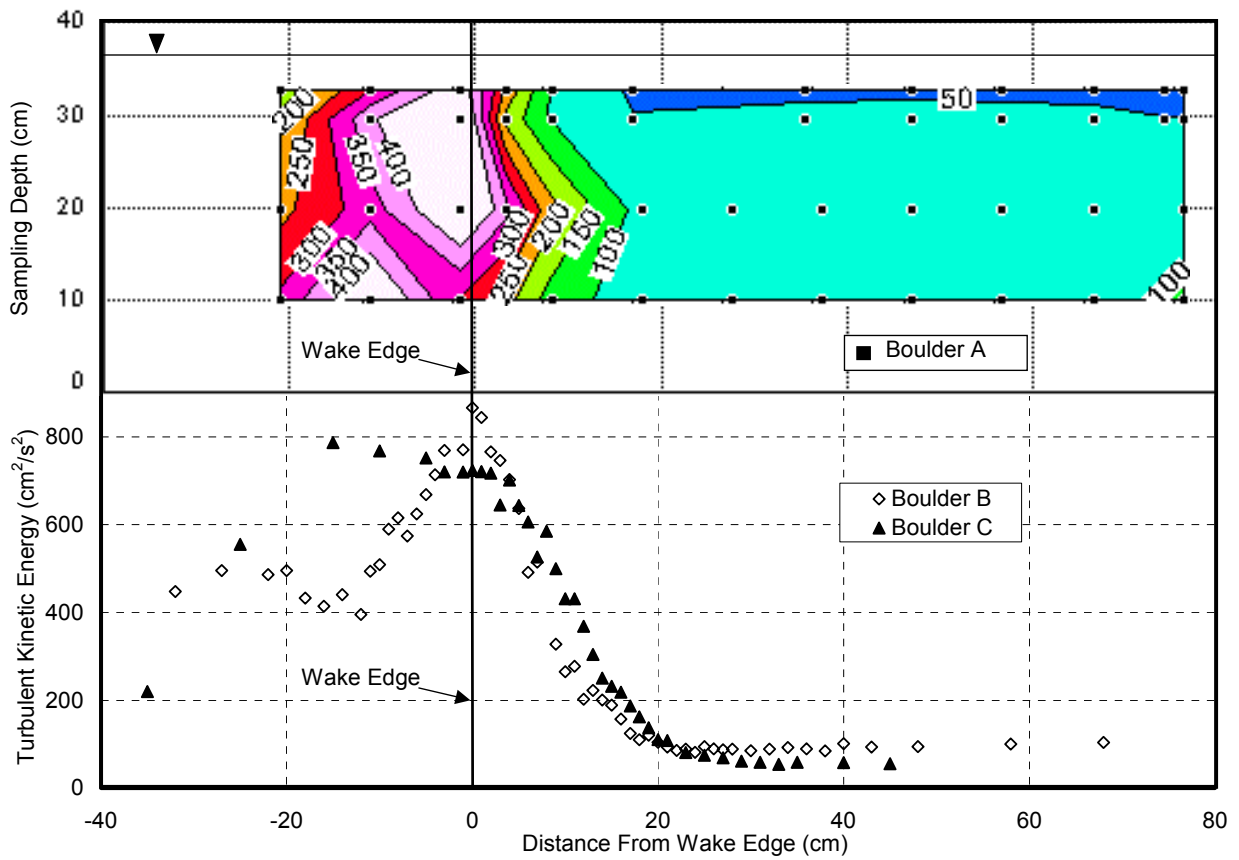


Figure 9. Turbulent Kinetic Energy Directly Downstream From the Boulders: window (Boulder A) and cross sections (Boulders B and C). Turbulent kinetic energy values are in cm^2/s^2 . Negative distance values on the x-axis indicate locations within the wake.

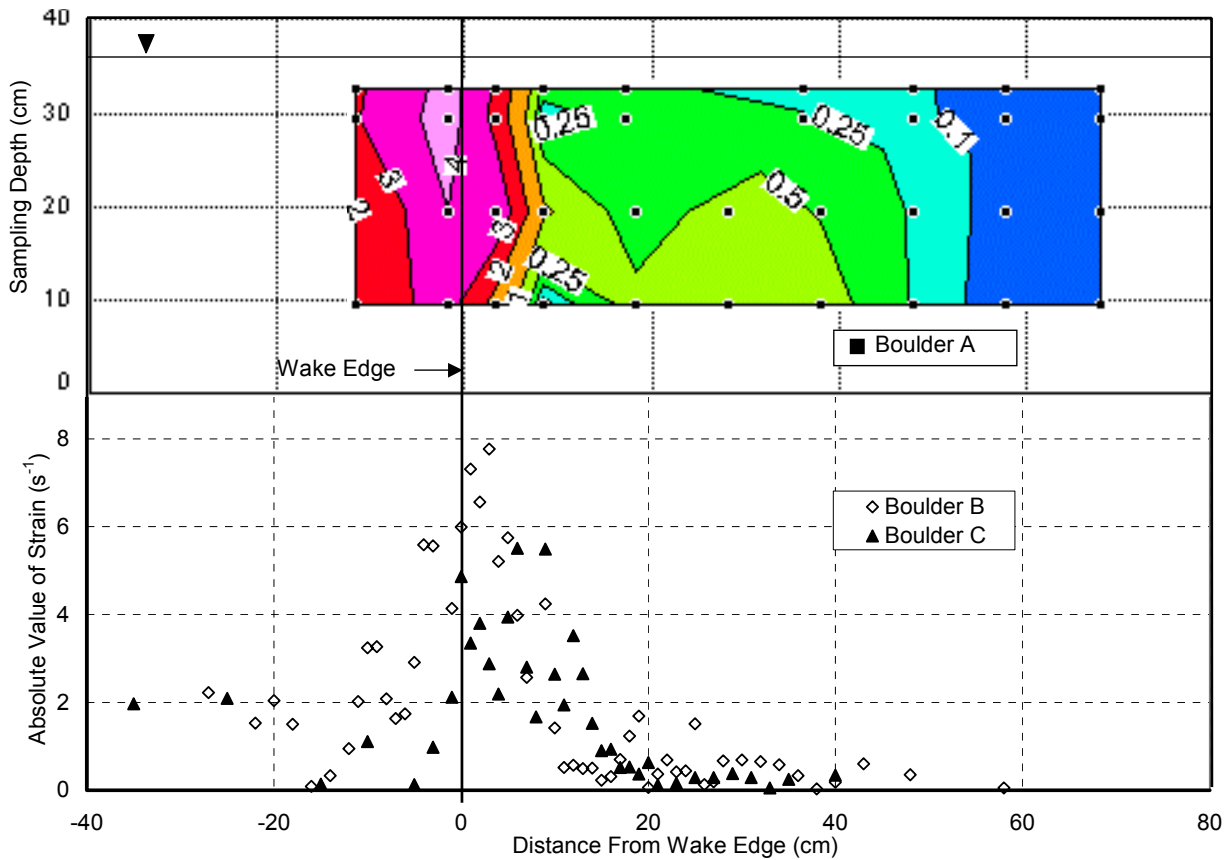


Figure 10. Absolute Value of Strain $|dU/dy|$ Directly Downstream From the Boulders: window (Boulder A) and cross sections (Boulders B and C). Strain values are in s^{-1} . Negative distance values on the x-axis indicate locations within the wake.

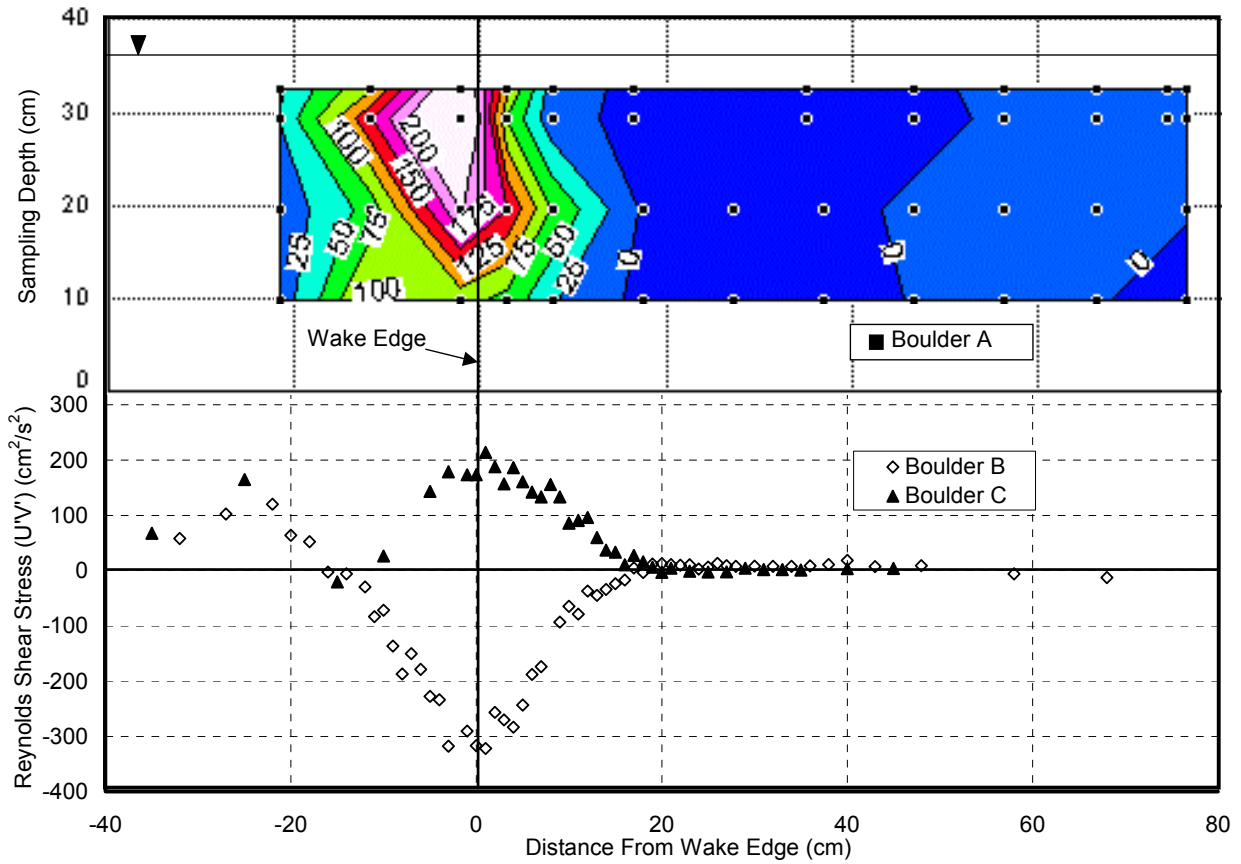


Figure 11. Reynolds Shear Stress Tensor $\overline{u'v'}$ Directly Downstream From the Boulders: window (Boulder A) and cross sections (Boulders B and C). Reynolds shear stress tensor values are in cm^2/s^2 . Negative distance values on the x-axis indicate locations within the wake.

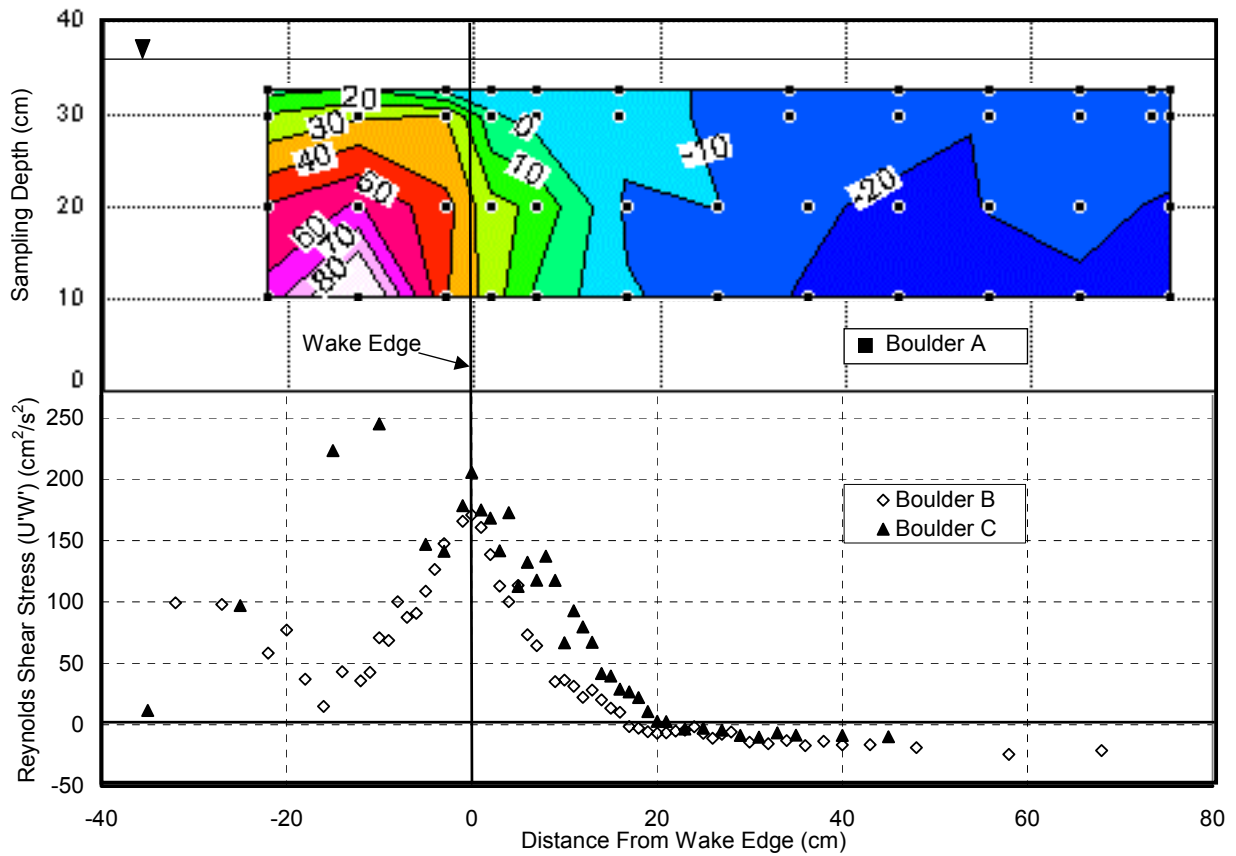


Figure 12. Reynolds Shear Stress Tensor $\overline{u'w'}$ Directly Downstream From the Boulders: window (Boulder A) and cross sections (Boulders B and C). Reynolds shear stress tensor values are in cm^2/s^2 . Negative distance values on the x-axis indicate locations within the wake.

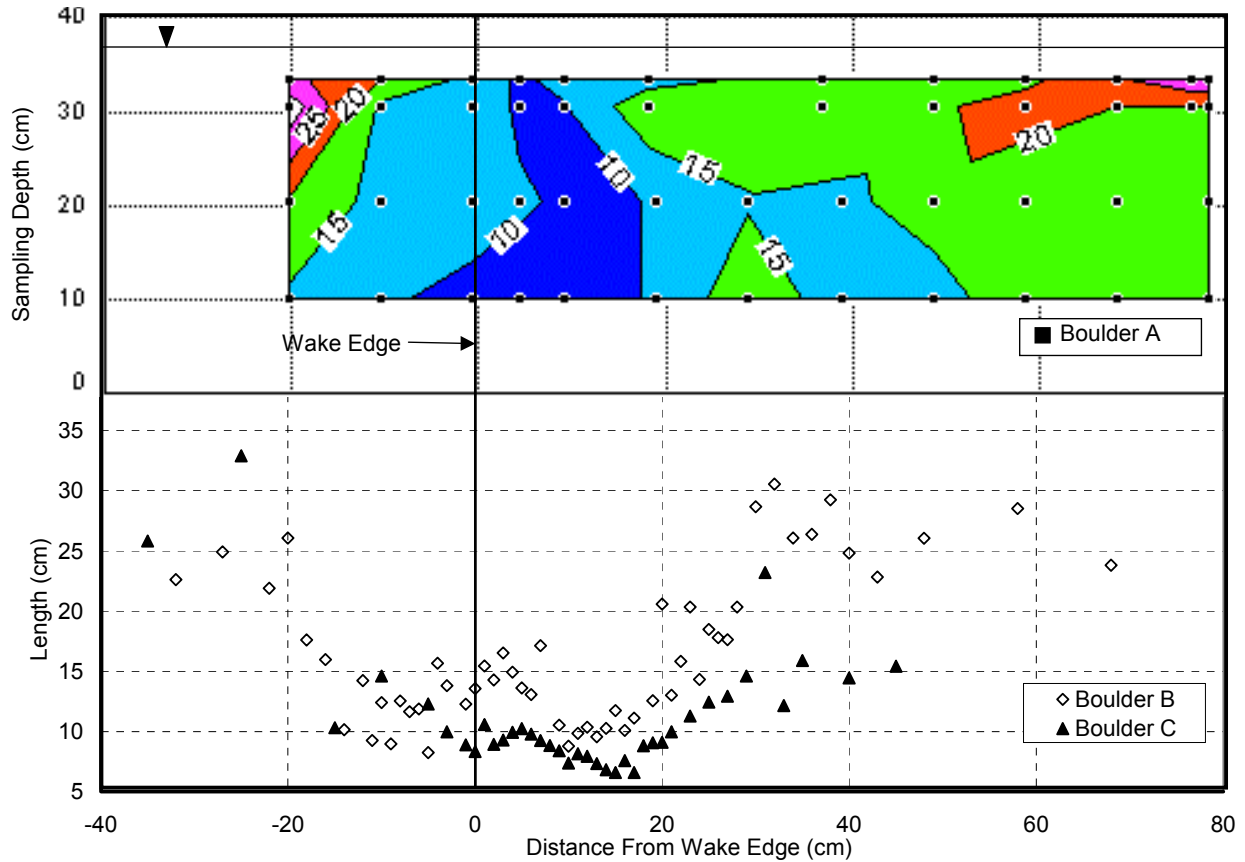


Figure 13. Eddy Length Scale Based on Approach U_{mag} Directly Downstream From the Boulders: window (Boulder A) and cross sections (Boulders B and C). Eddy length scale values are in cm. Negative distance values on the x-axis indicate locations within the wake.

In addition to windows and cross sections collected directly downstream from the Boulders, data were collected farther downstream to investigate the decay of turbulence within the wake region. Figure 14 presents the results of the data window collected three meters downstream from Boulder A at the apparent downstream extent of boulder influence. Data in Figure 14 are centered on the rock centerline and have the same shading scheme and contour intervals as the contour plots in Figures 8-13. Figure 15 presents the streamwise decay of TKE along the centerline of the wakes behind Boulders B and C.

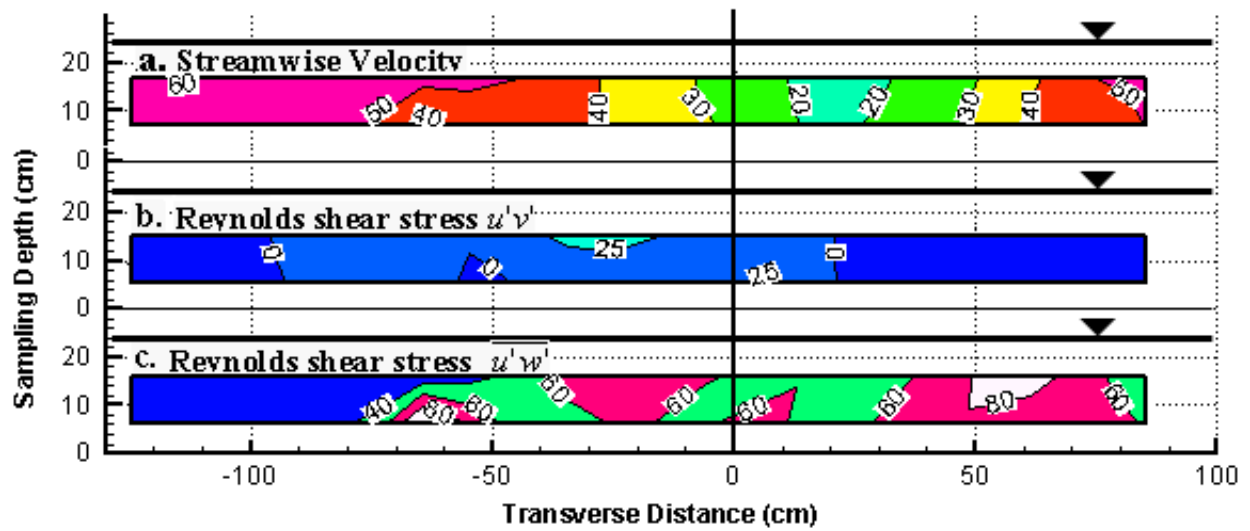


Figure 14. Relevant Flow Parameters at Three Meters Downstream from Boulder

A on 8/7/01. (a) Streamwise velocity (cm/s); (b) Reynolds shear stress tensor

$\overline{u'v'}$ (cm^2/s^2); (c) Reynolds shear stress tensor $\overline{u'w'}$ (cm^2/s^2). Zero on the

transverse axis represents the wake centerline.

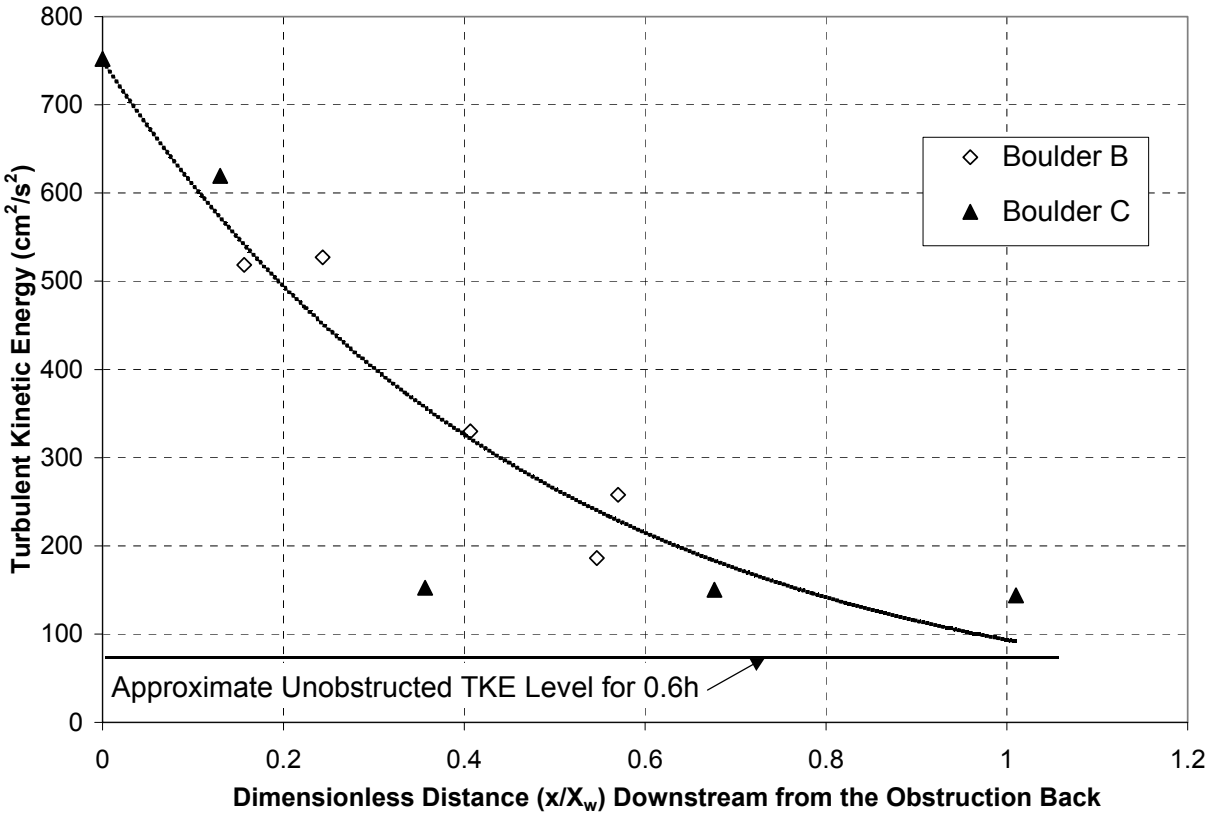


Figure 15. Streamwise Decay of Turbulent Kinetic Energy Along the Wake Centerline Downstream From Boulders B and C. Dimensionless distance is the distance downstream from the rock back (x) divided by the total apparent wake length (X_w).

Turbulence in Natural and Manmade Fishways

Ranges of TKE, absolute value of strain, and eddy length scales for data collected in the Clearwater River Basin, upstream from the Bonneville PSC, the selected jet, and selected mixer are presented in Table 3. Values presented in the Natural Gravel Bed River of Table 3 represent data collected from the upper 50% of the water column collected on the Lochsa and S.F. of the Clearwater Rivers. Raw and summary data for the selected jets and mixers along with the specifications for other tested jets and mixers are presented in Appendix C. Turbulence data

upstream of the Bonneville PSC is from Faber, *et. al.* (2000) and is available from the Army Corps of Engineers, Portland District.

Parameter	Units	Natural Gravel Bed River ¹		Bonneville PSC		Selected Jet		Selected Mixer	
		Min	Max	Min	Max	Min	Max	Min	Max
TKE	(cm ² /s ²)	15	870	34	440	2.6	390	8	340
Strain	(s ⁻¹)	0	7.8	0	2.6	0	5.9	0	0.48
Length Scale	(cm)	6	50	80	>1000	0.1	20	0.4	3

Table 3. Summary Table of Selected Turbulence Parameters in Natural and

Manmade Fishways. ¹ – Represents data collected from the upper 50% of the water column collected on the Lochsa and S.F. of the Clearwater Rivers (Faber, *et al.* 2000).

Jets and mixers were selected based on the ability to reproduce TKE, absolute value of strain, and eddy length scale results gathered during the gravel bed river characterization. A 15 cm diameter mixer with four blades run at 500 rotations per minute (RPM) was able to produce TKE and strain consistent with values recorded in the gravel bed rivers. Larger diameter mixers run at lower RPMs would theoretically increase the length scale while maintaining TKE levels, however, larger diameter mixers produced significant recirculating currents that affected turbulence parameters. A 1.4 cm diameter jet emitting 3 Newtons of momentum was able to produce TKE, strain, and eddy length scales consistent with values recorded in gravel bed rivers.

DISCUSSION

Unobstructed Turbulent Flow in Gravel Bed Rivers

Unobstructed velocity profiles compare well with previously published data on uniform and gradually varied flow in gravel bed channels (Figure 6 and Table 1). Matching velocity and TKE profiles to published data required use of the log-wake law rather than the log law due to the gradually varied nature of flow in the selected reaches (Song and Chiew, 2001). The dimensionless TKE profile was in agreement with both Nezu and Nakagawa's and Nikora and Goring's findings (Figure 7). The general increase in TKE above the findings of Nezu and Nakagawa (1993) for uniform flow may be attributable to the decelerating flow and large roughness elements in which most data were collected (Song and Chiew, 2001). This is in general accord with previously published data on gravel bed channels and indicates that general relationships such as the log-wake law and the turbulence decay models developed in controlled environments may be applicable to steady, unobstructed, gradually varied flow reaches of natural gravel bed rivers.

Obstructed Turbulent Flow in Gravel Bed Rivers

Velocity data collected from the boulder-influenced flow regions are in qualitative agreement with data published by Shamloo *et al.* (2001) (Figure 8). Wake widths depended upon the approach velocity, but ranged from 1D to 1.5D. These widths are slightly smaller than measured widths of 2D by Shamloo for hemispheres (2001). The smaller wake widths may be due to the higher approach turbulence and boulder roughness (Streeter *et al.* 1998). The relative widths of the boulders were too large for significant transverse pressure variations to cause alternating shedding vortices associated with a Von Karman vortex street leaving shedding

frequencies predicted by the Strouhal relationship significantly lower than observed (predicted~1/10Hz versus observed~2Hz).

Turbulence patterns both inside and outside of the Boulder wakes were highly influenced by the presence of the Boulders. The magnitudes of the ratio between maximum turbulence values in obstructed versus unobstructed flow regions found in this study are: TKE~6.8, strain~1.8, $\overline{u'w'}$ ~9.1, and $\overline{u'v'}$ ~14.8. These ratios are not universal but do provide basic relationships that will be useful to fish passage design.

Maximum values of TKE, strain, and Reynolds shear stress tensor $\overline{u'v'}$ directly downstream from the boulders reveal the location of the vortex street and the wake edge (Figures 9-11). Proper identification of wake regions is important for nutrient transport (Webel and Schatzmann, 1984) and many biological classification systems (Mobrاند Biometrics Inc., 1999). While the vortex street and wake edge of a protruding boulder may be easily distinguishable on the water surface, submerged wake regions are not easily distinguishable. Identifying the wake edge based upon coincidental peaks in TKE and strain appears to be more readily reproducible than investigation of mean velocity profiles (Figure 8).

Boulders A, B, and C were of three distinct geometries; however, the boulder shape did not significantly affect most turbulence parameters (Figures 9-13). The TKE within the wake of Boulder C exhibited a dual peak caused by vortex shedding from both the upstream and downstream corners of the boulder. The similarity in turbulence parameters between differently shaped boulders indicates that wake conditions may be approximated for various bluff object shapes if the wake edge and number of protruding edges is known.

The primary off-diagonal tensor of the Reynolds shear stress switches in the vortex street region from the $\overline{u'w'}$ orientation to the $\overline{u'v'}$ orientation confirming the presence of vortical

structures with vertical axes. Videler, *et al.* (1999) showed that swimming fish capture the kinetic energy in vertical axis coherent structures by producing counter-rotating vortices with their bodies. Energy extraction from a vortex by a swimming fish is only possible if the vortex has a vertical axis. In unobstructed flow regions most eddies have axes of rotation that are in the transverse direction which would prohibit energy extraction by most swimming fishes but in the vortex street of a protruding boulder energy extraction would be possible.

Eddy length scales in the vortex street were determined to be on the order of 10-15cm using the autocorrelation function (Figure 13). These values are corroborated by field observations of vortex diameters of approximately 10cm. Length scales on each side of the vortex street were larger than 20cm and tended to be slightly smaller than the flow depth. The eddy length scale is one of the most important turbulence parameters to aquatic biota. If eddy length is much larger than an aquatic organism, the eddy will be perceived as a secondary current and if the eddy size is much smaller, then the energy contained in the eddies will be negligible. However, if eddies are on the scale of the organism then turbulence can become a primary motivator for habitat selection (Cada and Odeh, 2001). For example, a 10 cm vortex diameter might be the appropriate size for energy extraction by an adult salmon but would probably be too large for a juvenile, on the order of 10cm in length, to successfully extract energy.

The fine scaled cross sections directly behind Boulders B and C exhibited similar trends to the windows behind Boulder A and add clarity to the overall trends observed within the coarse windows, depicting significant peaks that were not fully captured with the 10cm sampling grid. The most notable example of increased clarity from the fine scale cross sections is the W-shaped pattern that emerged within the eddy length scales behind Boulders B and C. The most probable explanation for the W-shaped pattern is that the local minima indicate the left and right edges of

a two-minute averaged vortex while the center peak is the full vortex diameter; the edge of a vortex passing through a control volume would exhibit shorter correlations than the full diameter of a vortex.

The TKE and strain at the wake zone edges were not significantly affected by the presence of the bed above 50% of the flow depth (Figures 9 and 10), implying that investigations not concerned with near bed conditions would not need to include vertical profiles of data within the wake region. This conclusion is relevant to juvenile salmonids, which are known to migrate in the upper fifty percent of the water column (ISRP, 1996). Migrating juvenile salmon encountering the wake zone edge would experience flow that is primarily two dimensional in the horizontal plane, implying that variations in flow depth selection within the top fifty percent of the water column by individuals near boulders is not related to hydraulic conditions.

The boulder influence on turbulence parameters decreases rapidly transverse to the flow outside of the vortex street, returning to background levels generally within half a boulder diameter from the wake edge (Figures 8-13). This area marked by background turbulence levels and locally accelerated streamwise velocity could provide favorable migration corridor habitat for juvenile salmonids. This advantage is partially offset by predation from the wake region.

Data were collected at the apparent downstream extent of the Boulder influence. Elevated TKE (50% above background, Figure 15) and $\overline{u'v'}$ (Figure 14b) along with depressed velocity (Figure 14a) and $\overline{u'w'}$ (Figure 14c) indicated the continued boulder influence. The continued presence of the wake beyond the visual extent of boulder influence indicates that visual identification should not be relied upon as the sole indicator of boulder influence for stream or biological classification systems.

Figure 16 presents a modified version of Figure 1 including new findings and corroborated results.

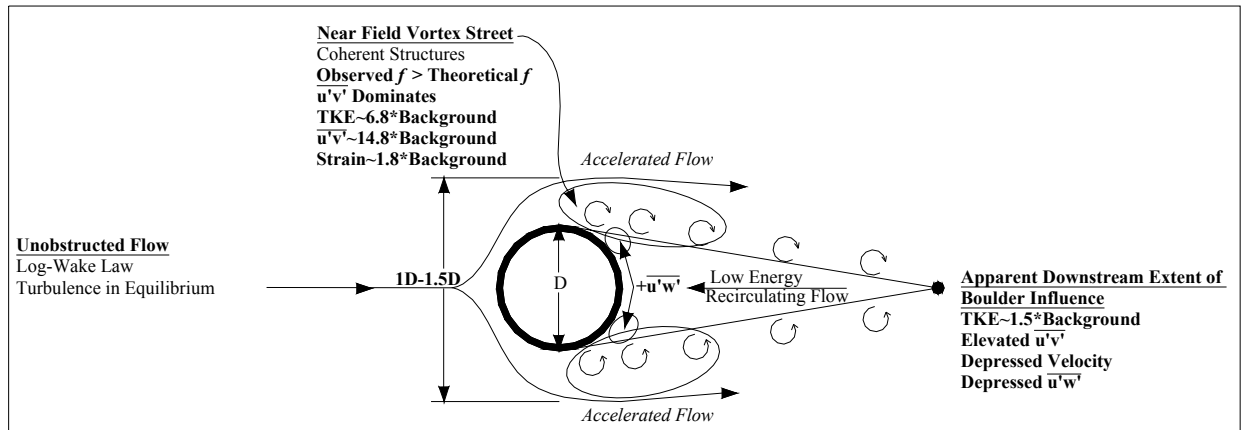


Figure 16. Summary of Gravel Bed River Findings. Bolded text are findings from this study while nonbolded text are corroborated findings.

Turbulence in Natural and Manmade Fishways

Many relevant turbulent parameters in natural corridors have been identified in the study of gravel bed rivers. In order to evaluate the performance of natural and manmade fishways a concise set of selection criteria were needed. Turbulence parameters that were deemed most important to migrating juvenile salmon include the fluctuation of turbulent intensity, strain, and turbulent length scales. TKE is a scalar quantity that is ideally suited for representing the amount of fluctuations an aquatic individual experiences. Since the lateral line only senses the change in velocity, the spatial change in velocity (strain), has been hypothesized to be a primary motivator in fish path selection (Nestler, 2002). As mentioned previously in this discussion, eddy length scales are extremely important in determining how an individual perceives the fluctuations characterized by the TKE.

Natural Fish Corridors

The primary emigration corridor for juvenile salmonids is the upper fifty percent of a gravel bed river water column (ISRP, 1996). Results from the upper fifty percent of the water column in gravel bed rivers of the Clearwater River Basin are presented in Table 3. The TKE and strain in the natural fish corridors studied exhibit large spatial variability while the macroscale turbulence diameters tend to be slightly larger than the average juvenile salmonid length indicating that juveniles are accustomed to a wide range of TKE and strain but the macroscale eddies tend to be fairly specific, on the order of one body length.

The gravel bed study showed a vast spatial diversity in turbulence parameters within the upper fifty percent of the water column. Theoretically, juveniles will not use all portions of this flow equally and will show tendencies for certain turbulent regimes. The wide range of TKE and strain represent the limits of possible turbulence values that may be attractive to juvenile salmonids. More precise determination of turbulence preferences would be possible with coupled fish-tagging and turbulence measurement studies.

Bonneville Prototype Surface Collector

Turbulent fluctuations upstream from the Bonneville PSC are within the range of turbulent fluctuations recorded in natural fish corridors indicating that the statistical fluid fluctuation experienced by juvenile salmonids are similar to those experienced in the natural fish corridors of the Clearwater River Basin.

Strain values are within the lower range of values recorded in natural fish corridors indicating that strain should not act as a deterrent to fish collection, however, strains were calculated by averaging velocities over two foot intervals and significant peaks in strain were most likely smoothed.

The major difference in turbulence structure between the natural corridors of the Clearwater River Basin and the Bonneville PSC is the turbulence scale. While turbulence length scales recorded in the gravel bed rivers were on the same order of magnitude as juvenile salmonids the turbulent length scales upstream from the PSC were between one and two orders of magnitude larger than the juvenile salmonids. Turbulence structures much larger than the individual are perceived as secondary currents that may confuse juvenile salmonids trying to determine the PSC Inlet location. The Bonneville PSC was selected as a typical surface collector. Results have generally been positive in that it does increase passage efficiencies and reduce mortalities, however, the PSC only collects twenty percent of the “run of the river” juveniles leaving a great deal of room for improvement (Ploskey, *et al.* 2000). The current success of the PSC is most likely due to the proper reproduction of turbulent fluctuations upstream from the PSC entrance but it may be possible to increase attraction rates by producing appropriately scaled eddy lengths.

Turbulent Mixer

The selected turbulent mixer produced turbulent fluctuations and strain levels that were within the range found in the natural fish corridors of the Clearwater River Basin. Due to the pulsating nature of flow from a small mixer, the eddy length scales were an order of magnitude smaller than the turbulent length scales recorded in the Clearwater River Basin. Larger diameter mixers run at fewer RPMs would increase the length scales while maintaining TKE values; tests of larger mixers resulted in the development of significant secondary currents within the flume and results could not be validated. The proper sizing of TKE and strain with length scales much smaller than the individual will allow investigators to determine the sensitivity of migrating juvenile salmonids to turbulence scale. Preliminary results indicate that the selected mixer tends

to reduce fish collection efficiencies in fish raceways (Hotchkiss, 2002) suggesting that the macro scale turbulence lengths are important fish guidance parameters.

Turbulent Jet

The selected turbulent jet produced TKE, strain, and eddy length scales that were similar to turbulence found in the Clearwater River Basin. Preliminary results indicate that fish passage rates in raceways are increased when the selected jet is oriented toward the juvenile collector (Hotchkiss, 2002). The preliminary results suggest that properly scaled induced turbulence may increase fish collection in fish raceways however, these results are preliminary and only provide indications of how actively migrating juvenile salmon will react in fish raceways.

Background turbulence levels in the reservoir style flume were insignificant compared to the turbulence generated by the mixer indicating that wall effects were not an issue, however, isotropic conditions did not occur due to the relatively short nature of the tank. Because the jets and mixers did not issue into fully isotropic ambient fluid the growth and decay rates of the induced turbulence may be slightly different than those in reservoir conditions. The potential for error due to lack of isotropy is small due to the general agreement with results published by previous investigators (White, 1991).

CONCLUSIONS

Gradually varied turbulent flow in natural gravel bed rivers can be approximated by the log-wake law and turbulence decay models developed for unobstructed flow in gravel bed channels. Turbulence in the natural migration corridors of gravel bed streams exhibits spatial variability related to the presence of natural obstructions. A vortex street occurs behind natural obstructions in gravel bed rivers, but due to the relatively large obstruction diameters, an alternating shedding of vortices should not always occur, and the frequency of shedding tends to be greater than the frequency of shedding predicted by the Strouhal relationship. The velocity profiles recorded around the boulders in gravel bed streams are consistent with the results reported by Shamloo *et al.* (2001). The location of the vortex street can be identified by the area of maximum TKE, strain, and $\overline{u'v'}$. Individual vortices were indistinguishable in the time series data due to the large background turbulence induced by the gravel bed environment; however, the eddy length scales were captured using the autocorrelation function and were shown to be significantly smaller within the vortex street than in unobstructed flow at the same distance from the bed.

The results of these data indicate that turbulent flow patterns in gravel bed rivers are greatly impacted by the presence of natural obstructions. These findings imply that the bed shear stress and consequently sediment transport properties in the immediate vicinity of natural boulders are significantly affected by the presence of the boulder and that turbulent fluctuations rotate from the U-W plane to the U-V plane within the vortex street. This switch in orientation, along with increased turbulence properties, has many implications for fish passage design. The vertical orientation of vortices within the vortex street along with the regular interval provides

both a predictable pattern and a vortex orientation that could allow for energy extraction from the flow by swimming fishes.

Turbulence parameters in the upper fifty percent of the water column in gravel bed rivers exhibit a wide range of values. If future fish path and turbulence collection efforts were coupled, more specific turbulence preferences could be established increasing the potential for juvenile attraction to induced turbulence.

The investigation of turbulence in gravel bed rivers provided limits for turbulence parameters that juvenile salmonids experience in natural migration corridors. The range of scalar fluctuation and strain values varied significantly pointing to the need for more specific definitions of migration corridors. The eddy size in natural migration corridors were on the order of magnitude of the juvenile salmonid length providing clear guidance for macroscale eddy reproduction goals.

Turbulence parameters in natural migration corridors, as measured in the gravel bed rivers of the Clearwater Basin, are easily reproducible with turbulent jets. Large mixers (>15cm) are required to reproduce appropriate eddy length scales making proper reproduction of all relevant turbulence parameters more difficult in the laboratory environment. TKE, strain, and eddy length scales were reproduced using a single 1.4 cm diameter oscillating jet while TKE and strain were reproduced using a single 15 cm mixer. The ability to reproduce most turbulent parameters with a single source indicates that complex arrays of jets and mixers may not be necessary for juvenile attraction.

The turbulent flow upstream of the Bonneville PSC is similar to the turbulent flow found in the natural migration corridor of the Clearwater River Basin with the exception that turbulent length scales in the Bonneville Reservoir are one to two orders of magnitude larger than

turbulent structures in the Clearwater River Basin. The Bonneville PSC has generally had positive results collecting juvenile salmonids (Ploskey, *et al.* 2000) but according to the preliminary results from the selected jet fish passage efficiencies might be increased if eddy length scales matched natural migration corridor lengths.

While complete data for fish guidance is not available preliminary results indicate that properly scaled induced turbulence may aid in fish collection and should be considered when designing fishways.

REFERENCES

- Cada, G.C., and Odeh M. (2001). "Turbulence at hydroelectric power plants and its potential effects on fish." *Report, U.S. Department of Energy*, Bonneville Power Administration.
- Chang, H. (1992). *Fluvial Processes in River Engineering*. Krieger Pub.
- Cullen, R. T. (1989). "Fish Habitat Improvement from Scour and Deposition around Fishrocks." Master's Thesis, Washington State University.
- Djilali, N., and Gartshore, I. S. (1991). "Turbulent Flow Around a Bluff Rectangular Plate. Part I: Experimental Investigation." *Journal of Fluids Engineering*, 113, 51-59.
- Faber, D., Rondorf, D., Odeh, M., Zimmerman, S. (2000). "Water Velocity Profiles at Bonneville Dam Prototype Surface Collector, Turbine Unit 5." *Draft Final Report USGS*, USACE, Portland District.
- The Federal Interagency Stream Restoration Working Group (FISRWG). (1998). *Stream Corridor Restoration Principles, Processes, and Practices*. <www.usda.gov/stream_restoration>, October, 2002.
- Hotchkiss, R. H. (2002). *Using Induced Turbulence to Assist Migrating Juvenile Salmon*. Presentation to The American Fisheries Society Annual Conference, Baltimore, MD, August 18-22.
- Independent Scientific Review Panel (ISRP). (1996). *Return to the River, Appendix D*. <www.nwcouncil.org/library/1996/96-6/default.htm>, October, 2002.
- Mobrand Biometrics, Inc. (1999) *The EDT Method – Draft*.
- Nakamura, Y. (1993). "Bluff-Body Aerodynamics and Turbulence." *Journal of Wind Engineering*, 49, 65-78.

- National Oceanic and Atmospheric Administration (NOAA). 2000. *Final Biological Opinion - Reinitiation of Consultation on Operation of the Federal Columbia River Power System, Including the Juvenile Fish Transportation Program, and 19 Bureau of Reclamation Projects in the Columbia Basin*. December 21, 2000.
- Nestler, J. (2002). "Integrated CFD/3-D Tracking Data and an Explanation of Outmigrant Movement Behavior: Insights for Improving Designs." *Presentation to the HydroVision 2002 Conference*, Portland, OR, July 30.
- Nezu, I., and Nakagawa, H. (1993). *Turbulence in Open-Channel Flows*. A. A. Balkema.
- Nikora, V. I., and Goring, D. G. (1998). "Effects of Bed Mobility on Turbulence Structure." *NIWA Internal Report No 48*.
- Nikora, V. I., and Goring, D. G. (2000). "Flow Turbulence Over Fixed and Weakly Mobile Gravel Beds." *Journal of Hydraulic Engineering*, ASCE, 126 (9), 679-690.
- Nowell, A. R. M., and Jumars, P. A. (1984) "Flow Environments of Aquatic Benthos." *Annual Review of Ecological Systems*, 15, 303-328.
- Okamoto, S., and Sunabashiri, Y. (1992). "Vortex Shedding from a Circular Cylinder of Finite Length Placed on a Ground Plane." *Journal of Fluids Engineering*, 114, 512-521.
- Papanicolaou, A. N., Diplas, P., Dancy, C. L., and Balakrishnan, M. (2001). "Surface Roughness Effects in Near-Bed Turbulence: Implications to Sediment Entrainment." *Journal of Engineering Mechanics*, March, 211-218.
- Papanicolaou, A., Strom, K., Schuyler, A., and Talebbeydokhti, N. (2003). "The Role of Sediment Specific Gravity and Availability on Cluster Evolution." *Journal of Earth Surface Processes and Landforms*, In Press, January, 2003.

- Ploskey, G., Schilt, C., Hanks, M., Skalski, J., Nagy, W., Johnson, P., Patterson, D., Kim, J., Lawrence, L. (2002). "Hydroacoustic Evaluation of a Prototype Surface Collector and In-Turbine Screens at Bonneville Dam Powerhouse 1 in 2000." *USACE Report No ERDC/EL TR-02-15*, USACE.
- Rennie, C. D., Fisher, T., and Millar, R. G. (1999). "Spatial Variability of Turbulent Velocity Structure in a Natural River." *Proceedings of the International Water Resources Engineering Conference*, Seattle, WA.
- Schlichting, H. (1979). *Boundary Layer Theory*, (Trans. by Kestin J.) McGraw-Hill.
- Shamloo, H., Rajaratnam, N., and Katapodis, C. (2001). "Hydraulics of Simple Habitat Structures." *J. Hydraulic Research*, 39, 351-366.
- Song, T., and Chiew, Y. M. (2001). "Turbulence Measurement in Nonuniform Open-Channel Flow Using Acoustic Doppler Velocimeter (ADV)." *Journal of Engineering Mechanics*, March, 219-232.
- SonTek. (2002). Personal Communication with Mr. Ben Macone, Sontek, Incorporated.
- Stone, M., Tritico, H., Hotchkiss, R., Papanicolaou, A., and Barber, M. (2002). "Characterizing Turbulence in Salmonid Bearing Streams to Improve Fish Passage at Hydroelectric Dams." *CD-ROM Proceedings from HydroVision 2002 Conference*, Portland, OR.
- Streeter, V., Wylie, E., and Bedford, K. (1998). *Fluid Mechanics*. McGraw-Hill.
- Tritico, H. M. (2002). "Turbulence in Gravel Bed Rivers and its Relevance to Fish Passage Technologies." Master's Thesis, Washington State University. In preparation. December, 2002.
- United States Geological Survey. (2002). <<http://water.usgs.gov>>, October, 2002.

- Videler, J. J., Muller, U. K., and Stamhuis, E. J. (1999). "Aquatic Vertebrate Locomotion: Wakes From Body Waves." *The Journal of Experimental Biology*, (202), 3423-3430.
- Webel, G. and Schatzmann, M. (1984). "Transverse Mixing in Open Channel Flow." *Journal of Hydraulic Engineering*, ASCE, 110 (4), 423-435.
- Wahl, T.L. (2000). "Analyzing ADV Data Using WinADV." *CD-ROM Proceedings, Joint Conference on Water Resources Engineering and Water Resources Planning & Management*, Minneapolis, MN.
- White, F. M. (1991). *Viscous Fluid Flow*. McGraw-Hill.
- Wolman, M.G. (1954). "A Method of Sampling Coarse River Bed Material." *Trans. Am. Geophys. Union*, Washington, D.C., 35, 951-956.

APPENDIX A

LITERATURE REVIEW

APPENDIX A – LITERATURE REVIEW

The purpose of this appendix is to provide an overview of studies that have been conducted on turbulent flow behind bluff objects as they relate to the flow regime behind a protruding rock. The study of turbulent flow behind bluff objects has followed a circular course. The first documentation of recirculation and vorticity began during the Renaissance Period with observations of flow behind boulders (Nezu and Nakagawa 1993). Understanding wakes behind complex objects such as boulders, bridges, or planes not only enables engineers to better predict flow but also translates into added safety and reduced costs. Driven by the necessity to understand flow behind “simpler” objects before being able to describe flow behind complicated objects the field of fluid dynamics has until recently concentrated on simple geometric objects. With the advent of Doppler technology, growing computational fortitude, and ever increasing knowledge of flow behavior, recent studies on turbulence behind nongeometric objects have set the stage for a comprehensive investigation of the turbulent flow behind a boulder in a gravel bed river. It is concluded that ample understanding of basic wake phenomena along with appropriate measurement devices exist thus laying the foundation for future work on turbulent flow behind nongeometric bluff objects.

Introduction

The phenomena of vortex shedding and wake recirculation behind bluff objects have been studied since the Renaissance period. Leonardo da Vinci (1452-1519) is attributed with first describing vortices (Nezu and Nakagawa 1993, and Richter 1998). Figure A1 is a self-portrait of

da Vinci presented to elucidate the importance and complexity of understanding the motion of flow behind an object. While Da Vinci focused on flow behind rocks and other river objects recent progress in understanding the motion of fluid behind objects, has focused on the flow around more geometric objects.



Figure A1. A Self Portrait by Leonardo da Vinci Along with a Qualitative Discussion of Flow Behind an Object (R. Soc. Of London).

Flow around geometric objects has the dual benefit of practicality and relative simplicity. Much of the current interest in understanding the flow behind bodies is its inherent connection with drag and vibration. Efforts to reduce the drag on an aircraft carrier (Streeter *et al.* 1998) and to reduce the vibration on the Tacoma Narrows Bridge (Serway 1994) show the cost and safety benefits of understanding the movement of fluid behind objects. Secondly, the introduction of geometric objects reduces the complexity of the interaction between the object and the fluid.

Work by investigators on geometrical objects has led to quantitative explanations for the phenomena of vortex shedding and wake recirculation under simplified conditions. Research on the flow behind nongeometric objects, which until recently has been hindered by the complexity

of the problem, is the ultimate goal of many fluid dynamicists. Flow behind objects such as sediment particles, islands, jetties, and biota represent a few of the many complex flow regimes that do not follow classic geometric form.

The author's interest in the flow patterns behind nongeometric bluff objects stems from research relating turbulence found in undammed rivers to fish swimming kinetics. In order to discuss more complicated matters such as reproducing appropriately scaled turbulence, and increasing swimming efficiency through hydrodynamics a complete understanding of the mechanics and patterns of flow within a wake region is first required.

The gap between da Vinci's qualitative descriptions of flow around boulders and the need for quantitative data has closed rapidly during the past century. The advent of computers and Doppler technology has allowed for accurate investigation and numerical simulation of the flow behind an object.

The objective of this appendix is to provide an overview of studies that have been published on turbulent flow behind bluff objects as they relate to the flow regime behind a protruding rock. This discussion can be divided into three sections. First it is necessary to discuss measurement techniques. This discussion will not only show what work has been performed, but will also discuss the benefits and constraints associated with each technique. The second portion of the review will concern itself with the vast knowledge and study of flow behind geometric objects and how the results relate to the flow regime behind an obstruction in a gravel bed river. The review will end with a discussion of the flow behind nongeometric objects.

Measurement Techniques

Flow Visualization

Alexandrou (2001) described flow visualization as a very useful tool in studying streamlines, and stream functions. Flow visualization is conducted either by flow seeding or by optical imagery. Studies that use flow seeding inject dye or other particulate matter that is visible to the eye or specialized cameras. The steady flow of particles from a fixed point provides an excellent view of a single streamline. Optical imagery uses optical tricks to draw out shadows produced by the moving flow field, the shadows are equivalent to a stream function. Either method produces a movie of the flow streamlines that allows for easy conceptualization of the stream function. The major limitation of flow visualization is that it is generally not considered a quantitative technique for describing flow. Semi-quantitative data can be collected on the frequency of vortex shedding, average size of vortices, the mean path of the vortex, and separation/reattachment locations for flows behind bluff objects. Flow visualization is further limited by the inability to describe small-scale turbulent fluctuations and by the inability to provide an Eulerian frame of reference. Nezu and Nakagawa (1993) remind us that while flow visualization is often treated as a qualitative tool, da Vinci, Reynolds, Bernoulli, Euler, Prandtl, and Schlichting all made their major contributions to the field of fluid dynamics using flow visualization. More recently, Kline *et al.* (1967) discovered the phenomena of turbulent bursting through flow visualization.

Hot Wire Anemometers

Hot wire anemometry was developed in the 1930s to provide quantitative results to the flow visualization technique. Hot wire anemometry is based on the concept that a hot wire will

be cooled by a high velocity stream faster than it will be cooled by a low velocity stream (Alexandrou 2001). In the 1960s the hot wire anemometer was coupled with pressure transducers to provide very accurate descriptions of velocity fluctuations. Hot wire anemometry has the limitation of being intrusive to the flow, and very delicate. The intrusion into the flow leads to uncertainties in flow response due to the measurement wire, while the delicacy prevents flow measurements anywhere beside the laboratory environment. Hot wire anemometers were used exclusively from the 1960s through the 1980s and some scientists still prefer them today.

Doppler Technology

Doppler technology is based on the phase shift of a wave as it bounces off of particles entrained in the flow stream. The amount of phase shift can be correlated to the speed of the particle. Assuming that the particle is travelling at the same rate as the water, you then know the flow speed. Doppler technology allows for non-intrusive three-dimensional measurement of relatively small sample volumes at frequencies high enough to capture turbulent fluctuations. Two general types of velocimeters are in use. Laser Doppler Velocimeters (LDVs) use the phase shift of a laser and exhibit the highest degree of accuracy established in a laboratory setting. Acoustic Doppler Velocimeters (ADV) use the phase shift of a pulsed sound wave and combine a high degree of accuracy with a compact setup that can be used in relatively harsh environments (Nikora *et al.* 1998). The late 1980s and 1990s saw increased use of Doppler technology and is now the preferred method for turbulent velocity sampling in many situations. Current work, such as that performed by Schuyler and Papanicolaou (2000) on the clustering effect of sediment particles combines flow visualization with LDV measurements.

During the summer of 2001, Stone *et al.* (2002) investigated the flow of water behind boulders protruding from a gravel bed stream. Figure A2 shows the gathering of quantitative data on the turbulent fluid motion behind a boulder.

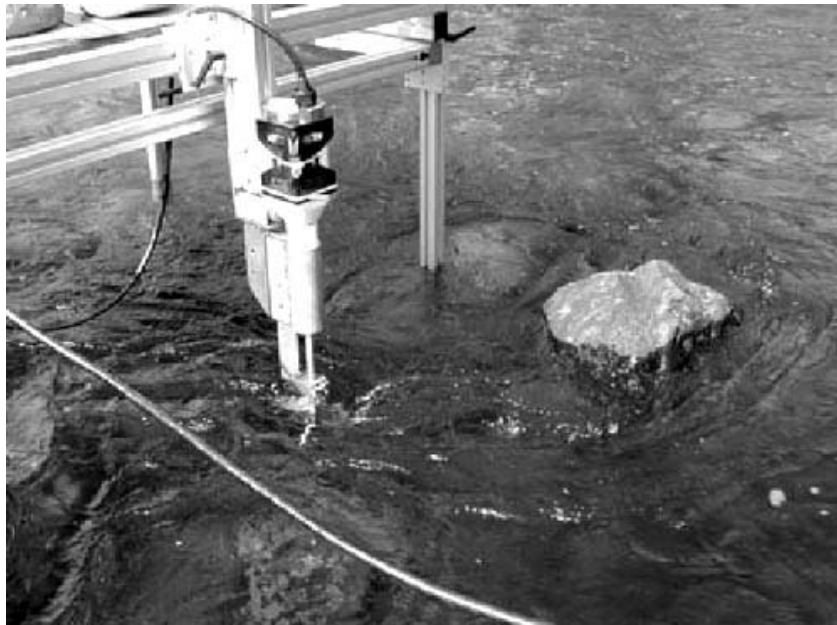


Figure A2. Quantitative Measurement of Turbulent Flow Behind a Boulder Using an ADV (Stone *et al.* 2002).

Numerical Modeling

Numerical modeling of complicated flow regimes has gained wide acceptance over the past decade as a tool that can predict and analyze complicated flow regimes. Numerical models solve complicated flow equations such as the Navier Stokes Equations at individual locations within the flow field. As computers continue to run faster and have more memory increasingly complicated flow regimes can be solved. Numerical models of the flow regime behind a circular cylinder have been created, the results of two such modeling exercises are available online at www.env.leeds.ac.uk/research/dynamics/vortex_anim and <http://www.fluent.com/solutions/examples/x170.htm>. The results of the flow regime behind a square cylinder can be found at anziamj.austms.org.au/v42/ctac99/kirk/home.html.

Flow Measurements behind Bluff Geometric Objects

Object Shape

The flow behind a bluff object is governed by the interaction between the flow and the object. In 1904 Prandtl provided the fluid mechanics field with the concept of boundary layers. While the boundary layer concept was initially presented theoretically, he was soon able to corroborate his theory with flow visualization along the bodies of spheres and thin plates (Schlichting 1979). Prandtl was able to relate the interaction between an object and the flow through pressure, viscosity, and shear variations. Prandtl's 2-D boundary layer equations as presented by Schlichting (1979) are:

$$\frac{du}{dx} + \frac{dv}{dy} = 0 \quad (\text{A.1})$$

$$\frac{du}{dt} + u \frac{du}{dx} + v \frac{du}{dy} = -\frac{1}{\rho} \frac{dP}{dx} + \nu \left(\frac{du}{dy} \right)^2 \quad (\text{A.2})$$

Where u and v are the velocities in the streamwise and transverse directions (x and y), P is pressure, ν is viscosity, and ρ is density. Schlichting (1979) provides a thorough discussion of boundary layer theory. It will suffice for our discussion to make the statement that the boundary layer formed by the interaction between object and flow drives the vortex generation and secondary circulation behind bluff objects. Due to the simple geometry of spheres and plates, hundreds of studies have been conducted analyzing the turbulent flow patterns that result (Schlichting 1979, Nezu and Nakagawa 1993, Djilali and Gartshore 1991, Ormieres and Provansal 1998). Conclusions related to the mechanics of vortex shedding, recirculation patterns within the wake region, and relative stability have been drawn for these objects and many other objects of varying complexity.

Studies on bluff geometric objects of increasing angular complexity have been conducted. To further understand the shedding processes from an object with uniform cross section while minimizing the influence of edge effects associated with the ends of the object, objects such as cylinders with high aspect ratios have been studied by Absil *et al.* (1990), Karniadakis and Triantafyllou (1992), Henderson (1995), and Matsumoto (1999). The flow around cubes and cubic rectangular cylinders are the second most common category of bluff geometric object studied. The study of cubic objects in flow stems from the large number of manmade objects such as buildings that are subjected to fluid forces (Nakamura 1993 and Nakamura *et al.* 1996). Secondly, Lakehal and Rodi (1997) point out cubic objects are highly angular and present configurations that are less dependant upon the Reynolds number of the flow and more dependant upon the orientation of the angles on the object.

Other geometric shapes have been studied to varying degrees. Wolochuk *et al.* (1996) studied the frequency of vortex shedding from equilateral triangle cylinders of varying aspect

ratios. The motivation for studying sharp edged bluff bodies is that frequency of vortex shedding is directly related to the width of the body and the velocity of the water. The dimensionless Strouhal Number can then be plotted against the Reynolds Number to develop a universal curve that can be used to determine the velocity of the upstream current. The Strouhal Number as defined by Vogel (1994) is:

$$St = \frac{fD}{U} \quad (A.3)$$

Where f is the frequency of shedding, D is the width of the object transverse to the mean flow, and U is the mean free-stream velocity. Miao *et al.* (1999) presented studies on prisms in an attempt to explain the varying curvature of the boundary layer in the near field of the downstream flow. Leweke *et al.* (1993) studied the formation of vortices downstream of a ring suspended in flow. Leweke's emphasis was to study the instability and flopping of vortex shedding modes between circular and helical patterns. Papangelou (1992), Piccirillo and Van Atta (1993), and others have studied objects of varying spanwise geometry (cones) and have found that the downstream fluctuation of water is not uniform in the spanwise direction as is the case in cylinders. Instead they have found that vortex shedding and downstream fluctuations occur in cellular locations (e.g. the base will shed vortices at a different frequency than the middle regions of the cone which will shed vortices at different frequencies than the upper portion of the cone). Drag coefficients for innumerable other object shapes have been determined and are presented in various fluid dynamics texts including Hoerner (1965) and Streeter *et al.* (1998).

Flow behind more complex geometric objects such as girders (Matsumoto, 1999) and crosses (Shirakashi *et al.* 1994) represent an increased understanding of the flow processes behind simple geometric objects and the necessity to understand increasingly complex situations.

The introduction of geometric objects such as cylinders (Strykowski and Sreenivasan 1990) and splitter plates (Kwon and Choi 1996, Nakamura *et al.* 1996, and Ozono 1999) into the downstream flow regime behind bluff objects represents the active effort to influence the flow regime behind a bluff object. The main concern of these papers is to reduce vibration and drag associated with the large coherent structures in the wake of bluff objects. Another example of recent attempts to understand increasingly complex flow situations are attempts to look at the interaction of arrays of bluff objects. Kolar *et al.* (1993) found that the resultant wakes from two similar objects mounted near each other and transverse to the flow could act in three separate modes. The first mode occurs when the individual wakes did not significantly act upon each other. The second mode occurs when the vortices are shed opposite in phase to each other. This results in a pulsed jet formation between the two wake regions. The third mode occurs when the two wake regions act as one large wake that would be similar to the wake behind a bluff body with a vertical orifice notch. Results from other more complicated arrays have been published including Polak and Weaver (1995).

Understanding of the mechanisms related to flow around bluff geometric objects has led to a greater understanding of boundary layer mechanics. The occurrence of boundary layers is not confined to motion around objects. Boundary layers also occur when fluid moves within objects such as pipes or channels. Increased understanding of boundary layers has allowed for better understanding, modeling, and design of orifices and other expansion flows as pointed out by Peters and Hirschberg (1993).

Studies on the Turbulent Flow behind Circular Cylinders

The mechanisms that drive the fluid movement in the wake region of a circular cylinder are functions of the Reynolds Number. According to Schlichting (1979) the flow behind a circular cylinder is divided into five regions which are dependant upon the Reynolds Number distribution. This distribution is presented in Figure A3 along with the vortex shedding modes for rectangular cylinders.

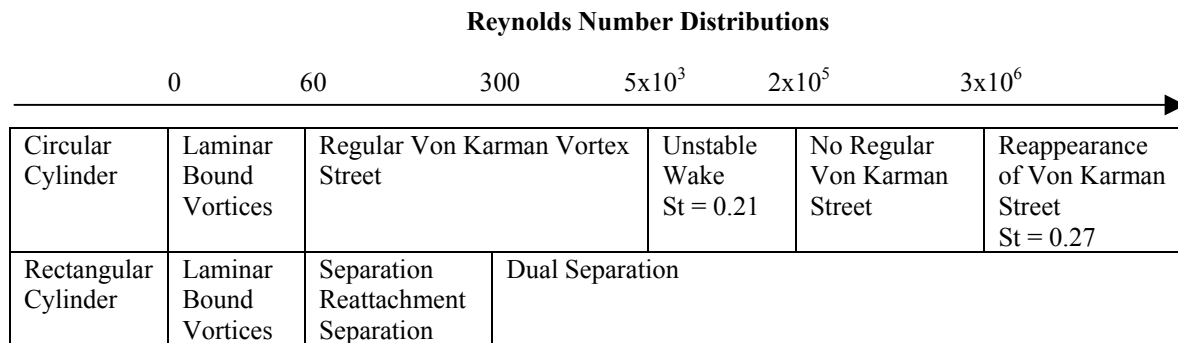


Figure A3. Vortex Shedding Modes for Circular and Rectangular Cylinders (Schlichting 1979, Arnal *et al.* 1991).

In the Reynolds Number range of zero to sixty, a laminar uniform wake appears. According to Henderson (1995) a pair of “bound” vortices of equal size are formed in the area of adverse pressure gradient. Henderson has also observed a slow periodic waviness within the wake at Reynolds numbers in the forty to fifty range. Between Reynolds Numbers of sixty and 5×10^3 a regular alternate shedding of vortices occurs. This regular shedding pattern is termed the regular Von Karman vortex street and is one of two intermediate steps toward a completely turbulent wake region.

Von Karman’s original work on circular cylinders occurred while he was working toward his masters degree under Prandtl. Prandtl expected the flow regime behind a circular cylinder to be composed of symmetrically shed vortices. Von Karman was able to prove mathematically

that symmetrically shed vortices were unstable, and in fact the only stable vortex shedding pattern is one in which the ratio of the width of the wake to the downstream distance between vortices is equal to 0.281. While Von Karman was not the first to note the phenomena of alternating shedding vortices, he was the first to prove its stable pattern and was also the first to correlate this pattern to wake drag (Von Karman 1957).

The second of the intermediate regions occurs between Reynolds Numbers of 5×10^3 and 2×10^5 . Within this region the Strouhal Number remains relatively constant at a value of 0.21 but the vortices that are shed no longer trail off behind the object in a regular path. This region has an apparent instability marked by two different modes of vortex shedding. As Persillon and Braza (1998) point out, the two different modes of vortex shedding cause large and small scale vorticity at two different frequencies. The interaction between the two vorticities causes amplitude and path modulations. At a Reynolds' Number of 2×10^5 the wake behind a circular cylinder turns fully turbulent. An obvious drop in the Drag coefficient along with the suppression of any regular Von Karman vortex street is observed. This region of suppressed vortex street occurs between Reynolds Numbers of 2×10^5 and 3×10^6 . Very few studies have been conducted on wakes within this region. The author speculates that this is due to the lack of harmful vibrations, excessive scour, or high drag within this region of flow. It is curious, however, that this region is centered on a Reynolds Number of 10^6 and that the kinematic viscosity of water at standard temperature and pressure is 10^{-6} m²/s. Therefore the area of suppressed vortex formation in water at standard conditions occurs when the metric product of the velocity of the water and the diameter of the cylinder is approximately equal to unity ($V \cdot D \approx 1$). For Reynolds Numbers at and above 3×10^6 the irregular Von Karman vortex street reappears at a Strouhal Number of approximately 0.27.

Studies on the Turbulent Flow behind Square Cylinders

The turbulent flow behind a square cylinder is made more complex by the addition of four corners to the object geometry. At most Reynolds numbers there may be as many as four vortices being shed at one time. There are at least four regions of flow characterized by the tendency of flow to separate and form vortices. Unlike circular cylinders, exact Reynolds Numbers cannot be applied due to the flow reattachment's dependence on the side ratio (length of the rectangle in the streamwise direction divided by the length of the rectangle in the transverse direction). A schematic of vortex shedding modes at approximate Reynolds Numbers is presented in Figure A3. At extremely low Reynolds Numbers there is no separation of the flow, and it is intuitive that at some Reynolds Number flow will separate at the leading two corners. Below Reynolds Numbers in the range of 100 to 300 the flow reattaches to the side wall and then separates a second time at the trailing corners forming a steady Von Karman vortex street (Arnal *et al.* 1991 and Nakamura *et al.* 1996). Above Reynolds Numbers of 300 the vortices that are spun off of the leading corners no longer reattach to the side wall of the rectangle and a second pair of vortices are shed from the trailing corners. This second pair of vortices serves to destabilize the wake behind the square cylinder by interacting with the upstream shed vortices in combinations that depend upon the frequency and phase of each vortex (Arnal *et al.* 1991 and Nakamura *et al.* 1996). Martinuzzi and Tropea (1993), and Lakehal and Rodi (1997) have reported this mode of vortex shedding through Reynolds Numbers of 4×10^4 .

Flow Measurements behind Nongeometric Objects

Nongeometric objects such as jetties, pilings, and biota are often recreated in laboratory environments. Two studies are of particular importance to the study of flow around a boulder in a gravel bed river. A study of the recirculation zone behind various islands in Rupert Bay, Quebec was conducted by Babarutsi *et al.* (1989). Babarutsi developed equations relating the distance from the islands to the reattachment point downstream to the depth of the water and the coefficient of friction. He also gave an empirical formulation for the strength of the recirculating flow as a function of mean stream velocity, depth, and the coefficient of friction. Additionally, due to the relatively low velocity to diameter ratio, Babarutsi discussed the occurrence of a steady recirculating wake bubble in which the shear layers on each side of the island are so far apart that they do not interact with each other. A second study by Shamloo *et al.* (2001) studies the effect of a large hemisphere on creating fish habitat in a gravel bed flume. The authors were most concerned with recirculation currents and scour holes at varying flow depths. Shamloo notes that when the depth of water is less than the height of the hemisphere the flow is two-dimensional and exhibits the Von Karman vortex street. He also notes that the length of the recirculation zone was one and a half times the diameter of the hemisphere. Shamloo continued to describe the wake region as being approximately twice the width of the body. Shamloo conducted both vertical and transverse profiles upstream and downstream of the hemisphere and shows zones of vertical recirculation along with regions of shear. Shamloo also placed a rock in the gravel bed flume and observed the scour hole created upstream but did not report any velocity measurements. He did note that the scour hole was much smaller than the scour hole created by the hemispheres. The complex geometry of the rock most likely resulted in a complex flow regime reducing the likelihood for the formation of high energy large coherent

structures. Shamloo called for further work to be conducted on more realistic geometries including rock clusters and stated that any further laboratory results should be supplemented with relevant field work.

REFERENCES

- Absil, L. H. J., Steenbergen, W., and Passchier, D. M. 1990 Time and spatial correlation measurements in the turbulent wake of a circular cylinder using laser doppler anemometry. *Applied Scientific Research*. 47, 247-271.
- Alexandrou, A. 2001 Measurement of Fluid Properties. In *Principles of Fluid Mechanics*, Chap 12.2. Prentice Hall.
- Arnal, M. P., Goering, D. J., and Humphrey, J. A. C. 1991 Vortex Shedding From a Bluff Body Adjacent to a Plane Sliding Wall. *J. Fluids Engineering*, 113, 384-398.
- Babarutsi, S., Ganoulis, J., and Chu, V. H. 1989 Experimental Investigation of Shallow Recirculating Flows. *J. Hydr. Eng.*, 115, 906-925.
- da Vinci, L. 1998 The Universe. In *The Notebooks of Leonardo da Vinci*, (ed. I. A. Richter), Chap 2.1. Oxford.
- Djilali, N., and Gartshore, I. S. 1991 Turbulent Flow Around a Bluff Rectangular Plate. Part I: Experimental Investigation. *J. Fluids Engineering*. 113, 51-59.
- Fluent. Flow Modeling Examples-Vortex Shedding.
<<http://www.fluent.com////////solutions/examples/x170.htm>>.
- Henderson, R. D. 1995 Details of the drag curve near the onset of vortex shedding. *Phys. Fluids*, 7, 2102-2104.
- Hoerner, S. F. 1965 *Fluid Dynamic Drag*, 2d ed., Hoerner.

- Hotchkiss, R. H., and Rondorf, D. 2001 Using Induced Turbulence to Assist Downstream Migrating Juvenile Salmonids. Presented to Bonneville Power Administration.
- Karniadakis, G., and Triantafyllou, G. 1992 Three-dimensional dynamics and transition to turbulence in the wake of bluff objects. *J. Fluid Mech.*, 238, 1-30.
- Kirkpatrick, M. P., Armfield, J. H. K., and Dixon, T. 2000 Simulation of vortex shedding flows using high-order fractional step methods.
<<http://anziamj.austms.org.au/V42/CTAC99/Kirk/home.html>>.
- Kline, S. J., Reynolds, W. C., Schraub, F. A., and Runstadler, P. W. 1967 The structure of turbulent boundary layers. *J. Fluid Mech.*, 30, 741-773.
- Kolar, V., Lyn, D. A., and Rodi, W. 1993 An Experimental Study of Interacting Coherent Structures in the Turbulent Near Wake Behind a Pair of Square Cylinders. *Applied Sci. Research*, 51, 417-421.
- Kwon, K., and Choi, H. 1996 Control of laminar vortex shedding behind a circular cylinder using splitter plates. *Phys. Fluids*, 8, 479-486.
- Lakehal, D., and Rodi, W. 1997 Calculation of the flow past a surface-mounted cube with two-layer turbulence models. *J. Wind Eng. and Ind. Aerodynamics*, 67and68, 65-78.
- Leweke, T., Provansal, M., and Boyer, L. 1993 Stability of Vortex Shedding Modes in the Wake of a Ring at Low Reynolds Numbers. *Physical Review Letters*, 71, 3469-3472.
- Martinuzzi, R., and Tropea, C. 1993 The flow around surface-mounted prismatic obstacle placed in a fully developed channel flow. *J. Fluids Engineering*, 115, 85-92.
- Matsumoto, M. 1999 Vortex Shedding of Bluff Bodies: A Review. *J. of Fluids and Structures*, 13, 791-811.

- Miau, J. J., Wang, J. T., Chou, J. H., and Wei, C. Y. 1999 Characteristics of Low-frequency Variations embedded in Vortex-shedding Process. *J. Fluids and Structures*, 13, 339-359.
- Nakamura, Y. 1993 Bluff-Body Aerodynamics and Turbulence. *J. Wind Eng. and Ind. Aerodynamics*, 49, 65-78.
- Nakamura, Y., Ohya, Y., Ozono, S., and Nakayama, R. 1996 Experimental and numerical analysis of vortex shedding from elongated rectangular cylinders at low Reynolds numbers $200 - 10^3$. *J. Wind Eng. and Ind. Aerodynamics*, 65, 301-308.
- Nezu, I., and Nakagawa, H. 1993 Brief History of Turbulence Research. In *Turbulence in Open-Channel Flows*, Chap 1.2. A. A. Balkema.
- Nikora, V. I., Goring, D. G., and Biggs, B. J. F. 1998 On gravel-bed roughness characterization. *Water Resources Research*, 34, 517-527
- Ormieres, D., and Provansal, M. 1999 Transition to Turbulence in the Wake of a Sphere. *Physical Review Letters*. 83, 80-83.
- Ozono, S. 1999 Flow control of vortex shedding by a short splitter plate asymmetrically arranged downstream of a cylinder. *Phys. Fluids*, 11, 2928-2934.
- Papangelou, A. 1992 Vortex shedding from slender cones at low Reynolds numbers. *J. Fluid Mech.*, 242, 299-321.
- Papanicolaou, A., Strom, K., Schuyler, A., and Talebbeydokhti, N. (2002). The Role of Sediment Specific Gravity and Availability on Cluster Evolution. *Journal of Earth Surface Processes and Landforms*, In Press, January, 2003.
- Persillon, H., and Braza, M. 1998 Physical analysis of the transition to turbulence in the wake of a circular cylinder by three-dimensional Navier-Stokes simulation. *J. Fluid Mech.*, 365, 23-88.

- Peters, M. C. A. M., and Hirschberg, A. 1993 Acoustically Induced Periodic Vortex Shedding at Sharp Edged Open Channel Ends: Simple Vortex Models. *J. Sound and Vibration*, 161, 281-299.
- Piccirillo, P. S., and Van Atta, C. W. 1993 An experimental study of vortex shedding behind linearly tapered cylinders at low Reynolds number. *J. Fluid Mech.*, 246, 163-195.
- Polak, D. R., and Weaver, D. S. 1995 Vortex Shedding in Normal Triangular Tube Arrays. *J. Fluids and Structures*, 9, 1-17.
- Schlichting, H. 1979 *Boundary Layer Theory*, (Trans. by Kestin J.) Chap 2. McGraw-Hill.
- Schuyler, A. and Papanicolaou, A. (2000). Image Analysis Technique to Track the Evolution of Sediment Clusters. *Journal of Experimental Techniques*, September/October 2000, Vol. 24, No. 5, SEM, p. 31.
- Schuyler, A. and Papanicolaou, A. (2000). The Effects of Cluster Bedforms on the Longitudinal Velocity. *Paper published in the Proceedings of the 2000 ASCE Water Resources Engineering and Water Resources Planning and Management Conference*, Minneapolis, MN, July-August 2000 (CD version).
- Serway, R. A. 1994 Forced Oscillations. In *Principles of Physics*, Chap 21.6. Saunders College.
- Shamloo, H., Rajaratnam, N., and Katapodis, C. 2001 Hydraulics of simple habitat structures. *J. Hydraulic Research*, 39, 351-366.
- Shirakashi, M., Bae, H. M., Sano, M., and Takahashi, T. 1994 Characteristics of Periodic Vortex Shedding from Two Cylinders in Cruciform Arrangement. *J. Fluids and Structures*, 8, 239-256.

Stone, M., Tritico H., Hotchkiss, R.H., and Papanicolaou, A. 2002 Characterizing Turbulence in Salmonid Bearing Streams to Improve Fish Passage at Hydroelectric Dams. Proposed paper for *HydroVision 2002*.

Streeter, V. L., Wylie, E. B., and Bedford, K. W. 1998 *Fluid Mechanics*, Chaps 5 and 7. McGraw-Hill.

Strykowski, P. J., and Sreenivasan, K. R. 1990 On the formation and suppression of vortex ‘shedding’ at low Reynolds numbers. *J. Fluid Mech.*, 218, 71-107.

University of Leeds, Institute for Atmospheric Science. Vortex Shedding Animation. <http://www.env.leeds.ac.uk/ias/dynamics/vortex_anim/>.

Vogel, S. 1994 Unsteady Flows. In *Life in Moving Fluids*. Chap 16. Princeton.

Von Karman, T. 1957 *Aerodynamics – Selected Topics in the Light of Their Historical Development*, Chap 3. Cornell University Press.

Wolochuk, M. C., Plesniak, M. W., and Braun J. E. 1996 The Effects of Turbulence and Unsteadiness on Vortex Shedding From Sharp-Edged Bluff Bodies. *J. Fluids Engineering*, 118, 18-25.

APPENDIX B

GRAVEL BED RIVER RESULTS

REACH FIGURES



Figure B1. Selected Reach on the South Fork of the Clearwater (Boulder A).



Figure B2. Selected Reach on the South Fork of the Clearwater (Boulder B).



Figure B3. Selected Reach on the Lochsa River (Boulder C).

SAMPLING PLATFORM PICTURES AND SPECIFICATIONS



Figure B4. Sampling Platform.

Specifications

The ADV stand was constructed to be flexible enough to allow critical positioning of the ADV probe while being rugged enough to minimize vibrations in the mountainous gravel bed tributaries of the Clearwater Basin. The stand was constructed from prefabricated Bosch[®] tubing and sliding components to allow for movement of the probe in the streamwise, transverse, and vertical directions. The stand was designed to have a one-meter vertical by one-meter transverse sampling window along with twenty-five centimeters in streamwise displacement. The stand

was also constructed with the flexibility to rotate the probe between -90° and 90° (where 0° is a downlooking configuration). Rotation of the probe allowed for the collection of data closer to the water surface than would otherwise be possible with a downlooking configuration. Each stand leg was adjustable so that the stand and probe could be leveled. Leveling the probe at each setup ensured accurate vertical and transverse cross sections were achieved. The ADV probe was mounted a minimum of 20cm upstream of the upstream stand legs to prevent disruption of the natural flow regime by the legs.

SURVEY RESULTS

7_10_01

Sunny 90

Survey of South Fork of Clearwater River South of Stites (upstream)

Station	+	HI	-	Elevation	H.Deg	x=radius	Coordinates	
							x (ft)	y (ft)
BM #2			0.005	99.96	0.0000	23.375	0	23.375
BM #1	0.045	99.955		100	280.2504	19.650	-19.326	3.553
BSA			-8.265	91.690	219.3940	194.375	-124.059	-149.636
BSB			-8.145	91.810	214.0450	185.160	-103.756	-153.359
BSC			-8.205	91.750	209.3139	172.840	-85.183	-150.391
BSD			-8.285	91.670	205.0409	167.195	-70.843	-151.445
BSE			-8.270	91.685	192.4748	153.905	-34.089	-150.082
BSF			-8.130	91.825	176.2436	151.105	9.462	-150.808
BSG			-8.070	91.885	162.2403	158.860	48.032	-151.425
BSH			-7.700	92.255	151.4919	169.085	79.844	-149.046
BSI			-7.485	92.470	140.4943	188.390	118.995	-146.051
BSJ			-7.670	92.285	131.0339	211.940	159.805	-139.215
BSK			-7.940	92.015	123.3745	251.530	209.434	-139.301
BSL			-8.290	91.665	120.3730	293.175	252.283	-149.348
BSM			-8.580	91.375	118.3643	327.725	287.704	-156.939
BSN			-9.060	90.895	118.2611	367.870	322.151	-175.173
BSO			-9.350	90.605	119.1812	407.170	355.069	-199.282
Opp. Bank at O			-8.450	91.505	125.2203	405.835	330.941	-234.905
RB			-7.270	92.685	176.2400	169.595	10.649	-169.26
x1			-7.920	92.035	175.3545	151.420	11.628	-150.973
x2			-7.700	92.255	174.2221	138.440	13.576	-137.773
x3			-7.650	92.305	173.2903	124.880	14.171	-124.073
x4			-7.410	92.545	171.4139	109.690	15.845	-108.539
x5			-7.475	92.480	168.2127	95.145	19.201	-93.187
x6			-7.725	92.230	164.5136	82.125	21.449	-79.274
WS Rock (~3" from top of rock)			-6.205	93.750	165.5451	82.765	20.143	-80.276
x7			-8.105	91.850	157.4727	70.440	26.626	-65.214
x8			-8.595	91.360	146.3348	64.615	35.604	-53.922
x9			-8.495	91.460	135.3857	57.905	40.478	-41.406
x10			-7.970	91.985	121.5506	52.030	44.163	-27.509
x11			-6.430	93.525	122.2954	37.970	32.024	-20.4
Rebar #1			-0.275	99.680		20.565		
Rebar #2			-1.520	98.435		32.820		
Bridge			4.500	104.455	90.2442	404.145	404.135	-2.904

Survey of South Fork of Clearwater River South of Stites (upstream)

Description	+	HI	Y	Elevation	H.Deg	Radius	Rotated and Translated Coordinates	
							x (ft)	y (ft)
BM #1	5.328	94.673		100.000	351.9044	180.785	-19.21113403	3.670814015
BM #2			5.29	99.963	358.2975	198.425	0	23.375
Rebar #1			5.050	99.723	351.2206	174.695	-20.30108777	-2.685157601
Rebar #2			3.795	98.468	359.1510	207.685	9.272734151	26.36070161
BS-A			-2.390	92.283	286.8742	266.685	-247.0807335	-102.0387233
BS-B			-2.335	92.338	292.9564	233.425	-207.0692195	-87.68100977
BS-C			-2.650	92.023	298.8222	204.290	-171.2539818	-79.58812166
BS-C-WS			-0.755	93.918	298.9767	205.660	-172.2069166	-78.45936412
BS-D			-2.770	91.903	314.6125	178.000	-119.4729235	-52.12345297
BS-E			-3.135	91.538	330.7650	149.065	-65.66224733	-46.0828082
BS-E-WS			-0.945	93.728	330.8050	Bat. Low	-65.66224733	-46.0828082
BS-F			-3.575	91.098	351.3658	128.130	-12.04277065	-48.51356944
BS-G			-3.500	91.173	22.6517	126.435	56.05596815	-57.27950037
BS-G-WS			-0.905	93.768	22.6183	126.635	56.06114402	-57.06644548
BS-H			-3.505	91.168	42.5319	147.055	106.9137844	-64.67853895
BS-I			-3.645	91.028	58.9736	189.470	170.0502267	-74.24448786
BS-I-WS			-1.380	93.293	59.0333	191.505	171.8807064	-73.33344892
BS-J			-3.775	90.898	70.8475	245.965	240.333438	-89.93833917
LB			-1.075	93.598	6.0047	156.130	23.00276003	-19.27973674
x1			-2.200	92.473	5.2367	151.655	20.58873656	-23.57541953
x2			-3.145	91.528	6.4586	142.150	22.91337099	-33.3091771
x3			-3.400	91.273	6.7500	129.735	22.39680258	-45.73263741
x4			-3.335	91.338	6.8800	116.830	21.37565993	-58.60020599
x4-WS			-0.900	93.773	6.6617	117.755	21.02336956	-57.63517466
x5			-2.350	92.323	6.2233	103.660	18.85213187	-71.58756404
BS 3' lmd UpStrm of Rock			-2.210	92.463	6.1483	97.665	18.18277529	-77.54653491
BS 3' lmd UpStrm of Rock @ WS			-0.900	93.773	7.0519	97.400	19.68800184	-77.95942062
x6			-2.210	92.463	8.0664	81.305	19.43134169	-94.12931783
x7			-1.865	92.808	9.3986	56.780	17.73786329	-118.6467301
x8			-2.470	92.203	12.5400	36.255	16.71046582	-139.2963473
x9			-2.370	92.303	14.5875	16.580	13.3648918	-158.704601
x10			-1.915	92.758	36.5167	5.520	12.68382817	-170.3280089
RB			-0.985	93.688	56.3133	4.575	13.24014054	-172.217067
FP-RB			0.395	95.068	146.6975	5.490	12.57665854	-179.3562076
RB-DS-L			-1.475	93.198	97.2119	69.625	78.70076205	-182.3134795
RB-DS-U			-1.135	93.538	93.1933	27.755	37.21518584	-175.8678371
RB-US			-0.940	93.733	273.1019	27.445	-17.94730041	-173.8335872
Rock/Top			-0.735	93.938	8.8197	97.770	22.72136507	-77.95383768
Rock/Upstream			-2.230	92.443	7.9000	97.145	21.09006812	-78.37429206
Rock/Downstream			-2.155	92.518	9.6647	98.170	24.20851571	-77.76417886
Rock/Left			-2.425	92.248	8.5375	99.050	22.41116548	-76.62074446
Rock/Right			-2.660	92.013	9.0125	95.960	22.79604592	-79.79142645
T/Trailing 18"Dia. Rock			-1.605	93.068	10.1267	98.630	25.06323986	-77.43185909
Submerged Rock/Top			-1.400	93.273	0.3203	113.760	8.058973698	-61.07187811
LB-DS-L			-1.415	93.258	45.0708	198.065	147.1541314	-32.43080294
LB-DS-U			-1.200	93.473	27.1353	168.515	83.61447967	-23.49104042
LB-US			-1.000	93.673	329.8383	187.590	-87.69010325	-14.36115042
FP-LB			3.430	98.103	6.5028	166.805	25.37132903	-8.776717847

7_25_01

Sunny 90

Survey of South Fork of Clearwater River South of Stites (upstream)

Description	+	HI	Y	Elevation	H.Deg	Radius	Rotated and Translated Coordinates	
							x (ft)	y (ft)
BM #1	0.208	104.793	0.2075	100.000	278.2746	18.083	-19.294	3.585
BM #2			0.17	99.963	358.1831	24.310	0.000	23.375
Rebar #1			-0.450	99.343	258.3208	18.565	-20.243	-2.711
Rebar #2			-1.650	98.143	1.3992	34.020	9.826	23.954
Leg 1			-7.735	96.870	155.0017	68.495	20.538	-65.632
Leg 3			-7.675	96.930	152.0725	69.865	24.330	-65.678
Leg 4			-7.535	97.070	153.3564	73.925	24.303	-70.045
T/ADV			-9.945	94.660	155.8142	68.705	19.682	-66.141

7_27_01

Sunny 85

Survey of South Fork of Clearwater River South of Stites (upstream)

Description	+	HI	Y	Elevation	H.Deg	Radius	Rotated and Translated Coordinates	
							x (ft)	y (ft)
BM #1	0.293	104.707	0.293	100.000	280.8025	16.834	-19.326	3.553
BM #2			0.258	99.965	0.8958	25.063	0.000	23.375
Rebar #1			0.04	99.747	258.9550	17.275	-20.483	-2.821
Rebar #2			-1.225	98.482	3.0933	34.68	9.676	23.748
Pos 1 Leg 1 Bed Surface			-7.35	92.357	164.6508	76.38	8.387	-76.962
Pos 1 Leg 1 Water surface			-6.295	93.412	164.8108	75.87	8.100	-76.490
Pos 1 Top of ADV			-9.33	95.190	164.6383	76.15	8.368	-76.732
Pos 1 Top leg 1			-7.105	97.415	163.0000	74.745	10.261	-74.987
Pos 1 Top leg 3			-7.115	97.405	161.2025	74.775	12.567	-74.556
Pos 1 Top leg 4			-6.945	97.575	161.2508	79.135	13.424	-78.831
Pos 2 Leg 1 Bed Surface			-7.705	92.002	154.3067	82.855	23.872	-79.762
Pos 2 Leg 1 Water Surface			-6.445	93.262	154.1908	83.065	24.100	-79.905
Pos 2 Top leg 1			-7.65	96.870	153.5908	82.195	24.625	-78.796
Pos 2 Top leg 2			-7.545	96.975	153.3392	86.52	26.449	-82.734
Pos 2 Top leg 3			-7.81	96.710	150.9342	82.045	28.121	-77.281
Pos 2 Top leg 4			-7.4	97.120	150.8958	86.39	29.836	-81.274
Pos 2 Top of ADV			-10.055	94.465	154.1217	82.705	24.076	-79.532

Survey of South Fork of Clearwater River South of Stites (upstream)							Rotated and Translated Coordinates	
Description	+	HI	Y	Elevation	H.Deg	Radius	x (ft)	y (ft)
BM #1	0.315	104.685	0.315	100.000	283.3439	17.635	-17.159	4.070
BM #2			0.31	99.995	0.0600	25.71	0.027	25.710
Rebar #1			-0.015	99.670	262.2503	17.685	-17.523	-2.385
Rebar #2			1.265	100.950	2.6328	35.33	1.623	35.293
Left Bank			-6.12	93.565	115.2167	34.165	30.909	-14.556
Strm Bed 1			-7.54	92.145	121.2858	38.01	32.483	-19.739
Strm Bed 2			-8.135	91.550	128.0183	41.225	32.478	-25.391
Strm Bed 3			-8.145	91.540	132.5625	43.2	31.819	-29.220
BS @ ADV			-7.66	92.025	162.4533	78.068	23.536	-74.436
WS @ ADV			-6.43	93.255	162.5933	78.19	23.391	-74.609
Leg 1			-7.485	97.013	161.6775	75.77	23.819	-71.929
Leg 3			-7.715	96.783	158.8236	76.265	27.550	-71.115
Leg 4			-7.55	96.948	159.2269	80.595	28.584	-75.356
BM 1	0.585	104.415	0.585	100.000	284.5475	17.875	-17.159	4.070
BM 2			0.54	99.955	0.0000	26.105	0.060	25.751
Left Bank			-5.82	93.595	112.6475	36.405	33.812	-14.242
Stream Bed 1			-7.035	92.380	118.4917	37.485	33.174	-18.108
""2			-7.65	91.765	124.9000	39.715	32.820	-22.951
""3			-7.895	91.520	128.8850	41.96	32.923	-26.568
""4			-8.08	91.335	133.6144	45.13	32.954	-31.358
""5			-8.26	91.155	137.9108	49.375	33.396	-36.867
""6			-8.275	91.140	142.2758	54.335	33.571	-43.202
""7			-8.155	91.260	145.8169	59.42	33.733	-49.380
""8			-8.165	91.250	148.9692	65.525	34.154	-56.371
""9			-7.535	91.880	151.8775	72.345	34.506	-64.026
""10			-7.145	92.270	154.1867	78.255	34.506	-70.668
""11			-7.175	92.240	156.6675	86.17	34.593	-79.345
""12			-7.12	92.295	158.7217	94.025	34.618	-87.837
""13			-6.99	92.425	160.6967	103.305	34.684	-97.719
""14			-6.82	92.595	163.2992	119.3	34.883	-114.489
""15			-7.325	92.090	165.2600	135.14	35.046	-130.913
""16			-7.47	91.945	166.7958	148.655	34.672	-144.947
""17			-7.165	92.250	167.4642	158.765	35.216	-155.200
""18			-6.64	92.775	168.3747	169.095	34.871	-165.847
Right Bank			-5.875	93.540	167.6317	171.325	37.500	-167.560
WL Upstream			-5.385	94.030	226.4475	236.045	-170.285	-163.649
WL @ Rope			-6.08	93.335	166.3406	135.96	32.775	-132.344
WL Downstream			-6.45	92.965	129.9781	183.05	140.881	-117.422
Stream Bed R. Rock			-7.955	91.460	156.4508	81.43	32.981	-74.876
"" U.S. Rock			-7.385	92.030	157.1639	79.885	31.446	-73.857
"" L. Rock			-7.735	91.680	156.0842	78.27	32.165	-71.781
"" D.S. Rock			-7.445	91.970	154.9692	79.54	34.091	-72.293
T/Rock			-5.965	93.450	155.8283	79.855	33.138	-73.081
T/Large Rock in Scour Hole			-6.89	92.525	154.2608	80.375	35.343	-72.619
BM1	-0.27	105.27	-0.27	100	217.5042	47.665	-17.158	4.070
BM2			-0.305	99.965	252.7803	36.86	0.008	25.686
WL Upstream			-6.09	94.18	293.4933	258.35	-36.782	254.408
WL @ Rope			-6.655	93.615	239.5483	69.195	-34.119	29.724
Right Bank			-6.62	93.65	236.7094	173.175	-134.088	58.835
Left Bank			-6.645	93.625	245.6589	21.355	11.482	14.691
BS @ ADV#2			-8.03	92.24	124.5675	78.375	35.993	-73.210
WS @ ADV#2			-6.705	93.565	124.5708	78.335	35.985	-73.170
Leg 1 SU 2			-7.6	97.4825	124.4400	78.26	36.158	-73.083
Leg 2 SU 2			-7.56	97.5225	123.5975	82.505	37.675	-77.220
Leg 3 SU 2			-7.72	97.3625	121.6664	77.395	39.824	-71.859
Leg 4 SU 2			-7.6	97.4825	121.0100	81.705	41.272	-76.019

Survey of South Fork of Clearwater River South of Stites (upstream)							Rotated and Translated Coordinates	
Description	+	HI	Y	Elevation	H.Deg	Radius	x (ft)	y (ft)
<i>Data from 8/1</i>								
BM #1	0.315	104.685	0.315	100.000	283.3439	17.635	-17.159	4.070
BM #2			0.31	-4.690	0.0600	25.71	0.027	25.710
Rebar #1			-0.015	-5.015	262.2503	17.685	-17.523	-2.385
Rebar #2			1.265	-3.735	2.6328	35.33	1.623	35.293
<i>Data from 8/7</i>								
BM #1	-0.215	105.215	-0.215	100.000	59.4958	14.22	-17.159	4.070
BM #2			-0.195	100.020	164.3675	20.375	0.054	25.744
Rebar #1			-0.55	99.665	36.1708	16.47	-17.355	-2.511
Rebar #2			-1.65	98.565	164.4442	30.27	1.588	35.520
BS #1			-9.975	90.240	0.0000	43.23	-20.822	-33.792
WS #1			-6.95	93.265	1.9850	42.49	-21.848	-32.488
BS #2			-8.985	91.230	282.7325	55.91	41.602	-28.082
WS #2			-7.03	93.185	282.7333	56.425	42.012	-28.393
Leg 1 BS			-7.935	92.280	315.4833	82.54	25.480	-71.860
Leg 1 WS			-6.97	93.245	315.4683	82.385	25.447	-71.707
Leg 1 Top			-7.525	97.503	315.3067	82.54	25.719	-71.772
Leg 3 Top			-7.56	97.468	312.6783	82.845	29.356	-70.653
Leg 4 Top			-7.44	97.588	313.0000	87.16	30.592	-74.815
Leg 4 Top SU 2			-7.78	97.248	306.8383	88.525	39.688	-71.938
Leg 3 Top SU 2			-7.53	97.498	306.2192	84.25	38.420	-67.750
Leg 1 Top SU 2			-7.675	97.353	308.7853	83.51	34.760	-68.872
T/ADV SU 2			-9.885	95.143	309.3472	83.835	34.172	-69.530
Leg 4 Top SU 3			-7.915	97.113	307.0567	91.26	40.702	-74.501
Leg 3 Top SU 3			-7.715	97.313	306.3650	87.05	39.605	-70.296
Leg 1 Top SU 3			-7.6	97.428	308.8208	85.785	35.742	-70.925
T/ADV SU 3			-10.48	94.548	309.5425	87.265	35.427	-72.735
Leg 4 Top SU 4			-8.235	96.793	301.6561	89.355	46.981	-68.451
Leg 3 Top SU 4			-8.155	96.873	301.0900	85.07	45.278	-64.426
Leg 1 Top SU 4			-8.135	96.893	303.6083	84.34	41.766	-65.862
T/ADV SU 4			-10.08	94.948	304.3408	86.295	41.866	-68.099
Stream Bed R. Rock			-7.955	91.46	156.45083	81.43	32.981	-74.876
"" U.S. Rock			-7.385	92.03	157.16389	79.885	31.446	-73.857
"" L. Rock			-7.735	91.68	156.08417	78.27	32.165	-71.781
"" D.S. Rock			-7.445	91.97	154.96917	79.54	34.091	-72.293
T/Rock			-5.965	93.45	155.82833	79.855	33.13834595	-73.08074135

8/16/01 Cloudy 67

Survey of the South Fork of the Clearwater (Stites)							Translated Coordinates	
Description	+	HI	Y	Elevation	H.Deg	Radius	x (ft)	y (ft)
BM #1	-0.740	105.740		100.000	0.0000	265.330	-81.267	261.650
Rebar #1			-1.030	99.710	1.3858	264.375	-74.873	260.618
BM #2			-0.790	99.950	355.9842	284.985	-101.225	280.606
Rebar #2			-2.285	98.455	354.1442	288.325	-110.683	283.141
BM #3			-6.140	94.600	87.4208	81.320	-0.029	-0.020
BM #3			-6.140	94.600	87.4075	81.350	0.000	0.000
BM #3	-0.27	99.870		94.600	76.8114	68.175	0.000	0.000
BS US			-2.875	91.995	150.0942	52.820	-40.042	-61.341
WS US			-0.890	93.980	150.0950	52.865	-40.020	-61.381
Leg 1 US			-2.515	97.168	147.9081	51.130	-39.213	-58.872
Leg 3 US			-2.455	97.228	144.2053	52.885	-35.445	-58.451
Leg 4 US			-2.605	97.078	146.3658	56.730	-34.955	-62.788
ADV US			-4.140	95.543	149.6781	52.760	-39.741	-61.097
BS DS1			-2.800	92.070	141.1792	53.995	-32.528	-57.623
WS DS1			-0.980	93.890	141.1833	54.170	-32.421	-57.761
Leg 1 DS1			-2.515	97.168	139.0983	52.670	-31.890	-55.364
Leg 3 DS1			-2.470	97.213	135.5575	54.525	-28.199	-54.483
Leg 4 DS1			-2.505	97.178	137.8092	58.300	-27.222	-58.750
ADV DS1			-3.405	96.278	140.9500	54.240	-32.206	-57.677
BM #3	0.005	99.595		94.600	87.0819	67.560	0.000	0.000
LB US			1.160	95.755	261.9083	418.420	-481.727	-62.335
Chan x1			-0.080	94.515	256.2833	416.435	-472.031	-102.185
WS x1			1.505	96.100	256.2117	416.350	-471.824	-102.670
RB US			1.295	95.890	250.2425	423.600	-466.136	-146.633
Chan x2			-2.755	91.840	229.0425	83.185	-130.293	-57.967
WS x2			-0.565	94.030	229.0631	83.430	-130.498	-58.105
Chan x3			-2.735	91.860	214.8550	63.015	-103.486	-55.149
Chan x4			-2.820	91.775	177.5750	53.145	-65.224	-56.537
Chan x5			-2.755	91.840	144.5183	57.660	-34.004	-50.392
WS x5			-0.665	93.930	144.3014	58.690	-33.226	-51.101
Chan x6			-2.705	91.890	127.3367	89.125	3.390	-57.493
Chan x7			-2.290	92.305	115.5875	124.060	44.421	-57.019
Chan x8			-2.345	92.250	109.7014	152.525	76.124	-54.858
WS x8			-0.890	93.705	109.6486	152.615	76.256	-54.756
RB@Chan8			-1.280	93.315	127.8428	190.820	83.218	-120.507
LB@Chan8			-1.060	93.535	80.7733	134.220	65.011	18.082
Rock #1			-2.555	92.040	98.1233	371.270	300.072	-55.901
WS Rock #1			-1.595	93.000	98.1358	371.220	300.011	-55.975
T/Rock #1			-0.725	93.870	97.9683	370.500	299.450	-54.800
Chan x9			-3.595	91.000	93.4850	370.300	302.143	-25.949
WS x9			-1.465	93.130	93.4533	370.400	302.255	-25.751
x1-LB			-0.938	93.657	93.1108	20.680	-46.823	-4.562
x2			-1.685	92.910	119.1642	23.725	-46.755	-15.001
x3			-2.045	92.550	134.8883	29.720	-46.416	-24.414
x4			-2.225	92.370	145.6769	37.830	-46.142	-34.682
x5			-2.650	91.945	152.8428	46.480	-46.257	-44.795
x6			-2.855	91.740	157.2217	55.275	-46.072	-54.403
x6-WS			-0.575	94.020	157.1333	55.320	-45.976	-54.412
x7			-2.575	92.020	160.9192	65.240	-46.145	-65.095
x8			-2.835	91.760	163.5125	74.125	-46.435	-74.516
x9			-2.090	92.505	165.9925	88.515	-46.047	-89.322
x10			-1.590	93.005	167.3967	98.685	-45.939	-99.746
RB			-0.950	93.645	168.5858	109.605	-45.782	-110.877
T/Rock #2			-0.025	94.570	153.8000	55.490	-42.973	-53.228
Up Rock #2			-2.780	91.815	155.8058	54.790	-45.018	-53.417
Down Rock #2			-2.615	91.980	152.5358	56.860	-41.249	-53.891
Right Rock #2			-2.635	91.960	155.0900	57.360	-43.313	-55.463
Left Rock #2			-2.915	91.680	153.6383	54.530	-43.259	-52.299
Flag			-2.5	92.095	128.8658	78.085	-6.674	-52.438

8/22/01 Cloudy 67

Survey of the Lochsa River (Agdar Campground)					Original Coordinates			
Description	+	Hl	Y	Elevation	H.Deg	Radius	x (ft)	y (ft)
BM #4	1.985	98.203		100.000	27.5000	42.170	19.472	37.405
BM #5			1.935	95.138	313.3875	38.780	-28.182	26.639
WS Upstream			-1.970	91.233	201.2686	76.460	-27.735	-71.252
BS Upstream			-2.120	91.083	201.7633	76.395	-28.325	-70.950
Leg 2 Upstream			-2.010	96.005	202.9442	74.700	-29.121	-68.790
Leg 3 Upstream			-2.400	95.615	204.7303	79.915	-33.432	-72.586
Leg 4 Upstream			-2.145	95.870	205.6833	75.750	-32.830	-68.266
ADV Upstream			-3.040	94.975	201.8967	76.565	-28.554	-71.041
WS DS1			-0.720	92.483	210.0975	77.695	-38.962	-67.220
BS DS1			-2.615	90.588	209.9808	79.08	-39.517	-68.499
Leg 2 DS1			-2.620	95.395	210.8258	77.39	-39.657	-66.457
Leg 4 DS1			-2.095	95.920	213.4683	78.46	-43.269	-65.451
Leg 3 DS1			-1.655	96.360	212.5453	82.62	-44.447	-69.646
ADV DS1			-3.295	94.720	209.7786	79.355	-39.412	-68.876
ADV DS2			-3.220	94.795	210.6672	78.965	-40.276	-67.921
ADV DS3			-3.545	94.470	212.2261	79.495	-42.392	-67.249
ADV DS4			-3.165	94.850	214.4033	80.315	-45.379	-66.266
ADV DS5			-3.130	94.885	216.3419	82.09	-48.647	-66.123
BM #5			1.940	95.143	313.4417	38.78	-28.157	26.666
RB #1			-0.625	92.578	195.3867	21.035	-5.581	-20.281
RB #2			-0.320	92.883	120.2983	107.255	92.605	-54.110
RB #3			0.150	93.353	110.8950	240.345	224.539	-85.721
CL 1			-2.240	90.963	130.2433	278.37	212.482	-179.837
WS 1			0.000	93.203	130.2317	278.54	212.648	-179.903
LB 1			0.135	93.338	137.4383	301.56	203.970	-222.114
LB 2			-0.225	92.978	148.2117	238.27	125.517	-202.529
CL 2			-2.985	90.218	146.0983	218.335	121.781	-181.217
WS 2			-0.195	93.008	146.0417	218.44	122.018	-181.184
LB 3			-0.715	92.488	202.0300	186.4	-69.917	-172.790
LB 4			-0.905	92.298	228.2483	222.885	-166.281	-148.420
CL 3			-4.775	88.428	241.8839	179.915	-158.684	-84.787
LB 4			-0.890	92.313	246.9417	336.785	-309.878	-131.908
CL 4			-5.015	88.188	255.9333	313.98	-304.565	-76.313
WS 4			-0.885	92.318	256.0950	313.505	-304.318	-75.339
RB 4			-0.885	92.318	280.2817	273.5	-269.108	48.816
RB 5			-0.950	92.253	281.2100	166.585	-163.407	32.385
RBx5			-0.805	92.398	247.8217	28.825	-26.692	-10.881
x5-2			-1.825	91.378	222.6883	49.865	-33.809	-36.653
x5-3			-2.000	91.203	218.1383	60.63	-37.443	-47.687
x5-4			-1.995	91.208	215.3050	70.02	-40.467	-57.142
Rock #2			-0.680	92.523	210.1933	71.155	-35.785	-61.502
x5-5a			-2.315	90.888	212.1467	80.5	-42.833	-68.158
R1-LF			-3.305	89.898	206.6856	81.78	-36.727	-73.069
R1-RF			-2.665	90.538	207.9683	78.965	-37.033	-69.742
R1-LB			-2.280	90.923	208.5517	83.545	-39.930	-73.385
R1-RB			-2.415	90.788	209.6533	80.38	-39.768	-69.853
R1-Top			-0.310	92.893	208.4367	80.995	-38.569	-71.222
x5-5			-2.960	90.243	210.3800	90.25	-45.642	-77.858
x5-6			-2.875	90.328	209.2650	100.665	-49.210	-87.817
x5-7			-3.115	90.088	208.1083	110.215	-51.927	-97.216
x5-8			-3.850	89.353	207.7650	113.89	-53.055	-100.777
x5-9			-2.965	90.238	207.8983	120.515	-56.389	-106.509
x5-10			-4.495	88.708	205.7633	131.4	-57.114	-118.338
x5-11			-3.485	89.718	204.7183	144.11	-60.261	-130.906
x5-12			-2.400	90.803	204.0933	156.18	-63.756	-142.574
x5-13			-1.605	91.598	204.1633	171.45	-70.181	-156.428
x5-LB			-0.770	92.433	202.7750	185.855	-71.947	-171.364

USGS GAUGING STATION RESULTS

Date	Stream Flow	Stream Flow	ΔQ	Work Day	ΔQ
	ft ³ /s	m ³ /s	m ³ /s/day	day	m ³ /s/work day
USGS Gauge 13338500 Near Stites Idaho					
7/24/01	375	10.62	0.00		
7/25/01	355	10.05	-0.57		
7/26/01	339	9.60	-0.45		
7/27/01	326	9.23	-0.37	0.25	-0.09
7/28/01	311	8.81	-0.42		
7/29/01	302	8.55	-0.25		
7/30/01	307	8.69	0.14		
7/31/01	404	11.44	2.75		
8/1/01	447	12.66	1.22	0.29	0.35
8/2/01	356	10.08	-2.58		
8/3/01	312	8.84	-1.25		
8/4/01	288	8.16	-0.68		
8/5/01	289	8.18	0.03		
8/6/01	284	8.04	-0.14		
8/7/01	264	7.48	-0.57	0.43	-0.24
8/8/01	248	7.02	-0.45		
8/9/01	238	6.74	-0.28		
8/10/01	229	6.48	-0.25		
8/11/01	221	6.26	-0.23		
8/12/01	213	6.03	-0.23		
8/13/01	209	5.92	-0.11		
8/14/01	203	5.75	-0.17		
8/15/01	198	5.61	-0.14		
8/16/01	190	5.38	-0.23	0.25	-0.06
8/17/01	183	5.18	-0.20		
8/18/01	177	5.01	-0.17		
USGS Gauge 13337000 on the Lochsa River Near Adgar Campground					
8/16/01	457	12.94	0.00		
8/17/01	442	12.52	-0.42		
8/18/01	431	12.21	-0.31		
8/19/01	419	11.87	-0.34		
8/20/01	411	11.64	-0.23		
8/21/01	406	11.50	-0.14		
8/22/01	400	11.33	-0.17	0.25	-0.04
8/23/01	399	11.30	-0.03		
8/24/01	395	11.19	-0.11		
8/25/01	388	10.99	-0.20		
8/26/01	378	10.70	-0.28		

Table B1. USGS Gauging Station Results for Each Sampling Event. (USGS 2002)

WOLMAN METHOD RESULTS

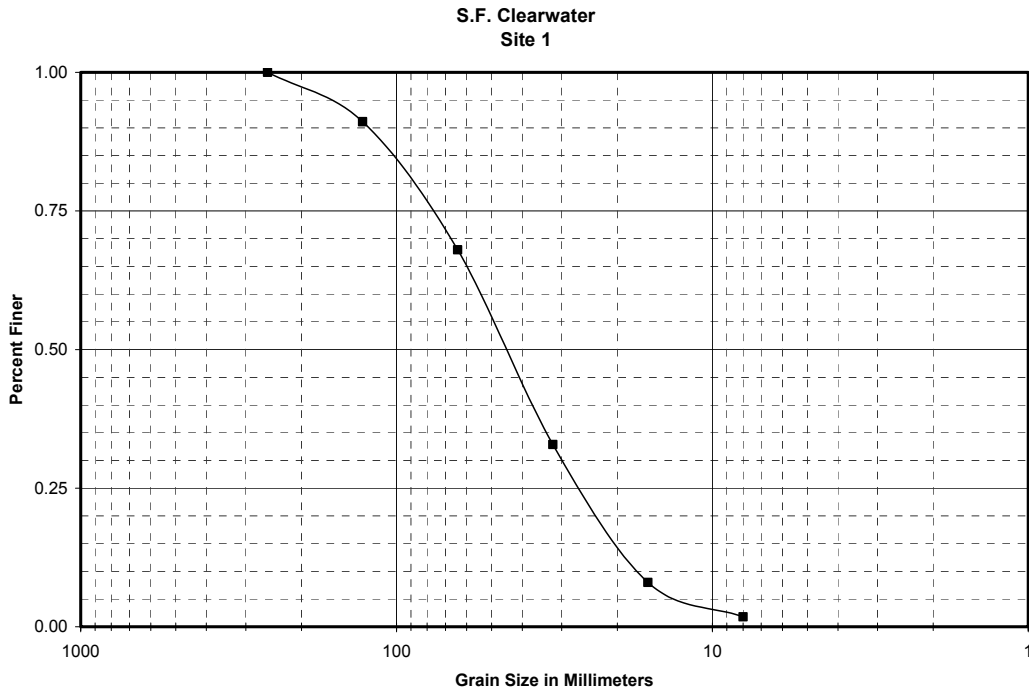


Figure B5. Grain Size Distribution, Boulder A - S.F. Clearwater. (Wolman, 1954)

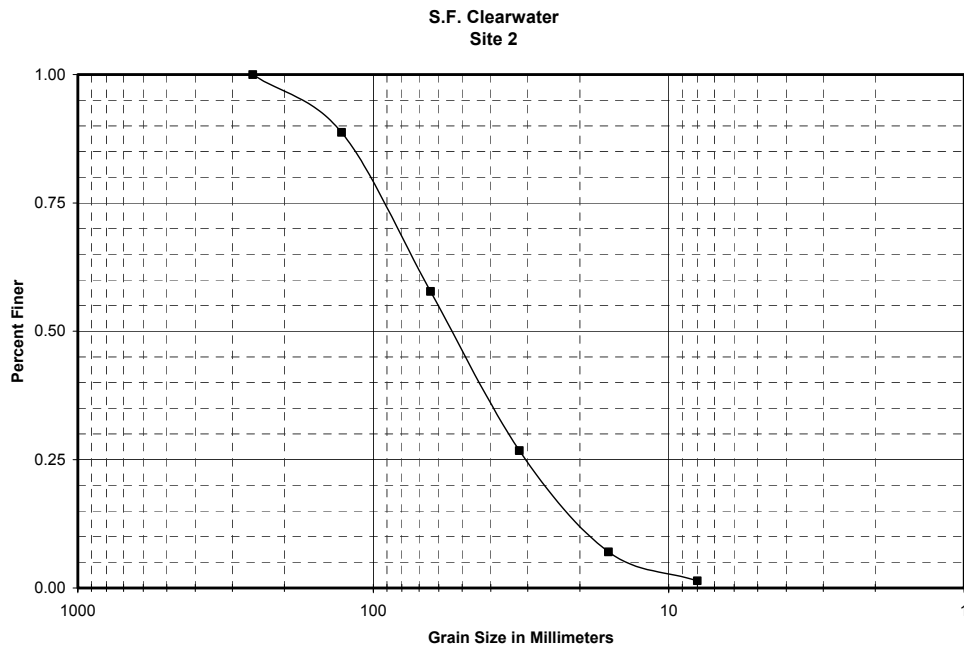


Figure B6. Grain Size Distribution, Boulder B - S.F. Clearwater. (Wolman, 1954)

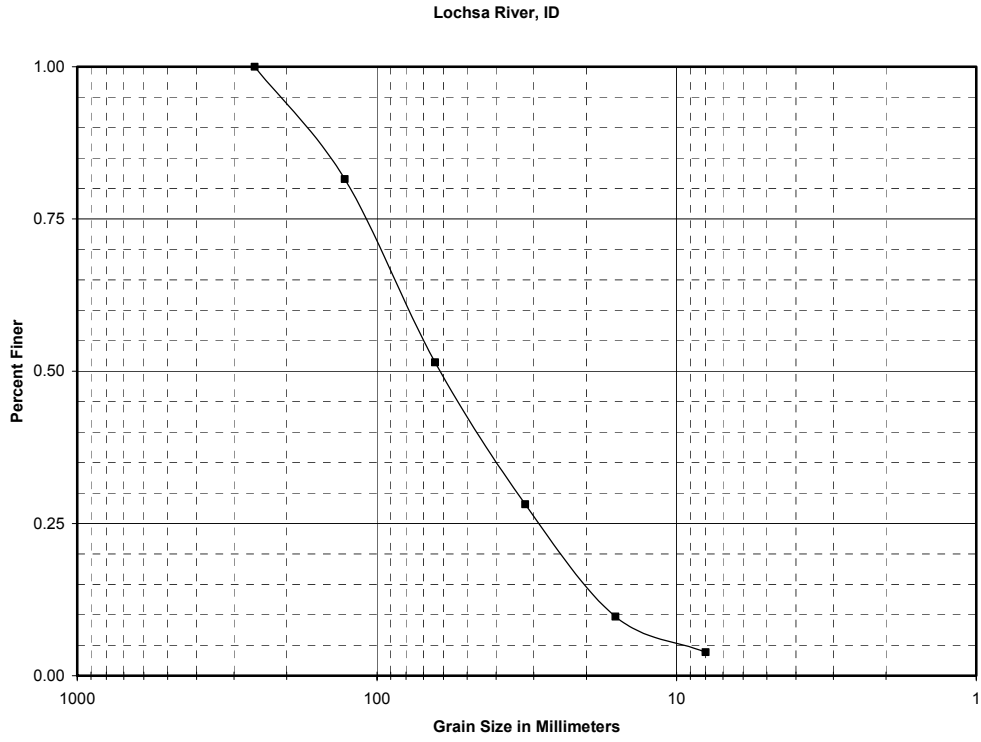


Figure B7. Grain Size Distribution, Boulder C – Lochsa River. (Wolman, 1954)

SHEAR VELOCITY CALCULATIONS

There are many methods for determining the shear velocity, U_* . The most common method for determining the global shear velocity is:

$$U_* = \sqrt{gHS} \quad (B1)$$

where g is the gravitational acceleration constant, H is the water depth (the hydraulic radius is the more exact term, but for large aspect ratios the depth is appropriate), S is the bed slope. This method gives a spatially averaged shear velocity for the entire reach (Results from this method are provided in Table B2). The most common method for determining the local shear velocity is:

$$U_* = \frac{\sqrt{-\overline{u'w'}}}{\sqrt{1 - \left(\frac{z}{H}\right)}} \quad (B2)$$

where $\overline{u'w'}$ is the time averaged Reynolds shear stress tensor in the u - w plane and z is the distance from the bed. Determination of U_* for $z = 0$ requires extrapolation of the vertical Reynolds shear stress tensor profile to the bed (Figure B8). Local shear velocity results are presented in Table B2.

Date	Global	Local
Equation	$U_* = \sqrt{gHS}$	$U_* = \frac{\sqrt{-\overline{u'w'}}}{\sqrt{1 - \left(\frac{z}{H}\right)}}$
Units	(cm/s)	(cm/s)
7/27	8.51	3.29
8/1	10.31	5.04
8/7	8.18	4.65
8/16	13.42	5.99
8/22	12.68	5.24

Table B2. Global and Local Shear Stress Values for Each Sample Date. (Nezu and Nakagawa, 1993).

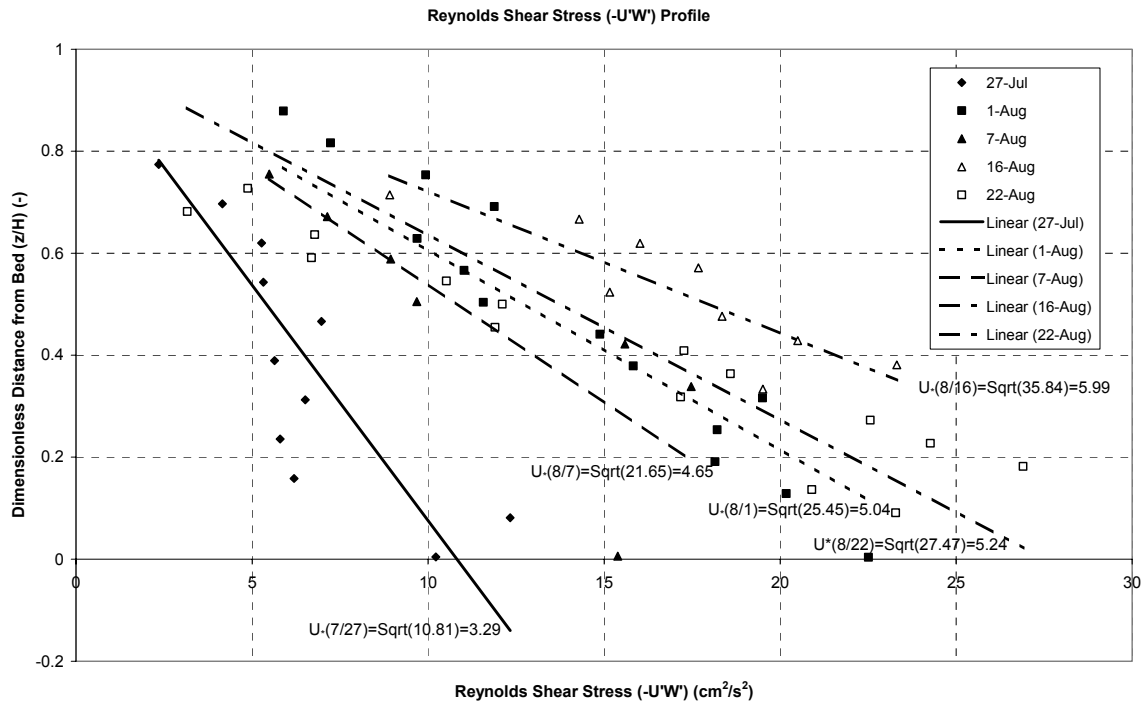


Figure B8. Determination of Local U_{*} . (Nezu and Nakagawa, 1993).

RELATIVE ROUGHNESS AND COLES' PARAMETER CALCULATIONS

The streamwise velocity distribution for each sample date fit the Log-Wake Law:

$$\frac{u}{U_*} = \frac{1}{\kappa} \ln\left(\frac{z}{k_s}\right) + 8.5 + \frac{2\Pi}{\kappa} \sin^2\left(\frac{\pi z}{2h}\right) \quad (\text{B3})$$

where u is the time averaged streamwise velocity at a point, U_* is the shear velocity calculated in the previous section, κ is the Von Karman Constant taken as 0.41, k_s is the relative roughness coefficient taken, Π is Coles' Parameter, z is the depth above the bed, and h is the total depth.

The relative roughness, k_s , and Coles Parameter, Π , can be determined by curve fitting each vertical profile. The relative roughness affects the slope of the curve fit while Coles' Parameter affects the translation of the curve fit. The velocity profiles along with the curve fit line and individual relative roughness and Coles' Parameters are presented in Figures B9-B13.

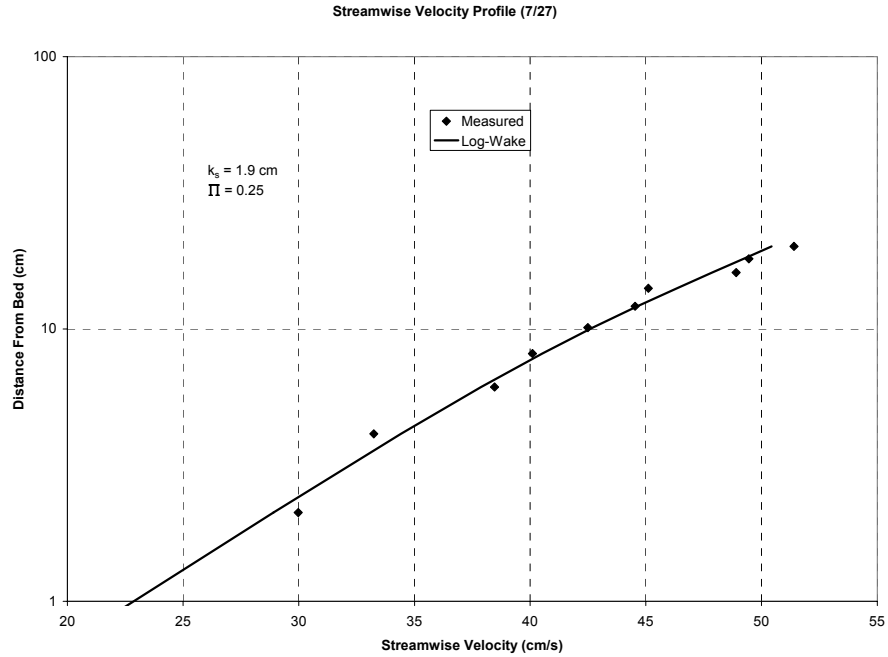


Figure B9. Streamwise Velocity Distribution, Relative Roughness, and Coles' Parameter on 7/27/01.

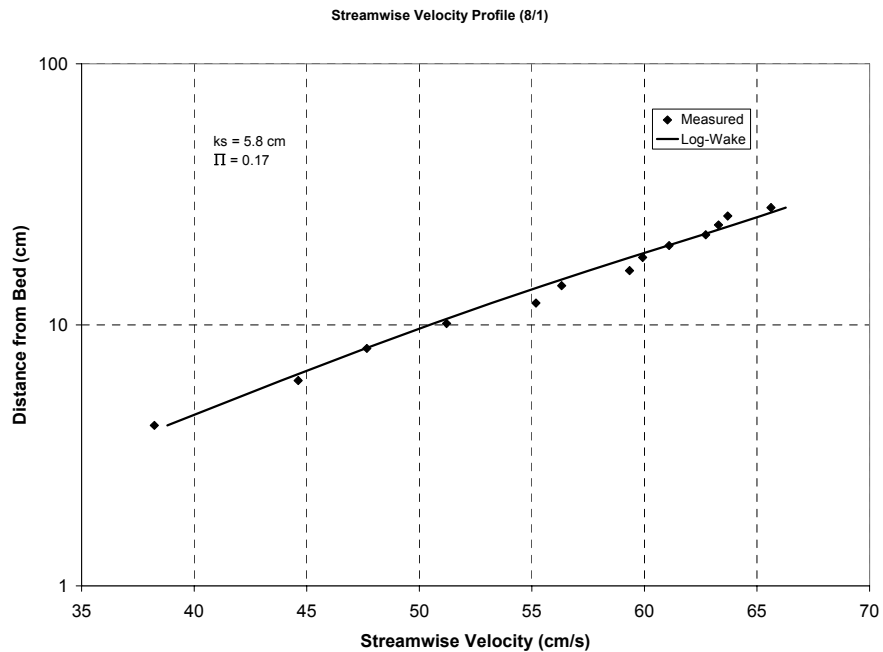


Figure B10. Streamwise Velocity Distribution, Relative Roughness, and Coles' Parameter on 8/1/01.

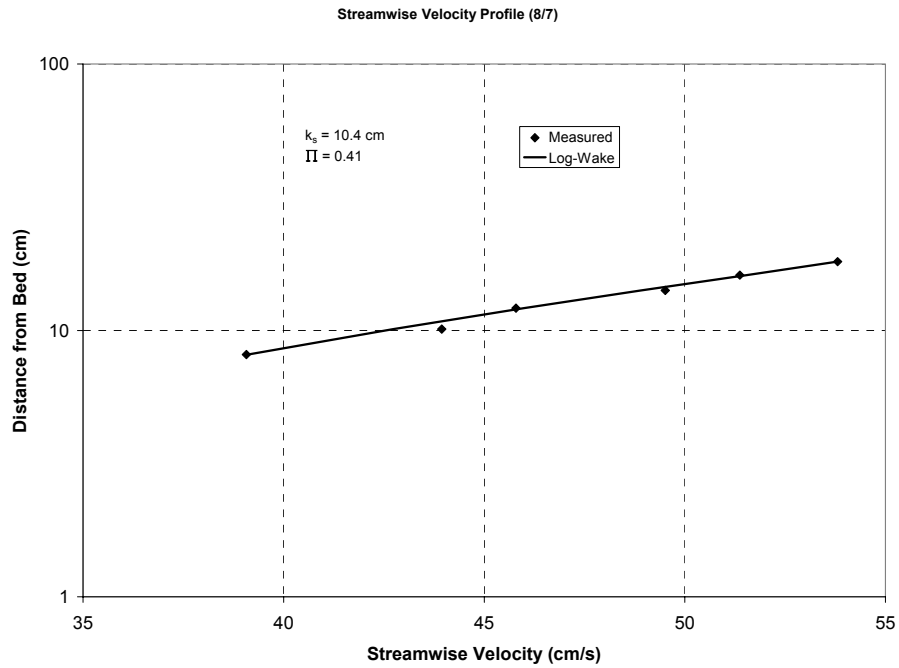


Figure B11. Streamwise Velocity Distribution, Relative Roughness, and Coles' Parameter on 8/7/01.

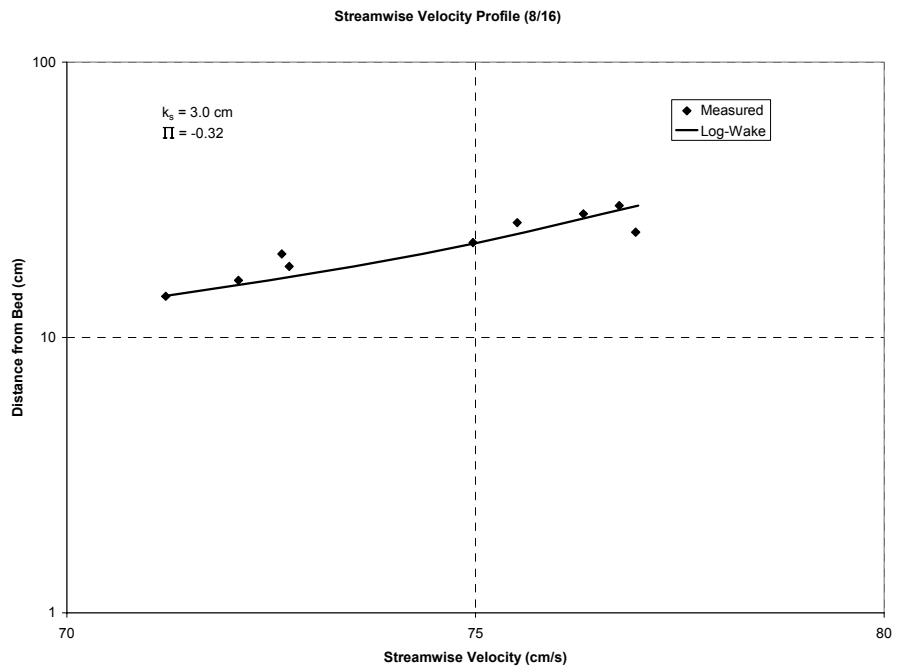


Figure B12. Streamwise Velocity Distribution, Relative Roughness, and Coles' Parameter on 8/16/01.

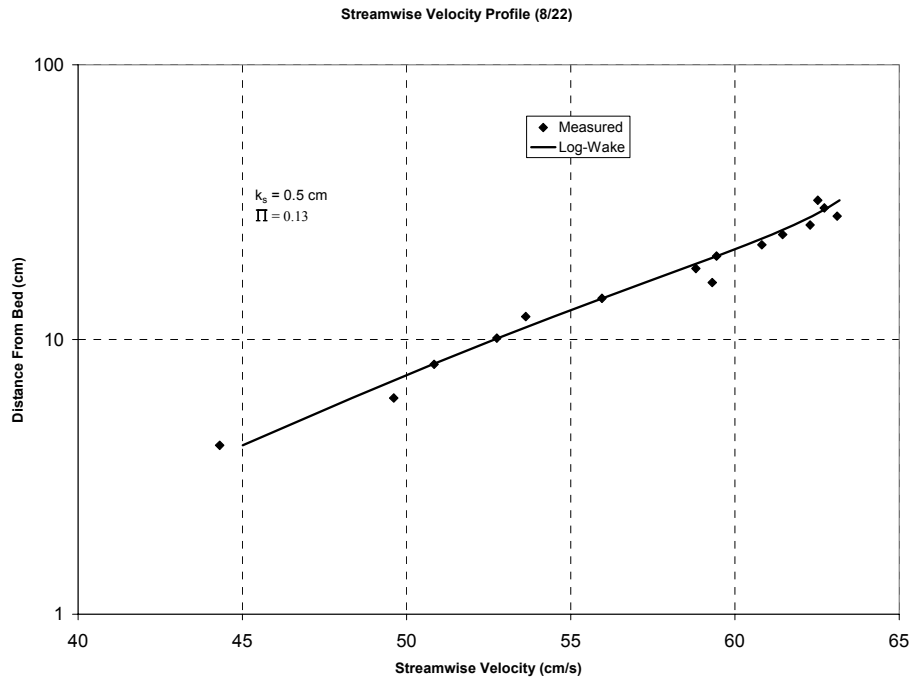


Figure B13. Streamwise Velocity Distribution, Relative Roughness, and Coles' Parameter on 8/22/01.

INCIPIENT MOTION CALCULATIONS

Determination of incipient motion for the mean particle size (d_{50}) at each of the sample locations can be achieved by using the Shields Diagram (Chang, 1992). While the Shields Method is not robust enough for determination of sediment load or scour depths it does provide an accurate estimation for whether mean particle sizes will move. The Shields Method provides the critical shear stress for incipient motion allowing the engineer to compare the critical shear stress to the measured shear stress. The steps for calculation of incipient motion are listed below.

1. Determine the ASCE Sedimentation Manual Parameter (1975): $\frac{d_{50}}{\nu} \sqrt{0.1 \left(\frac{\gamma_s}{\gamma} - 1 \right) g d_{50}}$

where ν is the eddy viscosity, γ_s is the specific weight of sediment (assumed to be 2.65), γ is the specific weight of water (assumed to be 1), and g is gravity (9.81 m/s²).

2. Determine the dimensionless critical shear stress from the Shields Diagram (Chang, 1992).
3. Calculate the critical shear stress from: $\tau_c = \tau_{*c} (\gamma_s - \gamma) d_{50}$

where τ_c is the critical shear stress and τ_{*c} is the dimensionless critical shear stress.

4. Calculate the bed shear stress: $\tau_0 = -\overline{\rho u' w'_0}$

where τ_0 is the bed shear stress, ρ is the fluid density (taken as 1000 kg/m³), and $\overline{u' w'_0}$ is the Reynolds shear stress tensor at the bed. The Reynolds shear stress tensor at the bed is shown in Figure B8.

The bed shear stress and critical shear stress values for each sample date along with all intermediate results are shown in Table B3. Each of the critical shear stress values is larger than the measured bed shear stress therefore incipient motion was not achieved during any of the sample dates.

Date	Units	7/27	8/1	8/7	8/16	8/22
d_{50}	mm	48	48	48	55	62
$-u'w'$	cm^2/s^2	10.8	25.5	21.7	27.5	35.8
ASCE Parameter	1	1.3E+04	1.3E+04	1.3E+04	1.6E+04	2.0E+04
\mathcal{T}^*_{c}	1	0.06	0.06	0.06	0.06	0.06
$\mathcal{T}_{0\text{c}}$	N/m^2	46.6	46.6	46.6	53.4	60.2
\mathcal{T}_0	N/m^2	1.1	2.5	2.2	2.7	3.6

Table B3. Incipient Motion Calculations. For Equations and discussion of parameters see proceeding text.

TURBULENCE DATA MANIPULATION PROCESS FOR

POINT 8-16-8-14

Raw ADV Data

The data that was collected by the SonTek ADV was saved in ASCII format as *.adv files. These files were output from WinADV without filtering as tab delimited files that could be viewed in spreadsheet form as shown in Table B4. The following tables will only show the first twenty five time instances collected at point 8-16-8-14. The complete raw and summary files for each sample point are presented in CD format in Appendix D.

Processed by: WinADV32 - Version 1.843 (October 2, 2000)
 Filename = 8_16_8
 Filtering = Unfiltered
 Scaling Options = Raw data
 WinADV Units = Metric

Time	Flag	Vx_1	Vy_1	Vz_1	COR0_1	COR1_1	COR2_1	SNR0_1	SNR1_1	SNR2_1
2036.74	14	4.66	-21.32	-6.06	94	91	94	16.8	15.9	15.9
2036.78	14	11.16	-20.72	-6.28	95	96	95	17.6	21.1	20.6
2036.82	14	9.72	-21.1	-3.66	95	90	95	11.6	12.9	13.8
2036.86	14	9.98	-12.12	0.94	97	95	96	19.8	16.8	17.6
2036.9	14	16.5	-12.26	1.76	96	95	95	15.5	12.9	15.9
2036.94	14	9.94	-14.68	6.62	85	81	86	10.8	12.9	12
2036.98	14	13.16	-21.62	10.66	86	91	86	12.9	12.9	15.9
2037.02	14	14.28	-19.62	18.88	74	73	84	13.3	17.6	18.5
2037.06	14	14.68	-26.66	18.02	90	88	92	25.8	30.5	33.1
2037.1	14	2.74	-16.36	9.22	93	92	89	19.4	17.2	20.2
2037.14	14	3.56	-17.58	7.86	93	92	96	18.1	15.9	21.1
2037.18	14	-8.9	-15.32	4	89	96	94	21.5	22.4	24.1
2037.22	14	-7.82	-10.72	4.44	96	97	97	22.8	20.6	29.2
2037.26	14	-4.38	-2.52	2.92	97	97	97	19.8	20.2	27.5
2037.3	14	-8.46	3.36	1.8	97	94	96	29.2	24.1	27.1
2037.34	14	-5	12.02	3.12	93	94	95	25.8	24.5	21.9
2037.38	14	-0.74	12.04	-4.38	90	92	93	17.6	15.5	17.6
2037.42	14	-6.04	9.3	-7.54	96	93	95	21.1	19.4	24.5
2037.46	14	-8.6	1.7	-11.02	91	88	91	18.9	21.1	25.4
2037.5	14	-2.96	2.88	-13.34	92	91	90	16.8	15.9	18.5
2037.54	14	-12.28	-0.1	-13.64	91	88	93	16.8	18.9	21.5
2037.58	14	-6	11.84	-11.88	92	96	93	22.8	25.4	26.7
2037.62	14	-25.62	8.5	-8.38	90	47	48	12	12	12
2037.66	14	9.58	2.1	-7.86	84	84	88	9.5	12	12.5
2037.7	14	-14.16	15.08	-7.92	94	93	89	14.6	15.9	20.6

Table B4. Raw ADV Data For Point 8-16-8-14.

Filtered ADV Data

Filtering for Signal to Noise Ratio and Correlation could also be conducted using WinADV. All data was with a Signal to Noise Ratio less than 10 or Correlation less than 70 were removed. Data highlighted in Table B4 were removed resulting in Table B5.

Processed by: WinADV32 - Version 1.843
 (October 2, 2000)
 Filename = 8_16_8
 Filtering = AvgCOR>70; AvgSNR>10
 Sampling Options = All samples
 Scaling Options = Raw data
 WinADV Units = Metric

Time	Flag	Vx_1	Vy_1	Vz_1	COR0_1	COR1_1	COR2_1	SNR0_1	SNR1_1	SNR2_1
2036.74	14	4.66	-21.32	-6.06	94	91	94	16.8	15.9	15.9
2036.78	14	11.16	-20.72	-6.28	95	96	95	17.6	21.1	20.6
2036.86	14	9.98	-12.12	0.94	97	95	96	19.8	16.8	17.6
2037.02	14	14.28	-19.62	18.88	74	73	84	13.3	17.6	18.5
2037.06	14	14.68	-26.66	18.02	90	88	92	25.8	30.5	33.1
2037.1	14	2.74	-16.36	9.22	93	92	89	19.4	17.2	20.2
2037.14	14	3.56	-17.58	7.86	93	92	96	18.1	15.9	21.1
2037.18	14	-8.9	-15.32	4	89	96	94	21.5	22.4	24.1
2037.22	14	-7.82	-10.72	4.44	96	97	97	22.8	20.6	29.2
2037.26	14	-4.38	-2.52	2.92	97	97	97	19.8	20.2	27.5
2037.3	14	-8.46	3.36	1.8	97	94	96	29.2	24.1	27.1
2037.34	14	-5	12.02	3.12	93	94	95	25.8	24.5	21.9
2037.38	14	-0.74	12.04	-4.38	90	92	93	17.6	15.5	17.6
2037.42	14	-6.04	9.3	-7.54	96	93	95	21.1	19.4	24.5
2037.46	14	-8.6	1.7	-11.02	91	88	91	18.9	21.1	25.4
2037.5	14	-2.96	2.88	-13.34	92	91	90	16.8	15.9	18.5
2037.54	14	-12.28	-0.1	-13.64	91	88	93	16.8	18.9	21.5
2037.58	14	-6	11.84	-11.88	92	96	93	22.8	25.4	26.7
2037.7	14	-14.16	15.08	-7.92	94	93	89	14.6	15.9	20.6
2037.74	14	7.2	13.04	-17.12	86	80	74	18.5	17.2	18.5
2037.78	14	-17.8	3.02	-11.9	81	92	87	11.6	16.3	19.4
2037.9	14	-28.36	4.48	-19.4	88	93	92	19.8	23.2	24.5
2037.98	14	-12.48	-0.8	-14.76	85	85	80	15.1	14.6	17.2
2038.02	14	-24.36	-4.18	-12.24	92	94	94	21.1	24.5	25.8
2038.06	14	-21.26	6.86	-11.66	79	89	49	15.5	16.3	16.3

Table B5. Filtered ADV Data For Point 8-16-8-14.

Rotated and Filtered ADV Data

Data were rotated such that the x-axis on a cartesian coordinate system was oriented with the mean streamwise velocity in the upstream velocity profile. For data collected in the upstream velocity profile data were rotated such that the mean transverse velocity was null while the mean vertical velocity was maximum (rotate such that α in Figure B14 is zero). Data collected behind the boulders were rotated to the same orientation as the upstream velocity profile. Proper orientation of the data downstream from the boulder was achieved by adding the rotation angle of the upstream data to the angle between each stand setup (Figure B14).

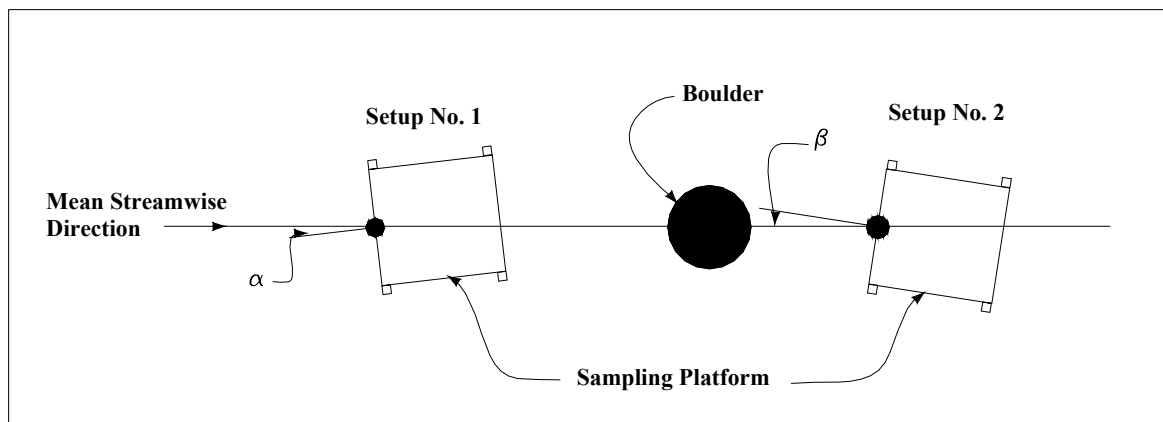


Figure B14. Data Rotation Angles for Orientation to Mean Streamwise Direction.

The rotated data is presented in Table B6. The instantaneous velocity angle in the horizontal plane is calculated in Column G. A correction factor is necessary when the streamwise velocity is less than zero (Column F) to account for the inverse tangent function acting over the 0 to π domain. The magnitude of the horizontal velocity is calculated in Column H. The rotation angle (7.74 degrees for point 8-16-8-14) is subtracted from the original angle of attack in Column I. Individual rotated velocity components are then recalculated in Columns J

and K. The stand was designed such that it was leveled with the earth based on bubble levels. Mean z values are therefore very close to zero. Data collected upstream from the obstruction were rotated about the y-axis in a similar manner to the rotation below. All time averaged vertical velocities behind the obstruction were assumed to be related to the obstruction influence.

Time	Flag	Vx_1	Vy_1	Vz_1	Correction	Angle	X-Y Mag	Rotated	Rotated	Rotated
					Factor			Angle	Vx	Vy
[A]	[B]	[C]	[D]	[E]	[F]	[G]	[H]	[I]	[J]	[K]
		cm/s	cm/s	cm/s	1	radians	cm/s	radians	cm/s	cm/s
2036.78	14	11.16	-20.72	-6.28	0	-1.07	23.53	-1.21	8.26	-22.03
2036.86	14	9.98	-12.12	0.94	0	-0.88	15.70	-1.01	8.25	-13.35
2037.02	14	14.28	-19.62	18.88	0	-0.94	24.26	-1.07	11.50	-21.36
2037.06	14	14.68	-26.66	18.02	0	-1.06	30.43	-1.20	10.95	-28.39
2037.1	14	2.74	-16.36	9.22	0	-1.40	16.58	-1.53	0.51	-16.58
2037.14	14	3.56	-17.58	7.86	0	-1.37	17.93	-1.50	1.159	-17.89
2037.18	14	-8.9	-15.32	4	3.14	4.18	17.71	4.05	-10.88	-13.98
2037.22	14	-7.82	-10.72	4.44	3.14	4.08	13.26	3.94	-9.19	-9.56
2037.26	14	-4.38	-2.52	2.92	3.14	3.66	5.05	3.52	-4.67	-1.90
2037.3	14	-8.46	3.36	1.8	3.14	2.76	9.10	2.62	-7.93	4.46
2037.34	14	-5	12.02	3.12	3.14	1.96	13.0	1.82	-3.33	12.58
2037.38	14	-0.74	12.04	-4.38	3.14	1.63	12.06	1.49	0.88	12.02
2037.42	14	-6.04	9.3	-7.54	3.14	2.14	11.08	2.01	-4.73	10.02
2037.46	14	-8.6	1.7	-11.02	3.14	2.94	8.76	2.81	-8.29	2.84
2037.5	14	-2.96	2.88	-13.34	3.14	2.36	4.12	2.23	-2.54	3.25
2037.54	14	-12.28	-0.1	-13.64	3.14	3.14	12.28	3.01	-12.18	1.55
2037.58	14	-6	11.84	-11.88	3.14	2.03	13.27	1.90	-4.35	12.54
2037.7	14	-14.16	15.08	-7.92	3.14	2.32	20.68	2.18	-12.00	16.84
2037.74	14	7.2	13.04	-17.12	0	1.06	14.89	0.93	8.89	11.95
2037.78	14	-17.8	3.02	-11.9	3.14	2.97	18.05	2.83	-17.23	5.38
2037.9	14	-28.36	4.48	-19.4	3.14	2.98	28.71	2.84	-27.49	8.25
2037.98	14	-12.48	-0.8	-14.76	3.14	3.20	12.50	3.07	-12.47	0.88
2038.02	14	-24.36	-4.18	-12.24	3.14	3.31	24.71	3.17	-24.70	-0.86
2038.06	14	-21.26	6.86	-11.66	3.14	2.82	22.33	2.69	-20.14	9.66
2038.1	14	-34.26	9.02	-2.82	3.14	2.88	35.42	2.74	-32.73	13.55

Table B6. Rotated Data for Point 8-16-8-14.

Output from FORTRAN-90 Program

The rotated and filtered data was processed using a FORTRAN-90 program. The point files were input by calling a batch file. The batch file expedited the calculation process and allowed for calculation of spatial parameters such as strain. The batch file for the cross section collected behind Boulder B (from which sample 8-16-8-14 is a single point) is provided as Table B7.

The output from this batch file is shown in Table B8. The equations used for calculation of the turbulent intensities, turbulent kinetic energy, strain, and Reynolds shear stresses are presented in the Background and Methods Sections of the main text.

South Fork Clearwater X-Section.

date	setup no	input file	output file	flag	time	location
08.16.01	2	sfu8.prn	startblank	0	120	105
08.16.01	2	sfu8.prn	sf81680.prn	0	120	0
08.16.01	2	sfu8.prn	sf81682.prn	2	120	10
08.16.01	2	sfu8.prn	sf81684.prn	4	120	20
08.16.01	2	sfu10b.prn	sf8161044.prn	44	120	25
08.16.01	2	sfu10b.prn	sf8161046.prn	46	120	28
08.16.01	2	sfu8.prn	sf81686.prn	6	120	30
08.16.01	2	sfu10b.prn	sf8161042.prn	42	120	32
08.16.01	2	sfu10b.prn	sf8161040.prn	40	120	34
08.16.01	2	sfu10b.prn	sf8161038.prn	38	120	36
08.16.01	2	sfu10b.prn	sf8161036.prn	36	120	38
08.16.01	2	sfu8.prn	sf81688.prn	8	120	40
08.16.01	2	sfu10b.prn	sf8161034.prn	34	120	41
08.16.01	2	sfu10b.prn	sf8161032.prn	32	120	42
08.16.01	2	sfu10a.prn	sf8161030.prn	30	120	43
08.16.01	2	sfu10a.prn	sf8161028.prn	28	120	44
08.16.01	2	sfu10a.prn	sf8161026.prn	26	120	45
08.16.01	2	sfu10a.prn	sf8161024.prn	24	120	46
08.16.01	2	sfu10a.prn	sf8161022.prn	22	120	47
08.16.01	2	sfu10a.prn	sf8161020.prn	20	120	48
08.16.01	2	sfu10a.prn	sf8161018.prn	18	120	49
08.16.01	2	sfu5.prn	sf81650.prn	0	120	50
08.16.01	2	sfu10a.prn	sf8161016.prn	16	120	51
08.16.01	2	sfu10a.prn	sf8161014.prn	14	120	52
08.16.01	2	sfu10a.prn	sf8161012.prn	12	120	53
08.16.01	2	sfu10a.prn	sf8161010.prn	10	120	54
08.16.01	2	sfu10a.prn	sf8161008.prn	8	120	55
08.16.01	2	sfu10a.prn	sf8161006.prn	6	120	56
08.16.01	2	sfu10a.prn	sf8161004.prn	4	120	57
08.16.01	2	sfu10a.prn	sf8161002.prn	2	120	58
08.16.01	2	sfu10a.prn	sf816100.prn	0	120	59
08.16.01	2	sfu9a.prn	sf81690.prn	0	120	61
08.16.01	2	sfu9a.prn	sf81692.prn	2	120	62
08.16.01	2	sfu9a.prn	sf81694.prn	4	120	63
08.16.01	2	sfu9a.prn	sf81696.prn	6	120	64
08.16.01	2	sfu9a.prn	sf81698.prn	8	120	65
08.16.01	2	sfu9a.prn	sf816910.prn	10	120	66
08.16.01	2	sfu9a.prn	sf816912.prn	12	120	67
08.16.01	2	sfu9a.prn	sf816914.prn	14	120	68
08.16.01	2	sfu9a.prn	sf816916.prn	16	120	69
08.16.01	2	sfu9a.prn	sf816918.prn	18	120	71
08.16.01	2	sfu9a.prn	sf816920.prn	20	120	72
08.16.01	2	sfu9a.prn	sf816922.prn	22	120	73
08.16.01	2	sfu9a.prn	sf816924.prn	24	120	74
08.16.01	2	sfu9a.prn	sf816926.prn	26	120	75
08.16.01	2	sfu9a.prn	sf816928.prn	28	120	76
08.16.01	2	sfu9b.prn	sf816930.prn	30	120	77
08.16.01	2	sfu9b.prn	sf816932.prn	32	120	78
08.16.01	2	sfu9b.prn	sf816934.prn	34	120	79
08.16.01	2	sfu8.prn	sf816814.prn	14	120	80
08.16.01	2	sfu9b.prn	sf816936.prn	36	120	82
08.16.01	2	sfu9b.prn	sf816938.prn	38	120	84
08.16.01	2	sfu9b.prn	sf816940.prn	40	120	86
08.16.01	2	sfu9b.prn	sf816942.prn	42	120	88
08.16.01	2	sfu8.prn	sf816816.prn	16	120	90
08.16.01	2	sfu9b.prn	sf816944.prn	44	120	95
08.16.01	2	sfu8.prn	sf816818.prn	18	120	100
08.16.01	2	sfu8.prn	endblank	18	120	105

00.00.00

Table B7. Example Batch Input File for FORTRAN-90 Program. This batch file represents the data collected behind Boulder B from which 8-16-8-14 is a single point.

South Fl earwater X-Sion.

Date	Input file	output file	FL	Time	Loc	X Mean	Y Mean	Z Mean	X TI	Y TI	Z TI	Strain	TKE	-U'V'	-U'W'	-V'W'
					cm	cm/s	cm/s	cm/s	cm/s	cm/s	cm/s	s ⁻¹	cm ² /s ²			
8.16.1	sfu8.prn	sf81680.prn	0	120	0	72.03	-1.98	-0.96	7.92	6.67	5.28		104.17	12.53	20.94	-2.28
8.16.1	sfu8.prn	sf81682.prn	2	120	10	71.08	-2.28	-0.45	7.82	6.52	5.25	0.05	100.70	5.73	24.10	-0.28
8.16.1	sfu8.prn	sf81684.prn	4	120	20	73.06	-0.94	-1.4	7.31	6.62	4.72	0.35	94.62	-8.87	18.54	0.53
8.16.1	sfu10b.prn	sf8161044.prn	44	120	25	76.28	-1.85	-3.37	6.87	6.90	4.82	0.60	93.90	-7.29	16.19	-2.00
8.16.1	sfu10b.prn	sf8161046.prn	46	120	28	77.82	-0.24	-3.95	7.78	6.98	4.62	0.18	101.72	-18.55	16.36	1.43
8.16.1	sfu8.prn	sf81686.prn	6	120	30	77.19	-1.09	-2.61	6.95	6.43	4.36	-0.03	84.89	-11.03	13.39	1.64
8.16.1	sfu10b.prn	sf8161042.prn	42	120	32	77.69	-2.02	-3.58	6.99	6.44	4.69	0.33	89.68	-8.64	16.88	2.19
8.16.1	sfu10b.prn	sf8161040.prn	40	120	34	78.51	-2.81	-3.88	7.07	6.69	4.89	0.58	92.89	-7.93	12.88	-2.64
8.16.1	sfu10b.prn	sf8161038.prn	38	120	36	80.02	-1.92	-3.88	7.20	6.37	4.66	0.65	88.99	-7.81	15.47	1.25
8.16.1	sfu10b.prn	sf8161036.prn	36	120	38	81.1	-1.56	-4.58	7.30	6.18	4.40	0.69	85.52	-8.16	14.20	3.29
8.16.1	sfu8.prn	sf81688.prn	8	120	40	82.76	1.37	-5.04	6.62	6.55	4.44	0.67	89.32	-7.75	5.86	4.98
8.16.1	sfu10b.prn	sf8161034.prn	34	120	41	83.09	-1.86	-5.06	6.65	6.60	4.40	-0.19	87.43	-8.96	7.77	4.63
8.16.1	sfu10b.prn	sf8161032.prn	32	120	42	82.38	-1.04	-4.95	6.59	6.39	4.55	0.13	89.46	-13.02	11.07	7.76
8.16.1	sfu10a.prn	sf8161030.prn	30	120	43	83.35	-0.07	-5.88	7.50	6.80	4.41	1.51	94.81	-6.58	7.08	3.73
8.16.1	sfu10a.prn	sf8161028.prn	28	120	44	85.41	-0.1	-6.08	6.83	6.10	4.01	0.44	81.62	-2.93	1.69	6.57
8.16.1	sfu10a.prn	sf8161026.prn	26	120	45	84.23	0.2	-6.55	6.74	6.27	4.52	-0.42	89.07	-10.71	4.42	7.08
8.16.1	sfu10a.prn	sf8161024.prn	24	120	46	84.56	-0.46	-6.2	6.76	6.33	4.34	0.69	86.13	-9.88	5.14	8.48
8.16.1	sfu10a.prn	sf8161022.prn	22	120	47	85.62	-0.42	-6.69	6.85	6.76	4.48	0.37	93.97	-10.95	6.56	13.54
8.16.1	sfu10a.prn	sf8161020.prn	20	120	48	85.31	-0.33	-7.29	7.68	6.74	4.52	-0.06	104.51	-12.62	7.08	16.17
8.16.1	sfu10a.prn	sf8161018.prn	18	120	49	85.51	0.37	-7.06	7.70	7.11	5.01	1.69	120.70	-11.81	5.79	22.68
8.16.1	sfu5.prn	sf81650.prn	0	120	50	88.68	3.1	-6.27	7.98	7.19	4.51	1.23	110.48	3.54	2.67	21.04
8.16.1	sfu10a.prn	sf8161016.prn	16	120	51	87.97	0.91	-8.31	8.80	7.30	4.99	-0.70	124.88	-5.05	1.39	24.14
8.16.1	sfu10a.prn	sf8161014.prn	14	120	52	87.28	1.82	-8.1	8.73	8.57	5.43	-0.31	157.21	17.04	-10.10	36.12
8.16.1	sfu10a.prn	sf8161012.prn	12	120	53	87.35	1.85	-8.63	9.61	9.03	5.52	0.23	189.20	23.51	-13.47	34.92
8.16.1	sfu10a.prn	sf8161010.prn	10	120	54	87.73	2.53	-9.24	10.53	9.31	5.64	-0.50	200.86	33.84	-20.38	37.37
8.16.1	sfu10a.prn	sf816108.prn	8	120	55	86.36	1.22	-9.04	10.36	10.08	6.24	-0.49	222.78	44.81	-28.33	54.94
8.16.1	sfu10a.prn	sf816106.prn	6	120	56	86.75	0.16	-8.87	10.41	8.89	5.85	-0.57	202.61	37.02	-22.28	39.62
8.16.1	sfu10a.prn	sf816104.prn	4	120	57	85.21	-0.03	-9.17	11.93	12.92	6.60	-0.52	277.34	78.75	-31.35	49.23
8.16.1	sfu10a.prn	sf816102.prn	2	120	58	85.72	0.08	-8.95	11.14	10.13	6.71	-1.42	265.00	64.77	-36.45	53.23
8.16.1	sfu10a.prn	sf816100.prn	0	120	59	82.37	-0.05	-8.93	13.18	12.50	7.41	-4.24	327.95	93.05	-35.09	49.00
8.16.1	sfu9a.prn	sf81690.prn	0	120	61	73.01	-0.27	-8.35	18.25	14.58	9.10	-2.57	514.84	173.64	-64.50	55.67
8.16.1	sfu9a.prn	sf81692.prn	2	120	62	74.66	-1.69	-7.56	17.17	14.69	9.15	-3.98	491.35	187.85	-73.30	65.66
8.16.1	sfu9a.prn	sf81694.prn	4	120	63	65.05	-1.38	-6.76	20.82	16.55	10.75	-5.75	637.02	243.39	-113.61	65.38
8.16.1	sfu9a.prn	sf81696.prn	6	120	64	63.17	-3.31	-7.46	23.37	16.48	10.37	-5.21	702.90	283.39	-100.31	59.95
8.16.1	sfu9a.prn	sf81698.prn	8	120	65	54.62	-2.99	-7.93	23.49	17.61	11.66	-7.77	745.95	270.05	-113.06	64.73
8.16.1	sfu9a.prn	sf816910.prn	10	120	66	47.62	-4.23	-8.9	24.29	17.47	12.02	-6.56	766.03	256.43	-138.70	77.58
8.16.1	sfu9a.prn	sf816912.prn	12	120	67	41.49	-3.27	-8.8	26.55	18.15	12.14	-7.31	843.89	321.81	-160.86	68.71
8.16.1	sfu9a.prn	sf816914.prn	14	120	68	33.01	-2.65	-9.43	25.09	19.61	13.30	-5.99	866.17	316.86	-171.01	68.77
8.16.1	sfu9a.prn	sf816916.prn	16	120	69	29.5	-5.63	-10.24	22.72	19.14	13.00	-4.14	770.65	290.45	-165.68	88.10
8.16.1	sfu9a.prn	sf816918.prn	18	120	71	20.6	-1.93	-8.26	21.01	19.76	14.21	-5.56	769.09	317.61	-147.40	75.19
8.16.1	sfu9a.prn	sf816920.prn	20	120	72	12.82	-2.76	-9.78	20.00	18.88	13.20	-5.59	713.59	233.75	-126.41	49.75
8.16.1	sfu9a.prn	sf816922.prn	22	120	73	9.42	-3.75	-11.77	18.75	18.90	12.83	-2.91	668.43	227.36	-108.65	57.04
8.16.1	sfu9a.prn	sf816924.prn	24	120	74	7	-4.69	-11.12	17.85	17.87	12.12	-1.74	624.58	178.90	-90.81	47.77
8.16.1	sfu9a.prn	sf816926.prn	26	120	75	5.94	-5.75	-12.44	16.81	17.65	11.82	-1.63	574.41	150.14	-87.58	40.06
8.16.1	sfu9a.prn	sf816928.prn	28	120	76	3.74	-3.71	-11.54	16.98	18.62	12.23	-2.08	615.54	187.19	-100.29	56.85
8.16.1	sfu9b.prn	sf816930.prn	30	120	77	1.77	-4.26	-11.39	16.07	18.23	12.64	-3.27	589.77	136.35	-68.73	40.87
8.16.1	sfu9b.prn	sf816932.prn	32	120	78	-2.8	-2.36	-8.81	15.06	17.13	11.19	-3.24	509.26	71.61	-70.89	21.43
8.16.1	sfu9b.prn	sf816934.prn	34	120	79	-4.71	-1.11	-10.26	14.84	16.66	11.08	-2.02	494.00	83.21	-42.59	41.92
8.16.1	sfu8.prn	sf816814.prn	14	120	80	-6.84	0.41	-10.17	13.00	15.23	9.97	-0.95	395.38	29.40	-35.85	27.00
8.16.1	sfu9b.prn	sf816936.prn	36	120	82	-7.55	1.87	-9.62	13.74	15.26	11.16	0.33	440.80	5.85	-43.21	13.14
8.16.1	sfu9b.prn	sf816938.prn	38	120	84	-5.53	-0.07	-7.63	13.27	14.38	11.22	0.09	414.47	2.39	-14.98	21.35
8.16.1	sfu9b.prn	sf816940.prn	40	120	86	-7.19	2.55	-6.4	14.02	14.48	11.46	1.50	433.00	-52.42	-37.14	11.33
8.16.1	sfu9b.prn	sf816942.prn	42	120	88	0.49	2.41	-0.54	15.35	15.28	12.31	2.04	495.64	-64.11	-77.17	2.26
8.16.1	sfu8.prn	sf816816.prn	16	120	90	0.98	5.84	0.48	16.91	13.67	12.03	1.53	486.33	-120.26	-58.30	-14.60
8.16.1	sfu9b.prn	sf816944.prn	44	120	95	11.18	2.07	12.17	16.55	13.89	12.66	2.22	495.81	-102.52	-98.03	-28.46
8.16.1	sfu8.prn	sf816818.prn	18	120	100	23.21	2.28	19.45	15.09	13.41	12.84		447.98	-58.21	-99.35	12.95

Table B8. Example Output File for FORTRAN-90 Program. This output file

represents the data collected behind Boulder B from which 8-16-8-14 is a single point.

Description of Eddy Length Scale Calculations

The integral form of the eddy length scale calculation is:

$$L=U_{\text{mag}} \int_0^t R(t)dt \quad (\text{B4})$$

where U_{mag} is the approach velocity magnitude, t is the sampling period, and $R(t)$ is the autocorrelation function and is defined to be:

$$R(t)=\frac{\overline{s'_t s'_{t+\Delta t}}}{\overline{(s'_t)^2}} \quad (\text{B5})$$

where s'_t is the instantaneous fluctuation component of the velocity magnitude and $s'_{t+\Delta t}$ is the instantaneous fluctuation component of the velocity magnitude for the time lag Δt . Figure B15 depicts the method for which the autocorrelation function can be calculated in spreadsheet form. The autocorrelation function can be plotted and the area under the curve represents the temporal eddy length scale (Figure B16). The eddy length scale is then determined by multiplying by the approach velocity magnitude.

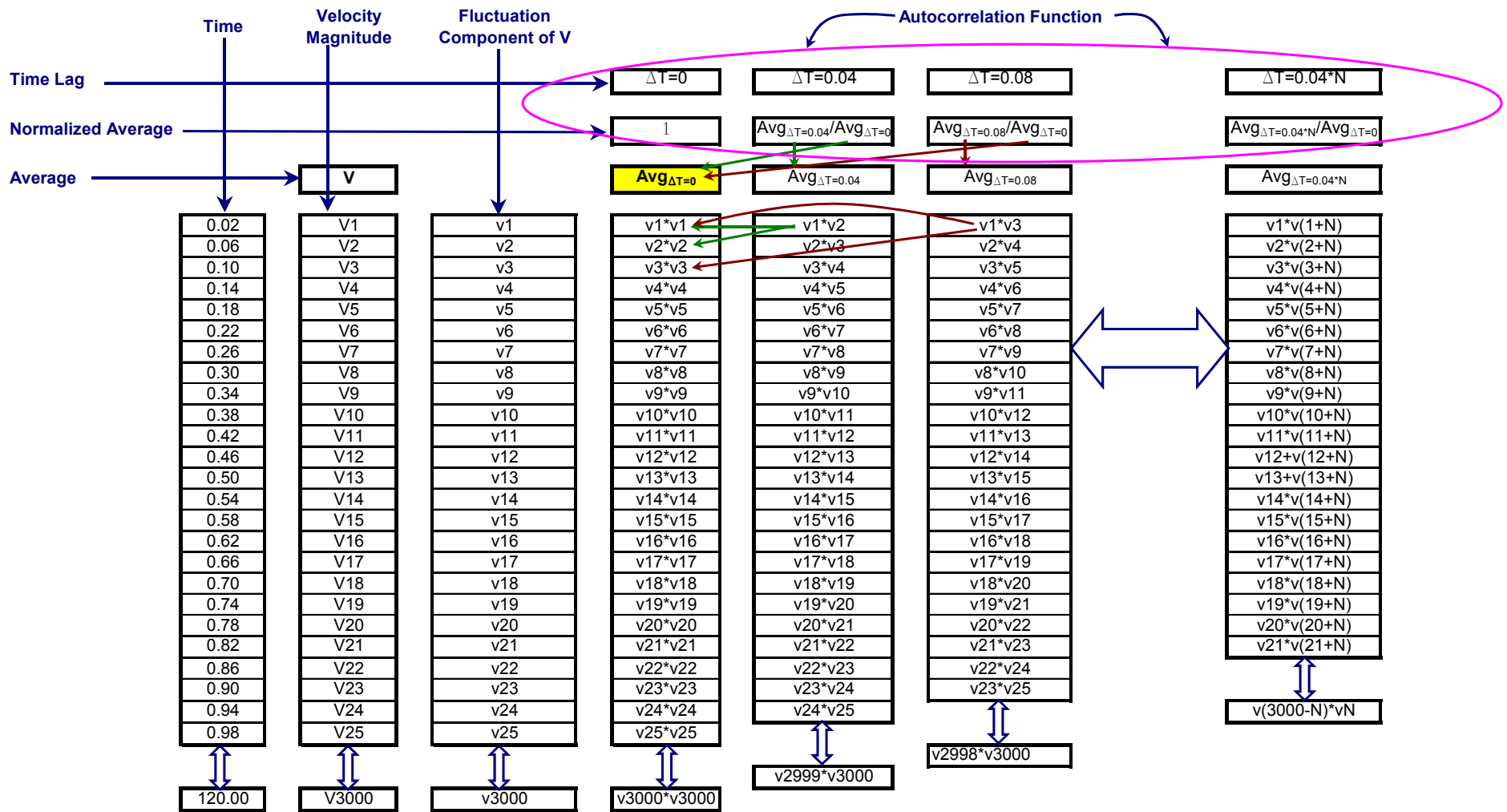


Figure B15. Autocorrelation Calculation Diagram.

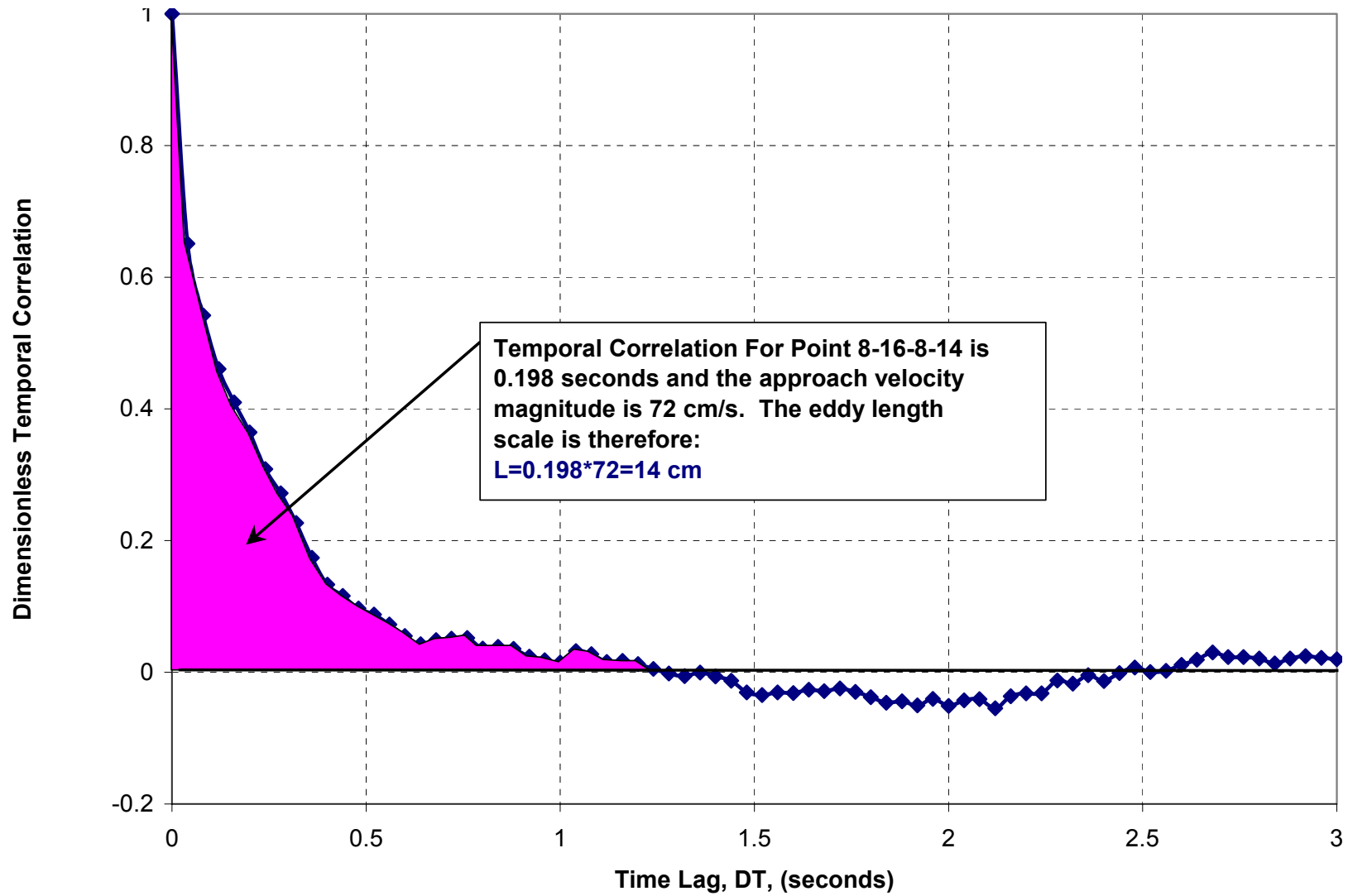


Figure B16. Length Scale Diagram For Point 8-16-8-14.

VERTICAL PROFILE FIGURES

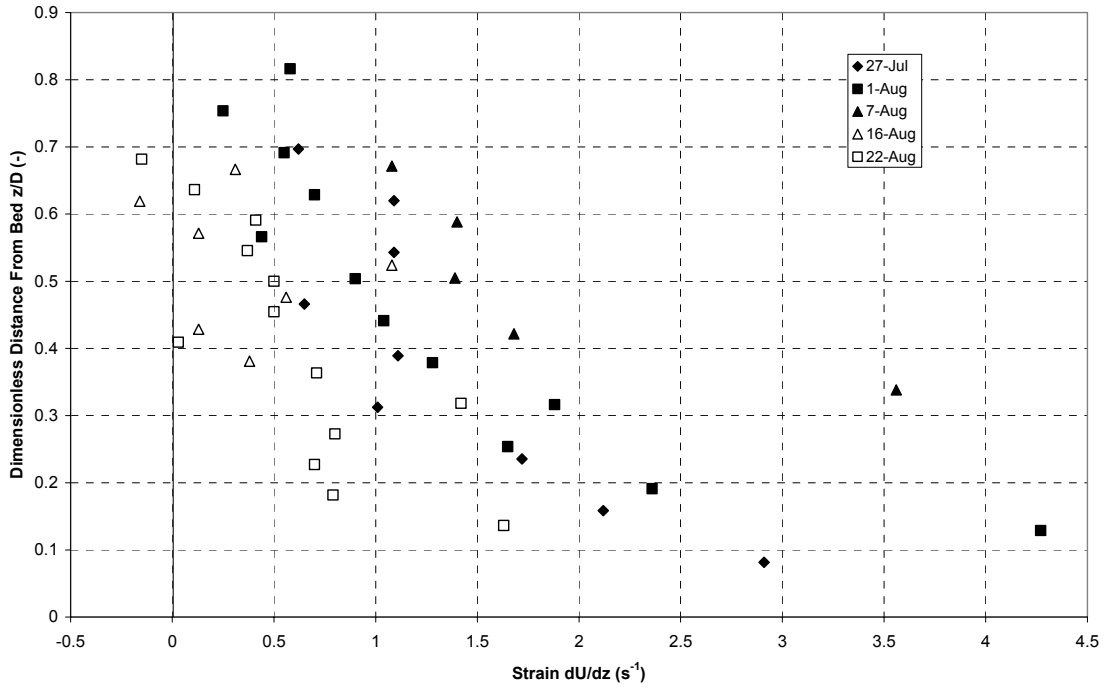


Figure B17. Strain Profiles for Unobstructed Flow.

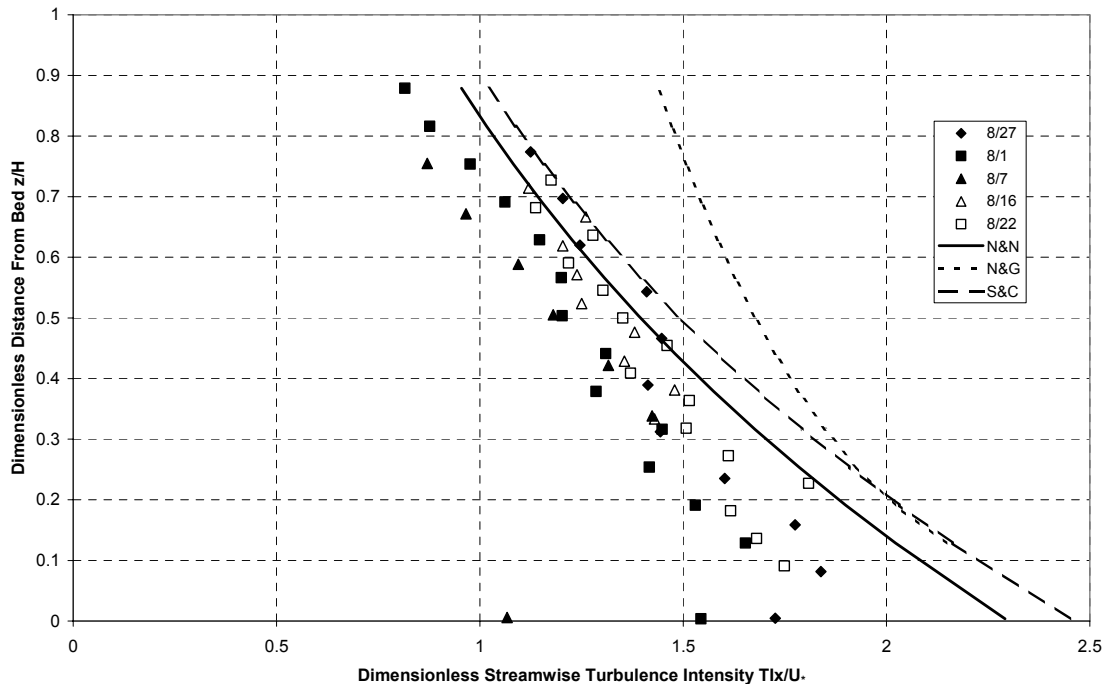


Figure B18. Dimensionless Streamwise Turbulence Intensity Profiles for Unobstructed Flow. N&N – Nezu and Nakagawa (1993); N&G – Nikora and Goring (1998); S&C – Song and Chiew (2001).

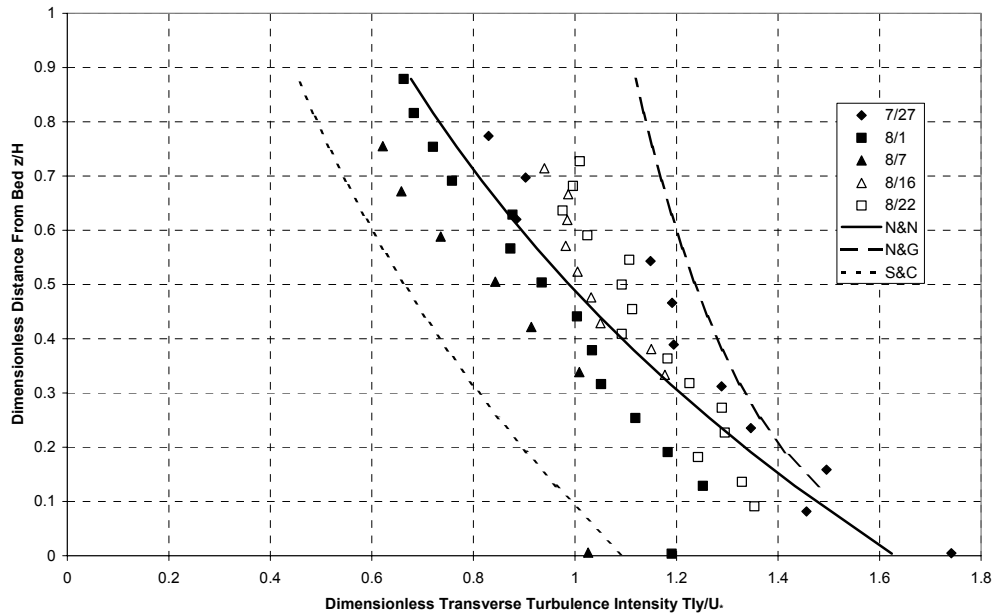


Figure B19. Dimensionless Transverse Turbulence Intensity Profiles for Unobstructed Flow. N&N – Nezu and Nakagawa (1993); N&G – Nikora and Goring (1998); S&C – Song and Chiew (2001).

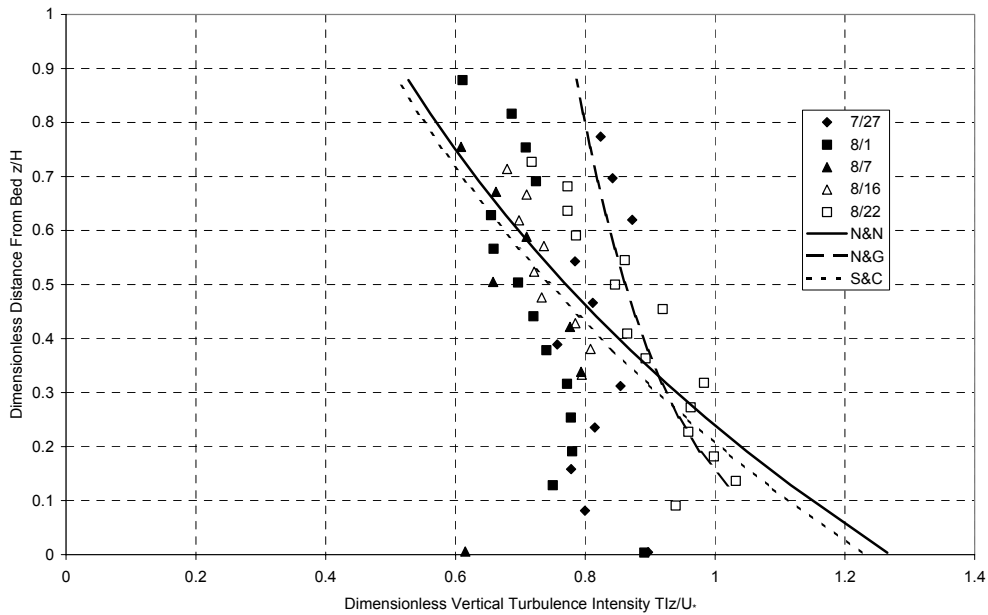


Figure B20. Dimensionless Vertical Turbulence Intensity Profiles for Unobstructed Flow. N&N – Nezu and Nakagawa (1993); N&G – Nikora and Goring (1998); S&C – Song and Chiew (2001).

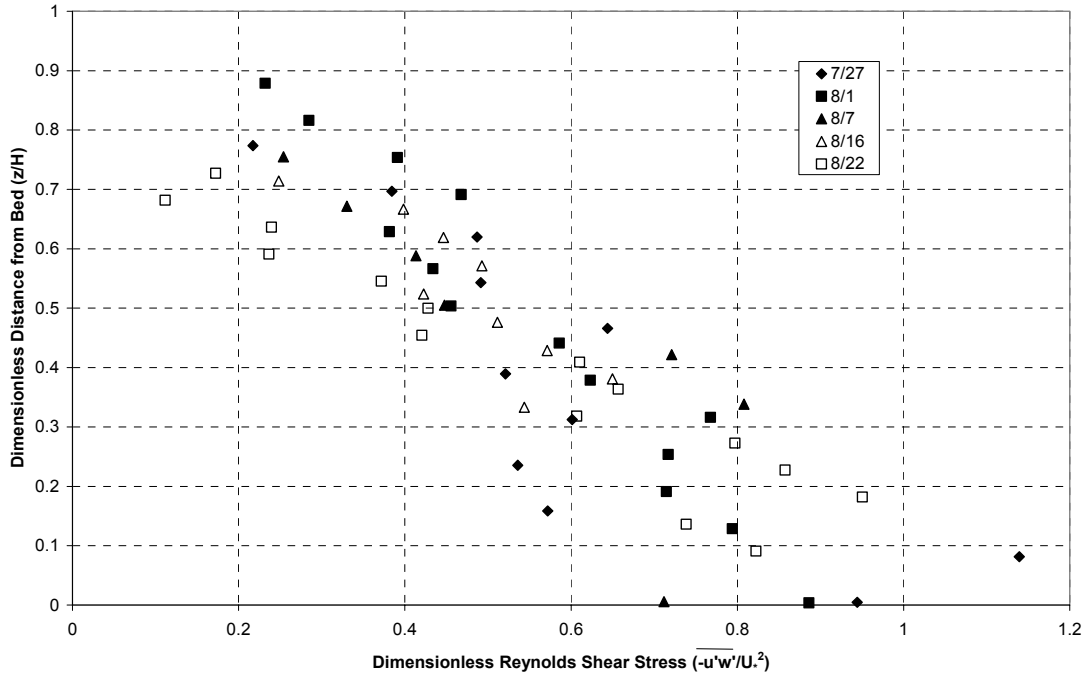


Figure B21. Dimensionless Reynolds Shear Stress Tensor $-\overline{u'w'}/U_*^2$ Profiles for Unobstructed Flow.

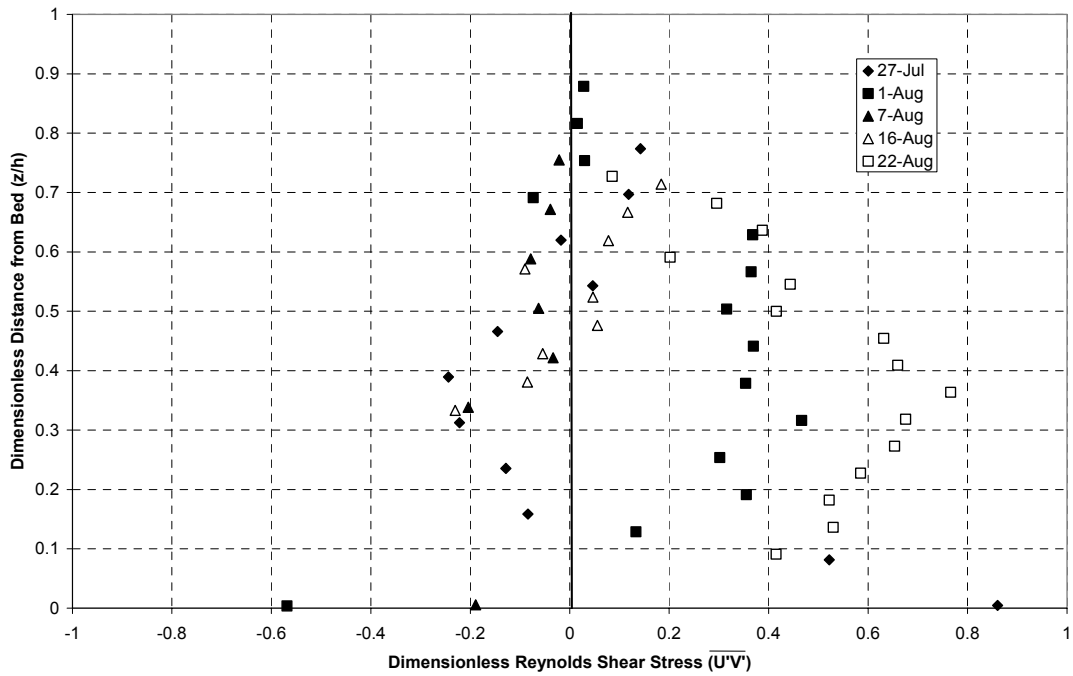


Figure B22. Dimensionless Reynolds Shear Stress Tensor $\overline{u'v'}/U_*^2$ Profiles for Unobstructed Flow.

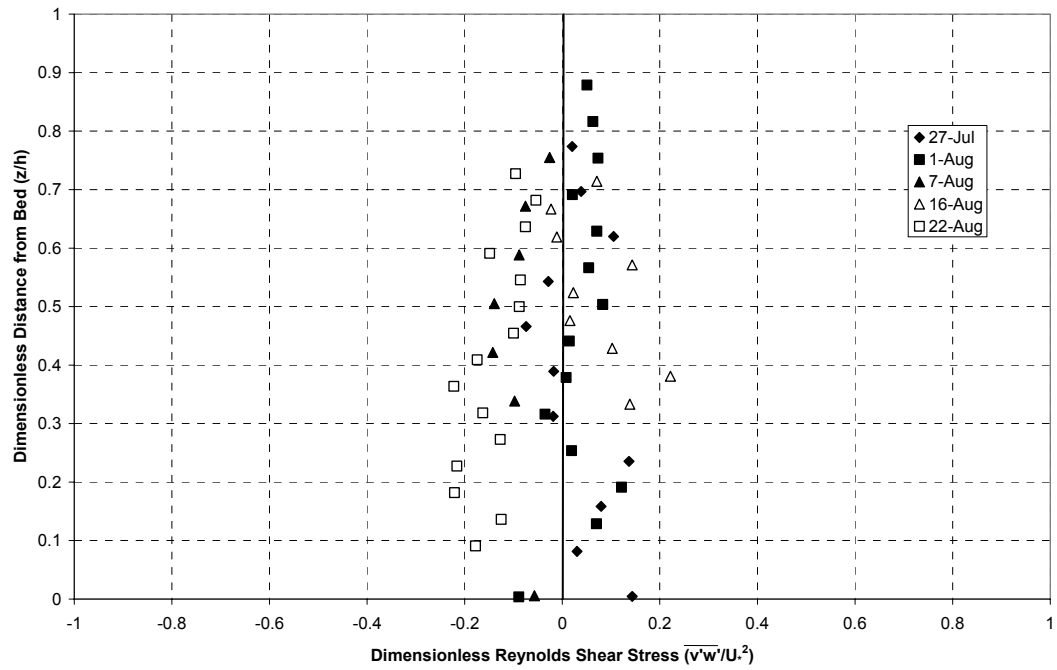


Figure B23. Dimensionless Reynolds Shear Stress Tensor $\overline{v'w'}/U_*^2$ Profiles for Unobstructed Flow.

OBSTRUCTED FLOW FIGURES

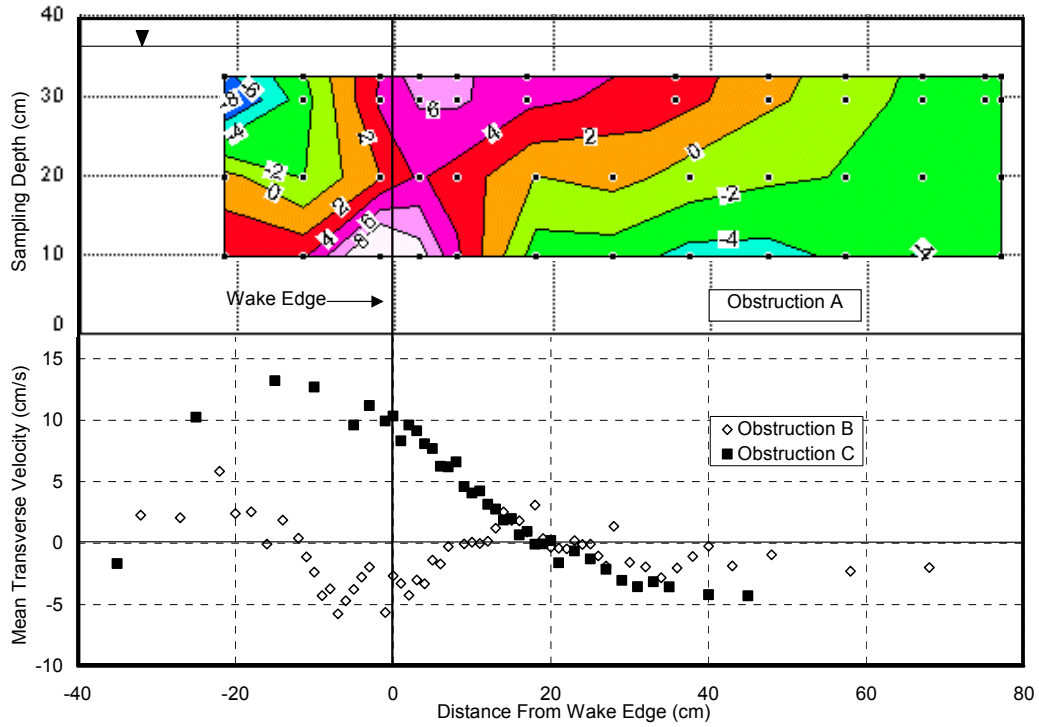


Figure B24. Transverse Velocity Directly Downstream from the Boulders.

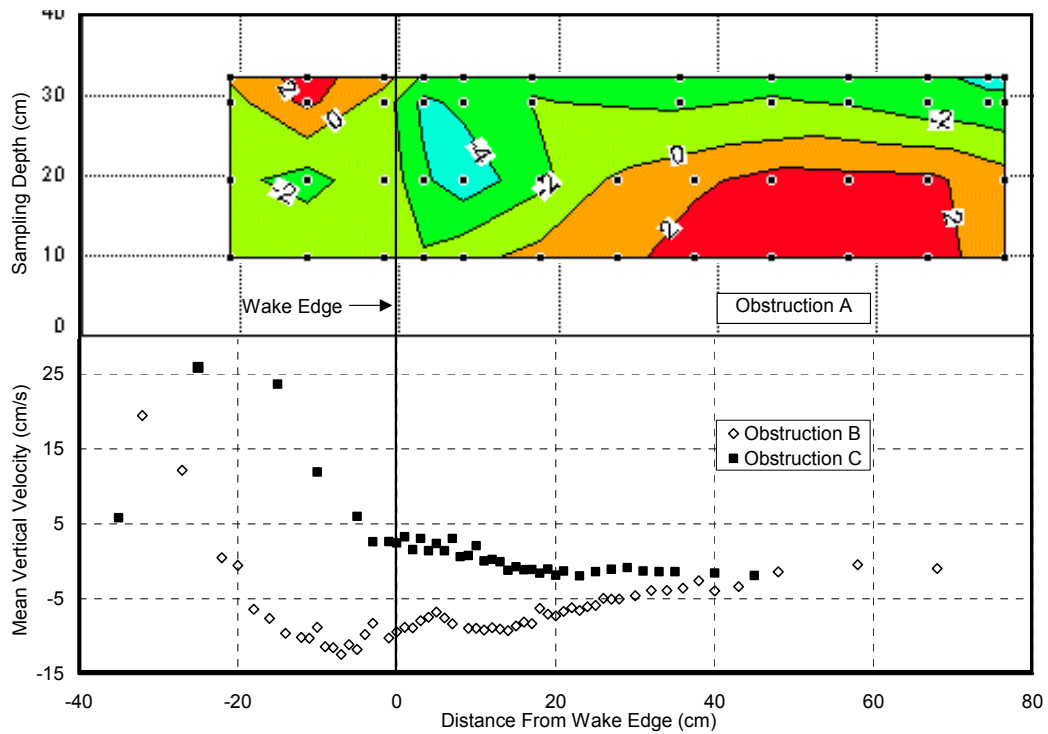


Figure B25. Vertical Velocity Directly Downstream from the Boulders.

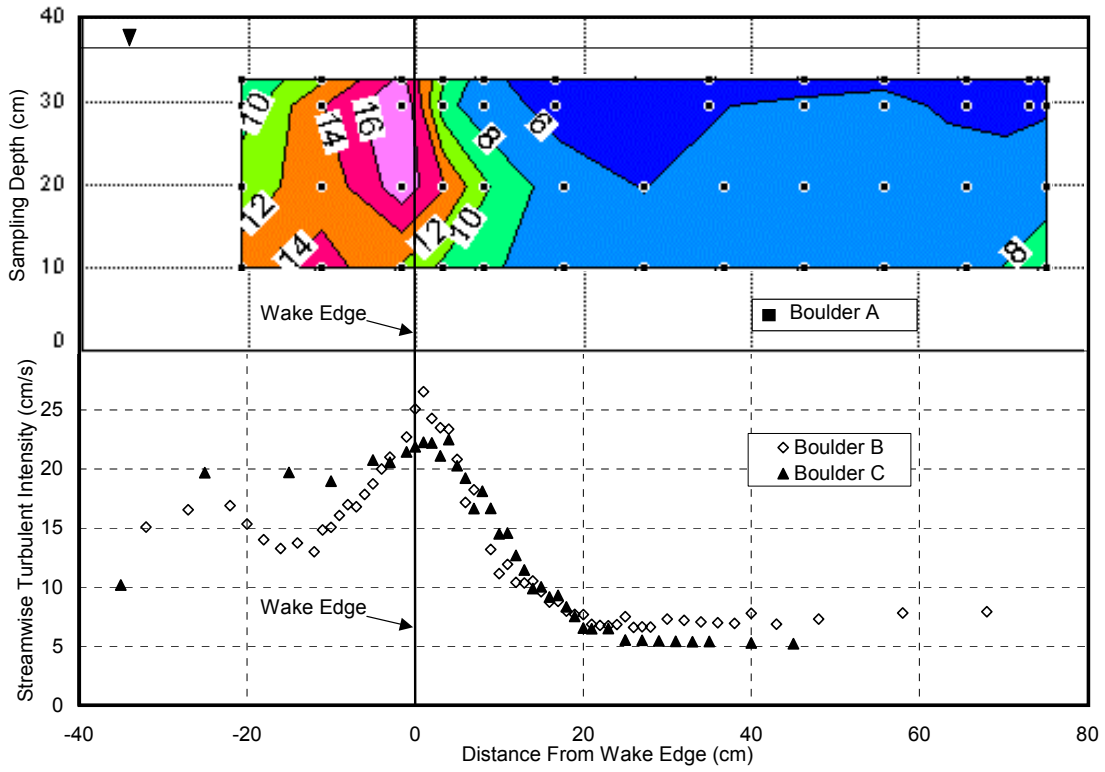


Figure B26. Streamwise Turbulent Intensity Downstream from the Boulders.

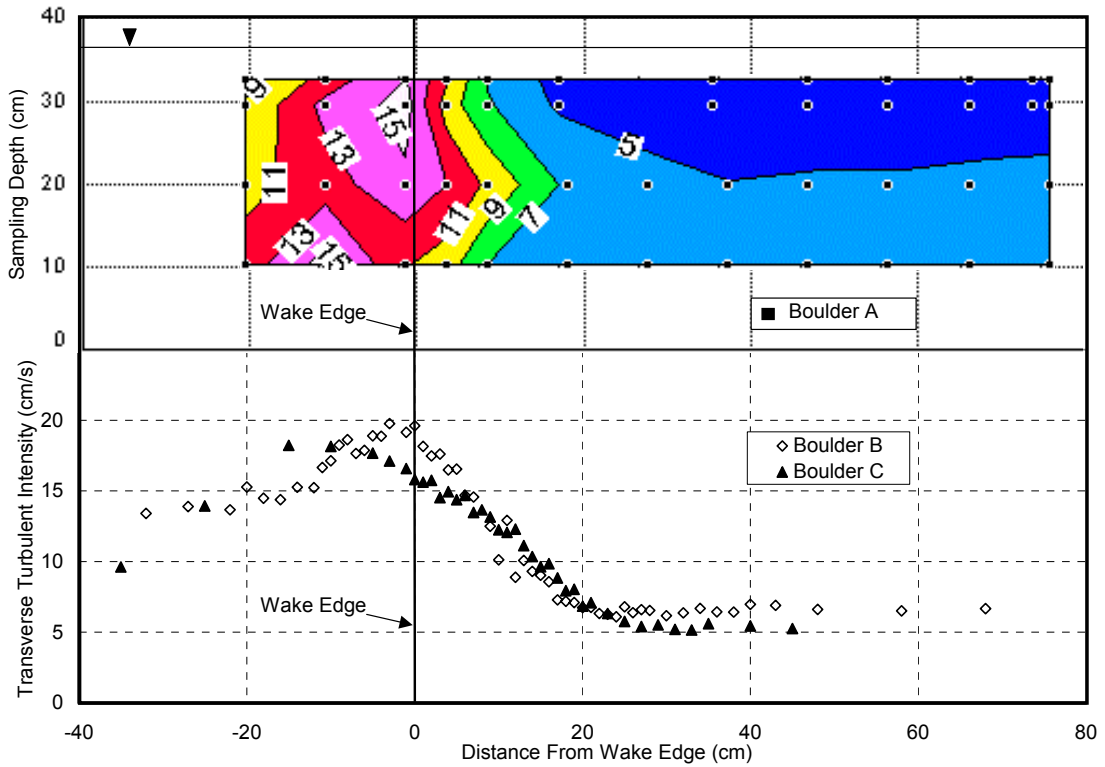


Figure B27. Transverse Turbulent Intensity Downstream from the Boulders.

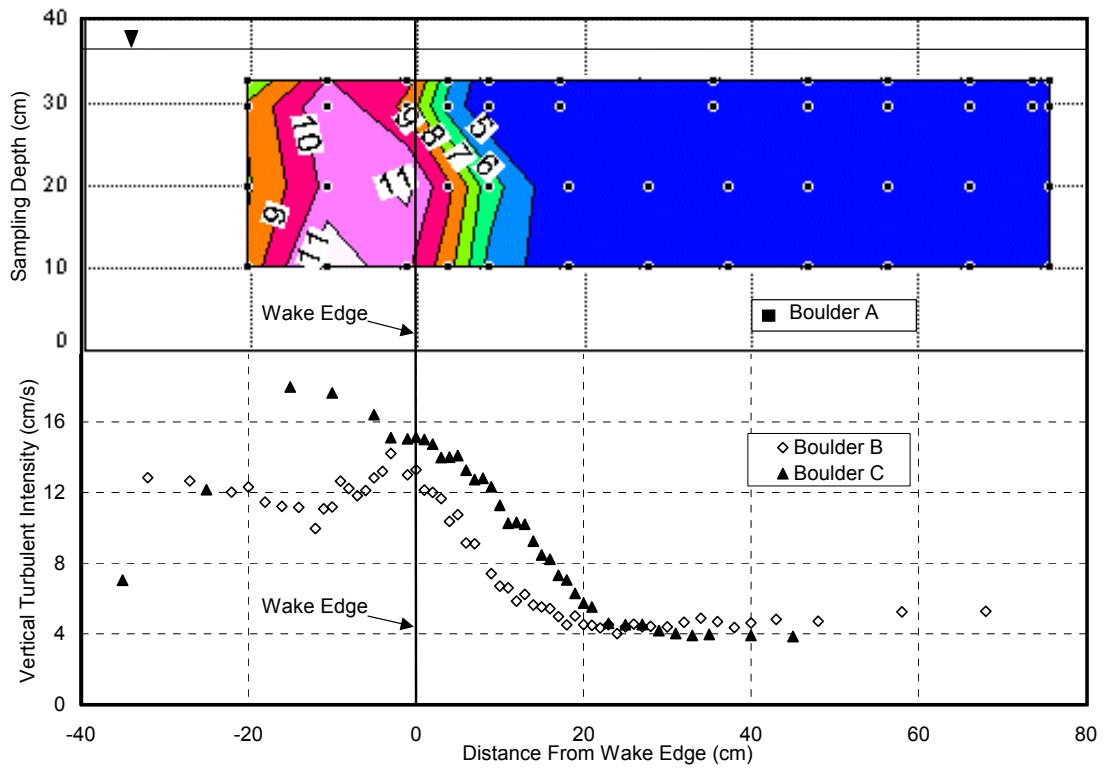


Figure B28. Vertical Turbulent Intensity Downstream from the Boulders.

REFERENCES

- Chang, H. (1992). *Fluvial Processes in River Engineering*. Krieger Pub.
- Nezu, I., and Nakagawa, H. (1993). *Turbulence in Open-Channel Flows*. A. A. Balkema.
- Nikora, V. I., and Goring, D. G. (1998). "Effects of Bed Mobility on Turbulence Structure." *NIWA Internal Report No 48*.
- Song, T., and Chiew, Y. M. (2001). "Turbulence Measurement in Nonuniform Open-Channel Flow Using Acoustic Doppler Velocimeter (ADV)." *Journal of Engineering Mechanics*, March, 219-232.
- United States Geological Survey. (2002). <<http://water.usgs.gov>>, October, 2002.
- Wolman, M.G. (1954). "A Method of Sampling Coarse River Bed Material." *Trans. Am. Geophys. Union*, Washington, D.C., 35, 951-956.

APPENDIX C

JET, MIXER, AND BONNEVILLE PROTOTYPE SURFACE COLLECTOR RESULTS

FLUME CONFIGURATION

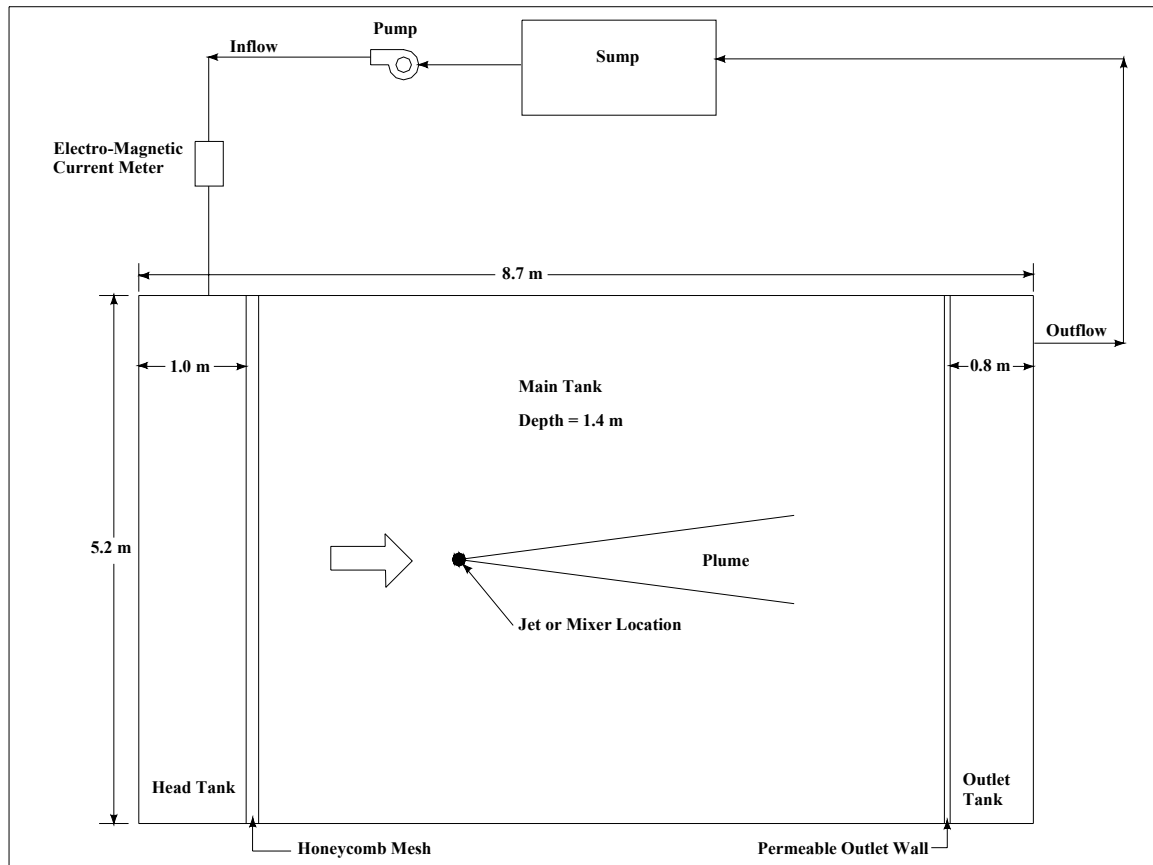


Figure C1. Flume Configuration. Plan View.

SUMMARY OF JETS AND MIXERS TESTED

Type	Diameter	Momentum
	(cm)	(N)
Jet 1, Flow 1	1.4	8.3
Jet 1, Flow 2	1.4	0.3
Jet 1, Flow 3	1.4	1.2
Jet 2, Flow 1	3.5	1.0
Jet 3, Flow 1	2.7	1.0
Oscillating Jet	1.4	1.0
Oscillating Jet	1.4	3.0
Propeller 1	23.5 (2 blades)	~500 RPM
Propeller 2	7.5 (4 blades)	~500 RPM
Propeller 3	15 (4 blades)	~500 RPM
Propeller 4	~ 15 (4 blades)	~500 RPM

Table C1. Summary Table of Jets and Mixers Tested. Momentum was used to quantify the flow from the jets (White, 1991) using the equation, $M = \rho QU$, where ρ is the water density, Q is the volumetric discharge from the jet, and U is the streamwise velocity measured at the outlet. The highlighted rows indicate the selected jet and selected mixer.

RESULTS FROM SELECTED JET

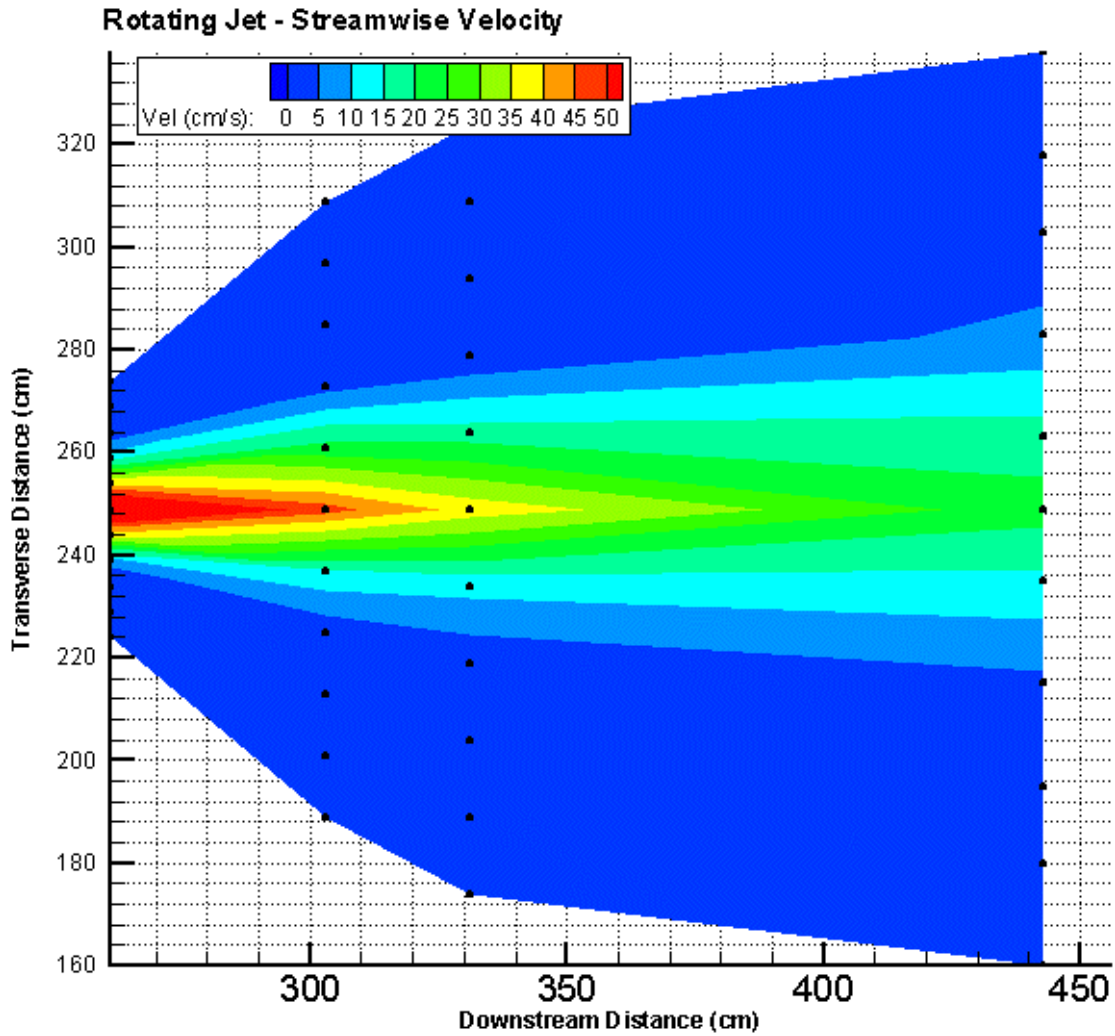


Figure C2. Streamwise Velocity From Selected Jet. Measured in the horizontal plane at the outlet centerline. The selected jet was an oscillating jet with a nozzle diameter of 1.5cm, exerting 3 Newtons of Momentum.

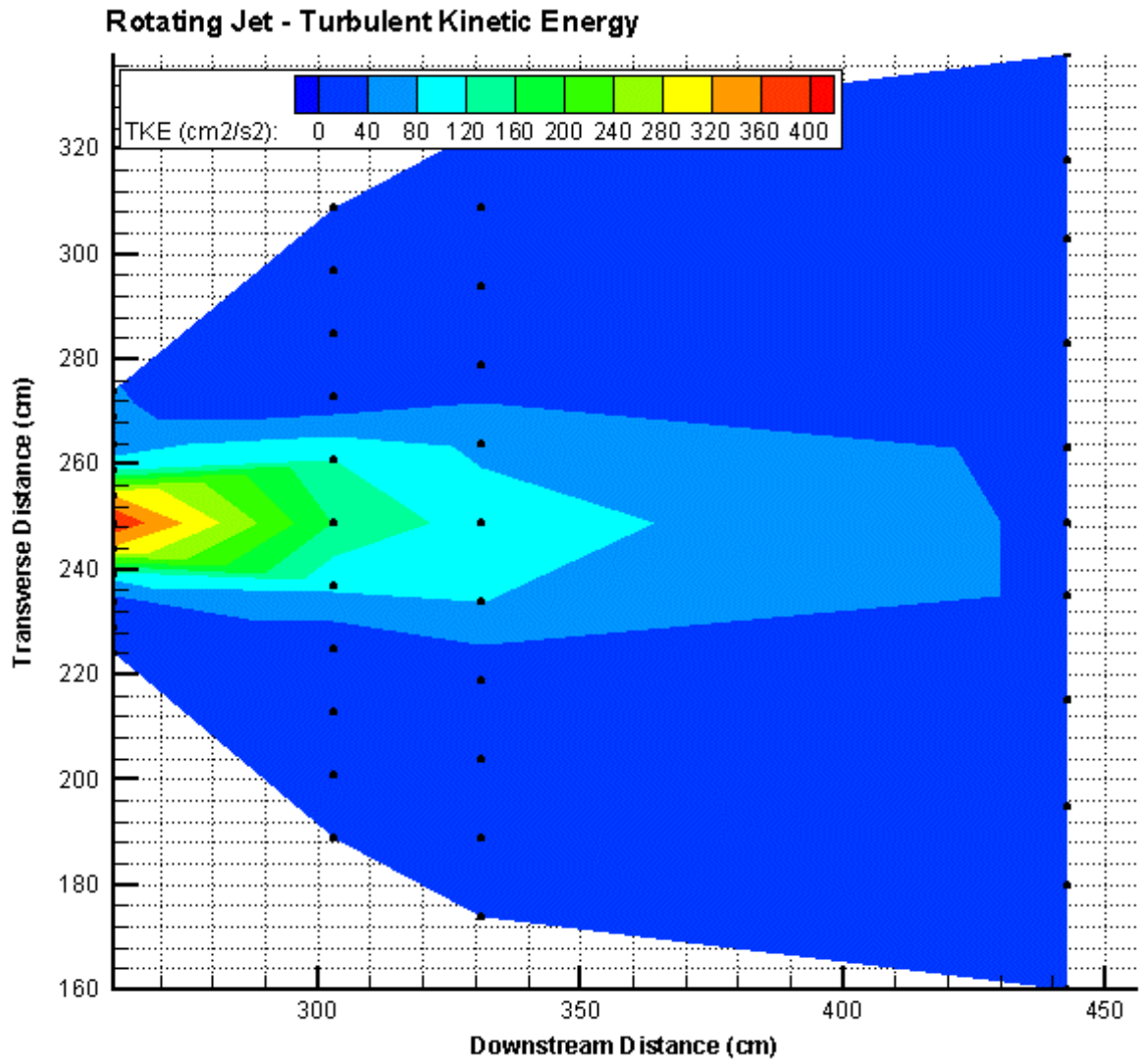


Figure C3. Turbulent Kinetic Energy From Selected Jet. Measured in the horizontal plane at the outlet centerline.

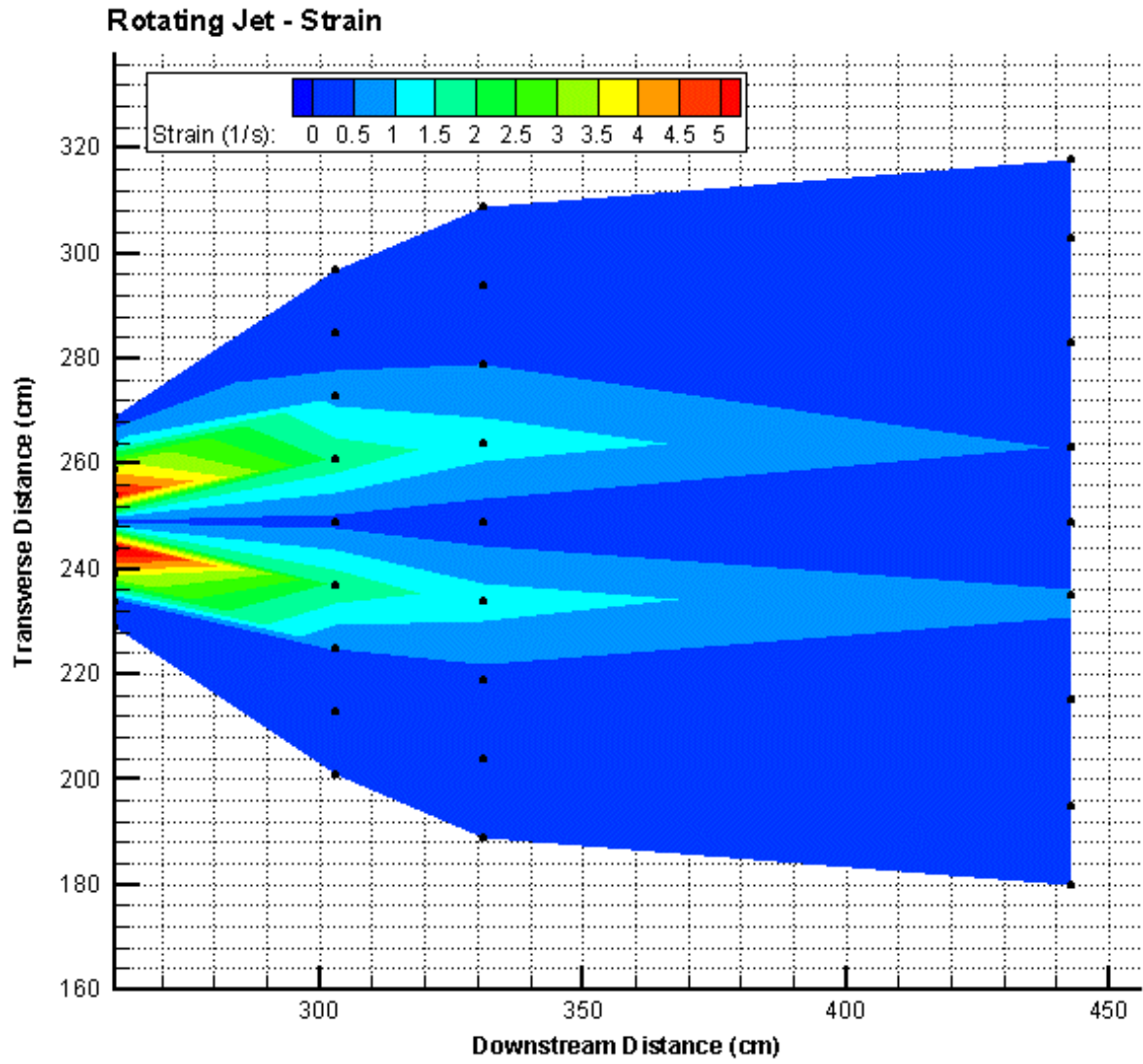


Figure C4. Strain From Selected Jet. Measured in the horizontal plane at the outlet centerline.

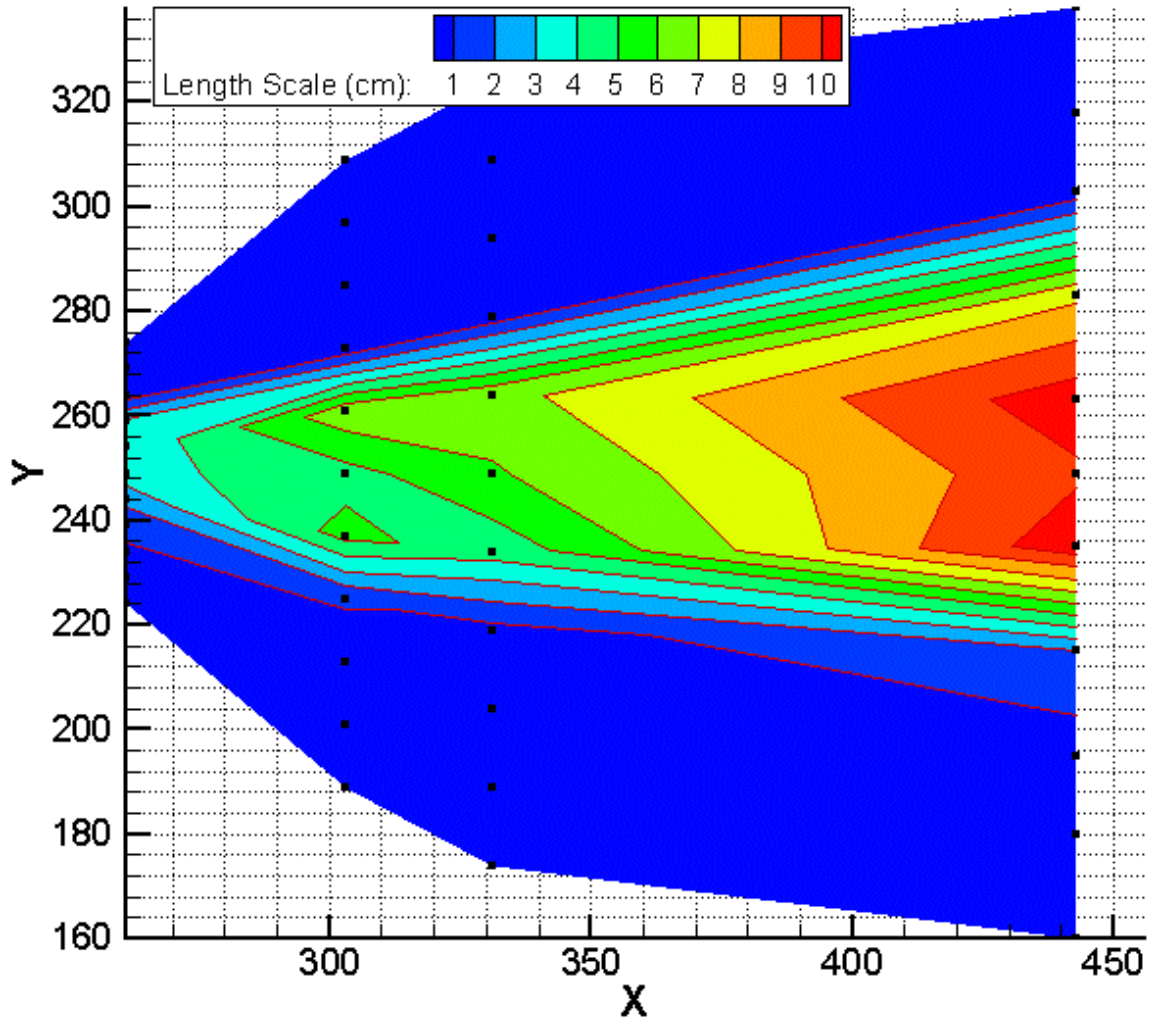


Figure C5. Eddy Length Scales From Selected Jet. Measured in the horizontal plane at the outlet centerline.

RESULTS FROM SELECTED MIXER

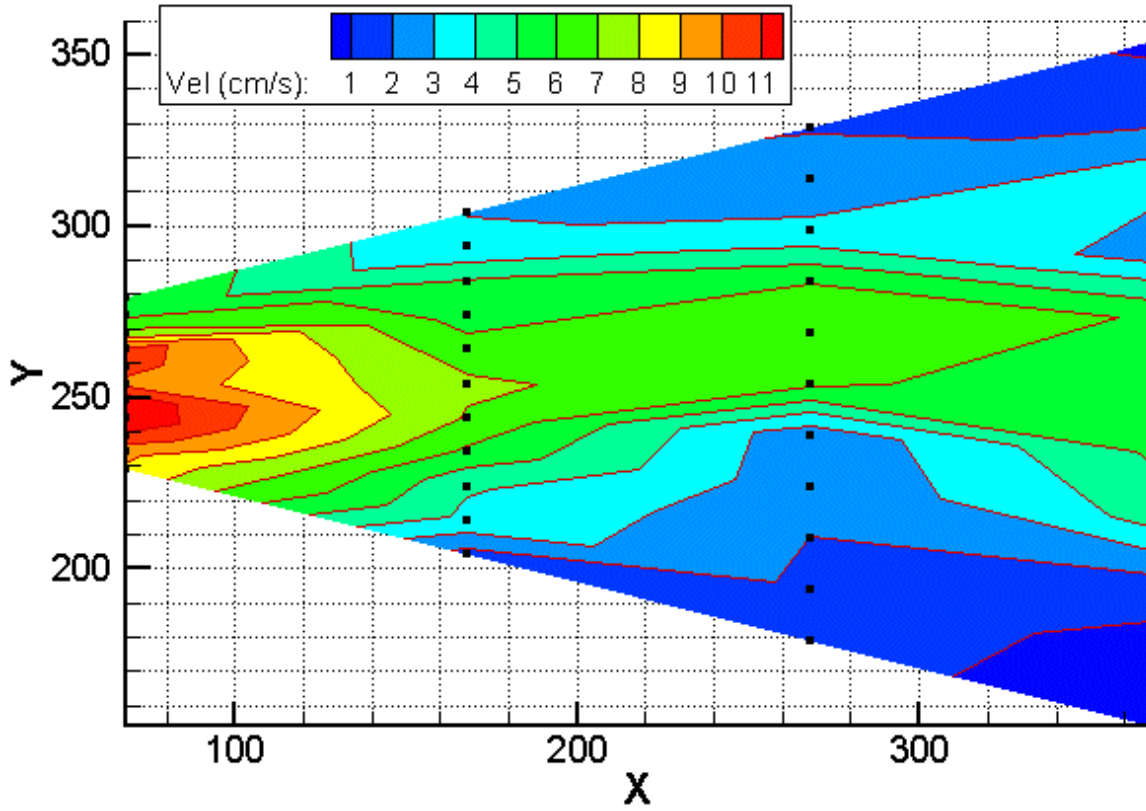


Figure C6. Streamwise Velocity from Selected Mixer. Measured in the horizontal plane at the outlet centerline. The selected mixer was 15 cm in diameter, with four blades, run at 500 rotations per minute.

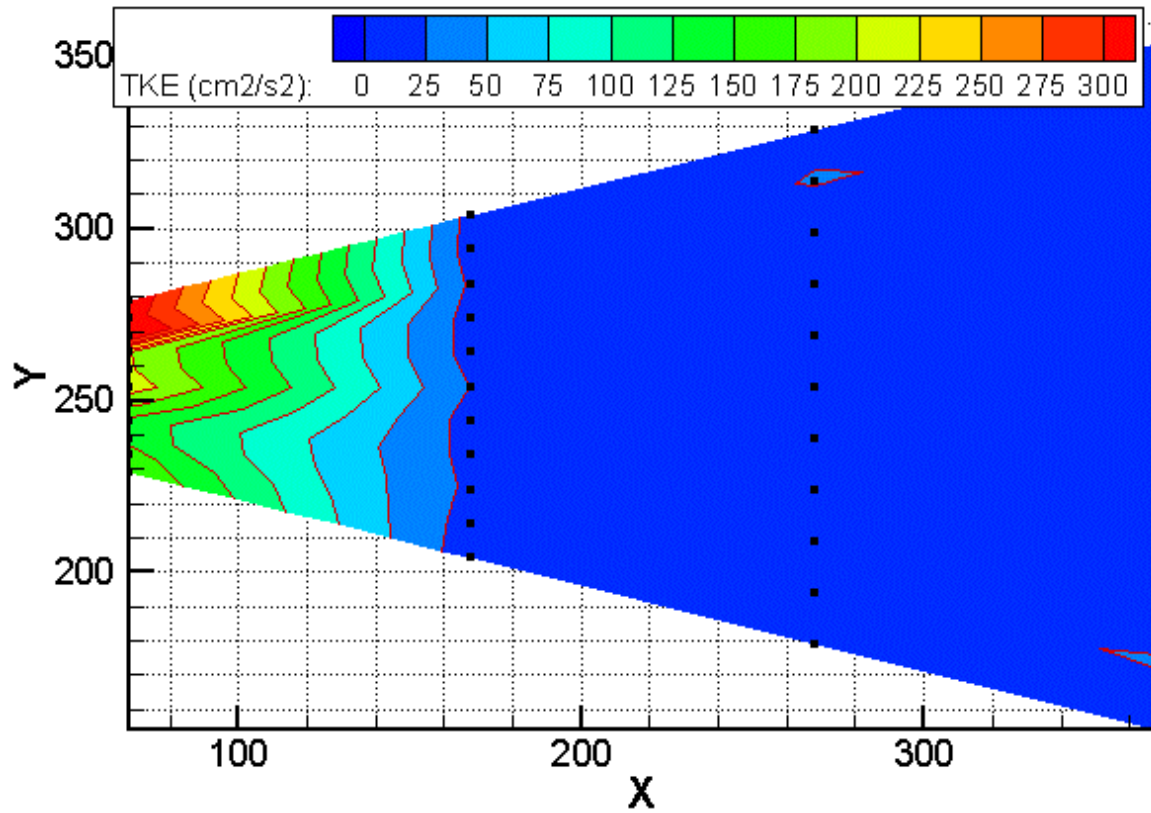


Figure C7. Turbulent Kinetic Energy from Selected Mixer. Measured in the horizontal plane at the outlet centerline.

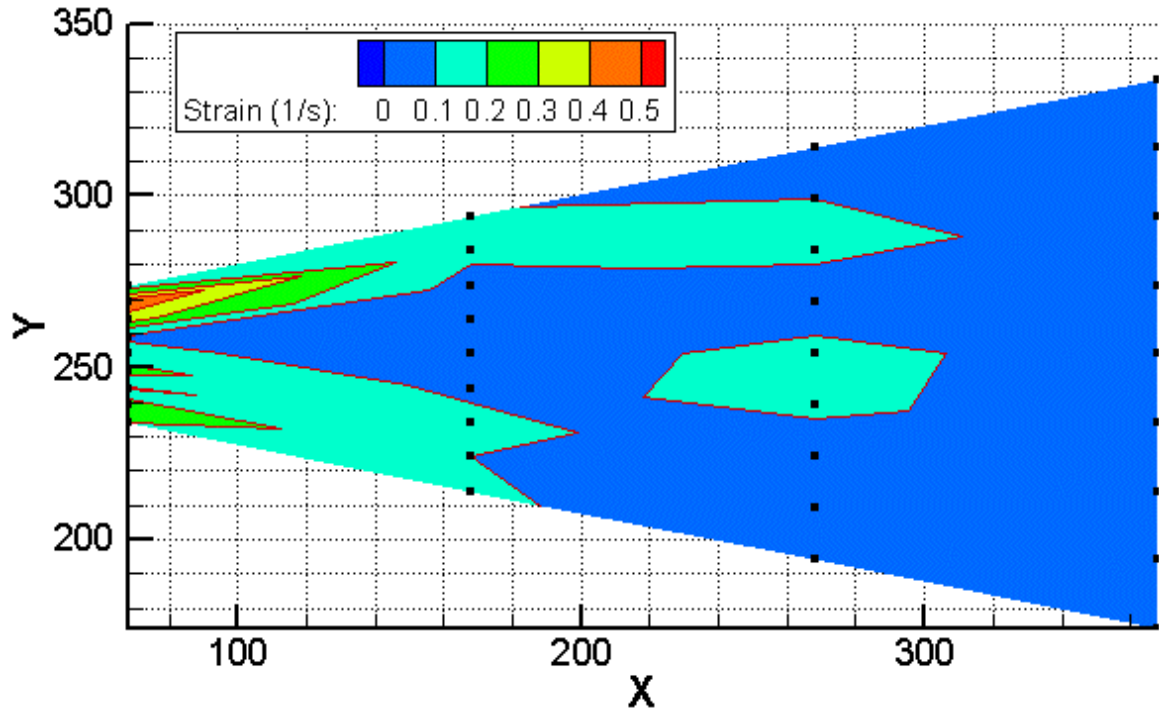


Figure C8. Strain from Selected Mixer. Measured in the horizontal plane at the outlet centerline.

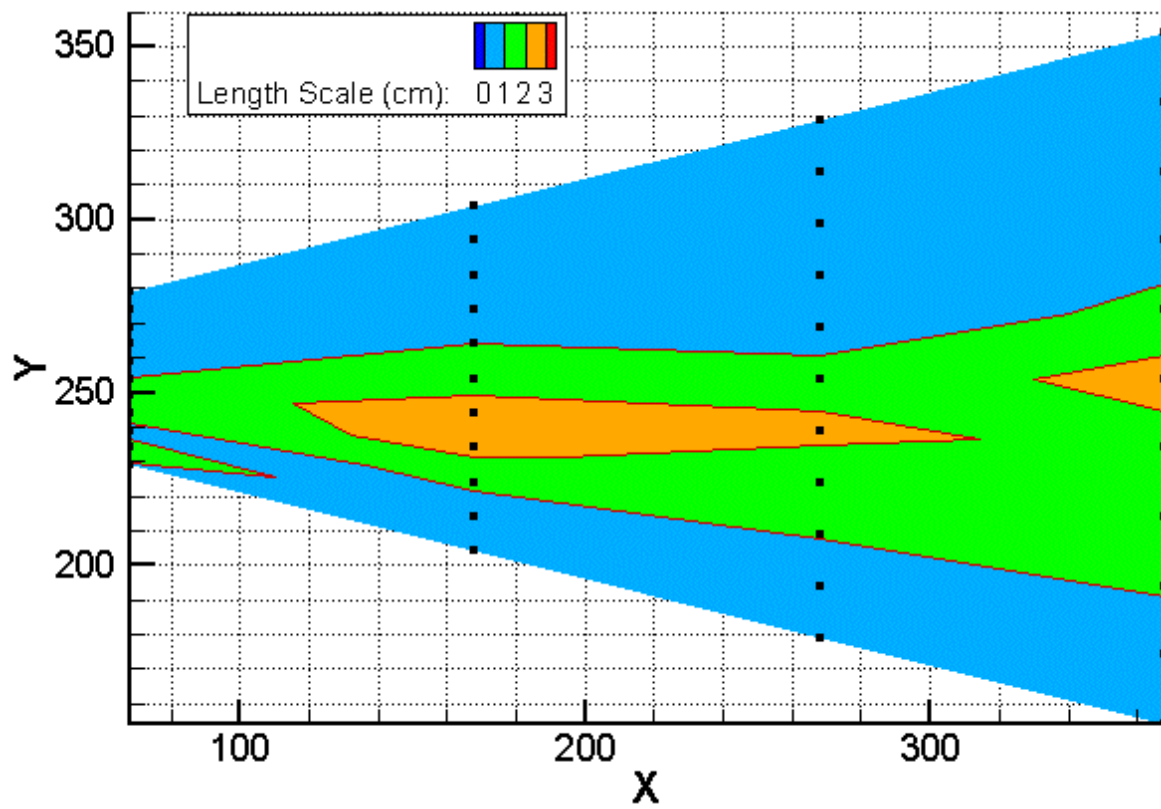


Figure C9. Eddy Length Scales from Selected Mixer. Measured in the horizontal plane at the outlet centerline.

RESULTS FROM BONNEVILLE PROTOTYPE SURFACE COLLECTOR

Turbulent Kinetic Energy and Strain Results from the Bonneville Prototype Surface Collector can be found in Faber (2000). Raw time series data from this study was provided by the United States Army Corps of Engineers, Portland District for determination of eddy length scales. Eddy lengths along with the sample number and location of each point are presented in Table C2.

Sample Number	Elevation (m)	Heading (degrees)	Northing (m)	Easting (m)	Length Scale (cm)
BON0001	21.7288	112.31944	220316.7753	496959.1712	488
BON0002	21.7288	112.31944	220316.4859	496959.8762	1076
BON0003	21.7592	112.31944	220316.4859	496959.8762	921
BON0004	21.7897	112.31944	220316.1965	496960.5813	636
BON0005	22.0031	112.31944	220317.0646	496958.4665	223
BON0006	22.0031	112.31944	220316.4859	496959.8762	339
BON0007	22.0031	92.31944	220317.1495	496960.0210	719
BON0008	22.0031	72.31944	220317.8226	496959.9305	907
BON0009	22.0031	132.31944	220315.9119	496959.5132	90
BON0010	22.0031	152.31944	220315.4966	496958.9756	174
BON0011	22.0031	112.31944	220315.9071	496961.2860	379
BON0012	22.0031	92.31944	220317.0878	496961.5438	438
BON0013	22.0031	72.31944	220318.2855	496961.3823	735
BON0014	22.0031	52.31944	220319.3557	496960.8211	492
BON0015	22.0031	132.31944	220314.8858	496960.6401	700
BON0016	22.0031	152.31944	220314.1471	496959.6836	372
BON0017	22.0031	172.31944	220313.7800	496958.5321	250
BON0018	22.0031	112.31944	220315.3283	496962.6960	393
BON0019	21.7897	172.31944	220312.2697	496958.7357	682
BON0020	21.7897	152.31944	220312.7975	496960.3914	284
BON0021	21.7897	132.31944	220313.8597	496961.7669	133

Table C2. Eddy Length Scales Upstream from the Bonneville Prototype

Surface Collector. Data reproduced with permission from the United States Army Corps of Engineers, Portland District.

BON0022	21.7897	92.31944	220317.0261	496963.0666	228
BON0023	21.8507	72.31944	220318.7484	496962.8344	249
BON0024	21.8507	52.31944	220320.2873	496962.0272	180
BON0025	20.4181	112.31944	220317.0646	496958.4665	1012
BON0026	20.4181	112.31944	220316.4859	496959.8762	1036
BON0027	20.4181	92.31944	220317.1495	496960.0210	692
BON0028	20.5095	72.31944	220317.8226	496959.9305	454
BON0029	20.5095	132.31944	220315.9119	496959.5132	228
BON0030	20.5095	152.31944	220315.4966	496958.9756	295
BON0031	20.5095	112.31944	220315.9071	496961.2860	572
BON0032	20.5095	92.31944	220317.0878	496961.5438	360
BON0033	20.5095	72.31944	220318.2855	496961.3823	699
BON0034	20.5095	52.31944	220319.3557	496960.8211	477
BON0035	20.5095	132.31944	220314.8858	496960.6401	247
BON0036	20.4791	152.31944	220314.1471	496959.6836	200
BON0037	20.4791	172.31944	220313.7800	496958.5321	305
BON0038	20.4791	112.31944	220315.3283	496962.6960	314
BON0039	20.4791	92.31944	220317.0261	496963.0666	328
BON0040	20.4791	72.31944	220318.7484	496962.8344	248
BON0041	20.4791	52.31944	220320.2873	496962.0272	596
BON0043	20.4791	152.31944	220312.7975	496960.3914	236
BON0044	20.5400	172.31944	220312.2697	496958.7357	303
BON0045	19.0160	112.31944	220317.0646	496958.4665	369
BON0046	19.0160	112.31944	220316.4859	496959.8762	547
BON0047	19.0160	92.31944	220317.1495	496960.0210	982
BON0048	19.0160	72.31944	220317.8226	496959.9305	909
BON0049	19.0160	132.31944	220315.9119	496959.5132	633
BON0050	19.0160	152.31944	220315.4966	496958.9756	463
BON0051	19.0160	112.31944	220315.9071	496961.2860	890
BON0053	19.0160	72.31944	220318.2855	496961.3823	654
BON0054	19.0160	52.31944	220319.3557	496960.8211	323
BON0055	19.0465	132.31944	220314.8858	496960.6401	166
BON0056	19.0465	152.31944	220314.1471	496959.6836	659
BON0057	19.0465	172.31944	220313.7800	496958.5321	78
BON0058	19.0465	112.31944	220315.3283	496962.6960	636
BON0059	19.0465	92.31944	220317.0261	496963.0666	223
BON0060	19.0465	72.31944	220318.7484	496962.8344	223
BON0061	19.0465	52.31944	220320.2873	496962.0272	200
BON0062	19.0465	132.31944	220313.8597	496961.7669	196

Table C2 – Continued. Eddy Length Scales Upstream from the Bonneville Prototype Surface Collector.

BON0063	18.9855	152.31944	220312.7975	496960.3914	503
BON0064	18.9855	172.31944	220312.2697	496958.7357	302
BON0065	17.0957	112.31944	220317.0646	496958.4665	339
BON0066	17.0957	112.31944	220316.4859	496959.8762	742
BON0067	17.0957	92.31944	220317.1495	496960.0210	521
BON0068	17.0957	72.31944	220317.8226	496959.9305	771
BON0069	17.0957	132.31944	220315.9119	496959.5132	255
BON0070	17.0957	152.31944	220315.4966	496958.9756	252
BON0071	17.1567	112.31944	220315.9071	496961.2860	501
BON0072	17.1567	92.31944	220317.0878	496961.5438	171
BON0073	17.1567	72.31944	220318.2855	496961.3823	436
BON0074	17.1567	52.31944	220319.3557	496960.8211	337
BON0075	17.1567	132.31944	220314.8858	496960.6401	266
BON0076	17.1567	152.31944	220314.1471	496959.6836	113
BON0077	17.1567	172.31944	220313.7800	496958.5321	138
BON0078	17.2481	112.31944	220315.3283	496962.6960	372
BON0079	17.2481	92.31944	220317.0261	496963.0666	552
BON0080	17.2481	72.31944	220318.7484	496962.8344	1134
BON0081	17.2481	52.31944	220320.2873	496962.0272	291
BON0082	17.2481	132.31944	220313.8597	496961.7669	447
BON0083	17.2481	152.31944	220312.7975	496960.3914	169
BON0084	17.2481	172.31944	220312.2697	496958.7357	385
BON0085	15.8156	112.31944	220317.0646	496958.4665	180
BON0086	15.8156	112.31944	220316.4859	496959.8762	403
BON0087	15.8156	92.31944	220317.1495	496960.0210	1014
BON0088	15.8156	72.31944	220317.8226	496959.9305	824
BON0089	15.9070	132.31944	220315.9119	496959.5132	210
BON0090	15.9070	152.31944	220315.4966	496958.9756	249
BON0091	15.9070	112.31944	220315.9071	496961.2860	192
BON0092	15.9070	92.31944	220317.0878	496961.5438	365
BON0093	15.9070	72.31944	220318.2855	496961.3823	339
BON0094	15.9070	52.31944	220319.3557	496960.8211	565
BON0095	15.9070	132.31944	220314.8858	496960.6401	487
BON0096	16.0899	152.31944	220314.1471	496959.6836	193
BON0097	16.0899	172.31944	220313.7800	496958.5321	344
BON0098	16.0899	112.31944	220315.3283	496962.6960	256
BON0099	16.0899	92.31944	220317.0261	496963.0666	394
BON0100	16.0899	72.31944	220318.7484	496962.8344	666

Table C2 – Continued. Eddy Length Scales Upstream from the Bonneville Prototype Surface Collector.

BON0101	16.0899	52.31944	220320.2873	496962.0272	293
BON0102	16.2728	132.31944	220313.8597	496961.7669	104
BON0103	16.1204	152.31944	220312.7975	496960.3914	180
BON0104	16.1204	172.31944	220312.2697	496958.7357	389
BON0105	19.1684	172.31944	220312.2697	496958.7357	196
BON0106	19.1684	152.31944	220312.7975	496960.3914	477
BON0107	19.1684	132.31944	220313.8597	496961.7669	433
BON0108	19.1684	112.31944	220315.3283	496962.6960	742
BON0109	19.1989	92.31944	220317.0261	496963.0666	335
BON0110	21.7897	112.31944	220317.0646	496958.4665	205
BON0111	21.7897	112.31944	220316.4859	496959.8762	289
BON0112	21.7897	72.31944	220317.8226	496959.9305	327
BON0113	21.7897	152.31944	220315.4966	496958.9756	700
BON0114	21.8202	112.31944	220315.9071	496961.2860	1101
BON0115	21.8202	72.31944	220318.2855	496961.3823	323
BON0116	21.8202	152.31944	220314.1471	496959.6836	863
BON0117	21.8202	112.31944	220315.3283	496962.6960	632
BON0118	21.8202	72.31944	220318.7484	496962.8344	622
BON0119	21.8202	152.31944	220312.7975	496960.3914	581
BON0120	18.7722	152.31944	220312.7975	496960.3914	397
BON0121	18.7722	112.31944	220315.3283	496962.6960	324
BON0122	18.7722	72.31944	220318.7484	496962.8344	348
BON0123	18.7417	72.31944	220318.2855	496961.3823	971
BON0124	18.7417	112.31944	220315.9071	496961.2860	552
BON0125	18.7417	152.31944	220314.1471	496959.6836	358
BON0126	18.7417	152.31944	220315.4966	496958.9756	688
BON0127	18.7417	112.31944	220316.4859	496959.8762	495
BON0128	18.7417	72.31944	220317.8226	496959.9305	529
BON0129	18.8026	112.31944	220317.0646	496958.4665	658
BON0130	18.8026	112.31944	220317.0646	496958.4665	455

Table C2 – Continued. Eddy Length Scales Upstream from the Bonneville

Prototype Surface Collector.

References

- Faber, D., Rondorf, D., Odeh, M., Zimmerman, S. (2000). "Water Velocity Profiles at Bonneville Dam Prototype Surface Collector, Turbine Unit 5." *Draft Final Report USGS, USACE, Portland District.*
- White, F. M. (1991). *Viscous Fluid Flow*. McGraw-Hill.

APPENDIX D

**CONTACT INFORMATION FOR ALBROOK HYDRAULIC
LABORATORY**

**CONTACT INFORMATION FOR ALBROOK HYDRAULIC
LABORATORY**

Raw and summary data for this project are available in CD Format from Dr. Rollin Hotchkiss who may be contacted at the address listed below.

Dr. Rollin H. Hotchkiss, Ph. D., P. E.
Director, Albrook Hydraulic Laboratory
Washington State University
P.O. Box 642910
Pullman, WA 99164